THE ROLE OF MERIDIONAL MODES IN PACIFIC CLIMATE VARIABILITY AND CHANGE

A Dissertation
Presented to
The Academic Faculty

by

Giovanni Liguori

In Partial Fulfillment
of the Requirements for the Degree
Doctor of Philosophy in the
School of Earth and Atmospheric Sciences

Georgia Institute of Technology
December 2018

THE ROLE OF MERIDIONAL MODES IN PACIFIC CLIMATE VARIABILITY AND CHANGE

Approved by:

Dr. Emanuele Di Lorenzo, Advisor
School of Earth and Atmospheric Sciences
Georgia Institute of Technology

Dr. Takamitsu Ito
School of Earth and Atmospheric Sciences
Georgia Institute of Technology

Dr. Jean Lynch-Stieglitz
School of Earth and Atmospheric Sciences
Georgia Institute of Technology

Dr. Jie He
School of Earth and Atmospheric Sciences
Georgia Institute of Technology

Dr. Antonietta Capotondi
Cooperative Institute for Research in Environmental Sciences
NOAA-Physical Sciences Division

Date Approved: October 8th, 2018

To my amore Julie,
our daughter Giorgia,
and those to come

ACKNOWLEDGEMENTS

None of this would have been possible without numerous people who lent their help or support. My deepest gratitude goes to Manu, my advisor. After inviting me to the east side of the Atlantic, you warmly welcomed me in Atlanta and in your group. Since then, the many one-by-one hours spent in your office largely shaped the scientist I have become, and perhaps the person I am. Your style, simultaneously brilliant, energetic, peaceful and calm, has been a source of inspiration, enthusiasm, vision, and will remain a role model. For that, I will eternally be grateful to you.

I wish to thank all the scientists that directly or indirectly helped with the research presented in this dissertation. I am deeply indebted to Pedro Di Nezio, who I consider a friend first and foremost. He welcomed me in into his lab and home, taught me much of what I know of CESM, and always finds time for our delightful scientific conversations. I also wish to thank Antonietta Capotondi for several insightful scientific conversations and for accepting to be part of my PhD committee. Thanks also to Daniel Vimont, Matthew Newman, Michael Alexander, Jason Furtado, Niklas Schneider, Shang-ping Xie, Clara Deser and George Philander, from which I have received invaluable insight at different stages of this dissertation.

I would like to extend my sincere gratitude to all the people that were part of the School of Earth and Atmospheric Sciences community during these past five years. Thank you Taka (Ito), for being an excellent teacher, a reference for good science, and for allowing me to unexpectedly visit your office and brainstorm on the whiteboard. Thank you Rob (Black) for our numerous conversations about atmospheric dynamics and for accepting my often unspoken requests for advice. Thank you Annalisa (Bracco) and Kim (Cobb). The former for her help in building most of my ocean dynamics knowledge, and the latter for her

sound advice on my next steps in academia. Thanks also to many past and present graduate students with whom I shared both work and leisure. I am grateful to Yohei, Sebastian, Filippos, Anh, Fabrizio, Daoxun, Youngji, Giangiacomo, Giulia, and Raj. A double thanks to Yohei for organizing our traditional dinner with Michael Alexander at every Ocean Sciences Meeting conference.

In more than five years in Atlanta, I was immensely fortunate to come across several exceptional individuals that now are lifelong friends. I would express my gratitude to Alice, you were always there, both the cornerstone and the glue of my social life; Giuseppe, I never had a brother except the wonderful three years we lived together; Simon, it was a pleasure to be pulled by your momentum; David, you constantly stimulate my intellect and provide shelter for my emotions. Thanks also to Amir, Mari, Giovanni and Cesar for the amazing moments spent together.

I am also extremely grateful to my parents, Angela e Gennaro, for their unconditioned support despite the struggle of having me thousands of miles from home.

The last words of this acknowledgement could not go to anybody else other than my amore. Julie, during those stressful days that inevitably characterize the life of a PhD student, you were my happy oasis where I would feel safe, warm and happy. Your adventurous spirit has filled my life with excitement and pushed us toward our next big adventure down under. You are my best friend, my travel mate, my teammate, my lover, my true love, my wife, and the mother of our wonderful daughter, Giorgia, who makes every day special and fills our hearts with pure joy and happiness. Julie, you are my everything.

CONTENTS

LIST OF FIGURES

SUMMARY

Decadal changes in Pacific climate affect long-term transitions in marine ecosystems and influence the statistics of weather including ocean and atmosphere extremes such as strong droughts, hurricanes and marine heatwaves. However, the physical mechanisms that generate decadal variance and how these dynamics will change under anthropogenic forcing remains unknown. This research utilizes statistical and physical modeling to investigate the role of extratropical El Niño-Southern Oscillation (ENSO) precursors such as Pacific Meridional Modes (PMMs) in driving Pacific decadal variability and change.

In the first part of this dissertation, we develop an interpretative framework for the Pacific decadal variability (PDV) in which the stochastic variability of the North Pacific Oscillation (NPO) energizes the decadal-scale sea surface temperature anomalies (SSTa) variability in the extratropics through PMM dynamics. The spatial evolution of the North PMM (NPMM) dynamics injects decadal variance into the tropics where the SSTa anomalies are amplified by the feedback dynamics characteristic of the ENSO system along the equatorial plane. After the SSTa are amplified in the tropics, ENSO teleconnections project the decadal-scale variance onto the climate modes of the extratropics (e.g., Pacific Decadal Oscillation and North Pacific Gyre Oscillation). The coupling between extra-tropics/tropics/extra-tropics acts as a primary mechanism to redden (e.g. energize the low frequency) the Pacific climate spectrum by prolonging the memory of the system to stochastic perturbation from the ENSO precursors.

In the second part of this dissertation, we use the interpretative framework to explore how the PDV has changed in the observational record, and how it is expected to change according to the Community Earth System Model (CESM) Large Ensemble (LENS) under

the RCP8.5 radiative forcing scenario. After designing a set of diagnostics to measure the interaction dynamics between NPMM and ENSO, we found that the variance of the NPMM increases in a warming climate because of an intensification of the thermodynamic coupling of the ocean and atmosphere, also known as the wind-evaporations-SST (WES) feedback. This feedback is dependent on the mean background state (i.e., warming of SST generates a stronger response in evaporation) and modulates the amplitude of the growth of NPMM.

In the third part of this dissertation, we investigate the relative importance of the NPMM and South PMM (SPMM) in ENSO and tropical Pacific decadal variability (TPDV) by performing experiments with the CESM model in which the NPMM and SPMM are selectively suppressed. We find that both meridional modes energize the tropical variance independently on different timescales. The absence of NPMM leads to a significant reduction of the tropical interannual variability (~35%), while the absence of the SPMM has no appreciable impact on ENSO but significantly reduces the TPDV (~30%). While the relative importance of the NPMM and SPMM may be model dependent, the stochastic atmospheric variability in the extra-tropics that energizes the meridional modes emerges as a key source of TPDV.

CHAPTER I

INTRODUCTION

El Niño Southern Oscillation (ENSO) and the Tropical Pacific Decadal Variability (TPDV) exert a strong influence on modes of Pacific decadal variability (PDV) such as the Interdecadal Pacific Oscillation (IPO) [*Power et al., 1999; Salinger et al., 2001*], the northern and southern expressions of the Pacific Decadal Oscillation (PDO) [*Mantua et al., 1997; Y Zhang et al., 1997*], and the North Pacific Gyre Oscillation (NPGO) [*Di Lorenzo et al., 2008*]. As oceanic and atmospheric teleconnections are able to link them on a wide range of temporal scales, these modes of variability may show dependencies [*Liu and Alexander, 2007*]. For instance, studies have shown that Eastern Pacific El Niño events (or Eastern Pacific Warming, EPW) impact the PDO through an atmospheric teleconnection to the Aleutian Low [*Alexander, 1992; Alexander et al., 2002*], which in turn drives the PDO [*Newman et al., 2011; Schneider and Cornuelle, 2005; Vimont, 2005*]. Similarly, the central Pacific El Niño (or Central Pacific Warming, CPW) contributes to the decadal variance of the NPGO through atmospheric teleconnections that modulate the NPGO driver—the North Pacific Oscillation (NPO) [*Di Lorenzo et al., 2010; Furtado et al., 2011*]. All these climate modes strongly impact the marine ecosystem, agriculture, hurricanes, and other extreme weather events on a global scale, particularly over North America and Asia [*Chavez et al., 2003; Di Lorenzo et al., 2008; Gershunov and Barnett, 1998; Mantua et al., 1997; Roemmich and Mcgowan, 1995*].

Tropical Pacific climate variability originates locally [e.g., *Chowdary et al., 2012; Wang and Mehta, 2008*] and through its connections with subtropical and extratropical Pacific climate variability mostly from the North Pacific [e.g., *Anderson, 2003; Barnett et al., 1999; Deser et al., 2004; Vimont et al., 2001; Vimont et al., 2003*]. Locally generated tropical Pacific variability is

mostly associated with stochastic atmospheric forcing and feedback mechanisms acting along the equatorial plane and associated with the ENSO system (e.g., zonal modes dynamics). For instance, the westerly wind burst and the Madden-Julian oscillation can generate perturbations that are amplified by zonal modes dynamics and lead to mature expressions of El Nino. Recent studies have revealed how subtropical and extratropical stochastic atmospheric forcing can generate a large-fraction of tropical Pacific variability through positive feedback associated with thermodynamic coupling between the ocean and the atmosphere. More specifically, thermodynamically-controlled transient growing modes excited by stochastic forcing propagate towards the equator, where they can interact with ENSO. Therefore, they are often referred to as "meridional modes" [*Chiang and Vimont, 2004; Servain et al., 1999*]. This set of dynamics, initiated by stochastic atmospheric variability, has been principally used to investigate interannual variability, but it is still unclear to what extent these mechanisms explain decadal variability.

1.1 Stochastic Atmospheric Forcing and ENSO Precursors

Several studies have documented precursor dynamics in the ocean and atmosphere that lead to an El Niño event. Historically, ENSO precursors were first associated with dynamics acting along the equatorial plane, but more recently, studies have shown that extra-tropical dynamics can also lead to mature expressions of El Niño. On the equator, ENSO precursors include westerly wind bursts (WWBs) [*Fedorov, 2002; Kessler and Kleeman, 2000; McPhaden, 1999; McPhaden and Yu, 1999; Moore and Kleeman, 1996; 1997a; b*], and in the extra-tropics, they are associated with extra-tropical wind forcing (ETWF), which acts via the "seasonal footprinting mechanism" (SFM) [*Vimont et al., 2001; Vimont et al., 2003*] and the "trade wind charging" (TWC) mechanism [*Anderson, 2003; Anderson et al., 2013a*]. Although

these mechanisms differ markedly, both WWB and ETWF precursor dynamics originate in stochastic atmospheric variability.

As named by Luther et al. [*1983*], WWBs are short-lived episodes of strong westerly winds observed in the equatorial Pacific near the Dateline that occur as a result of local intraseasonal atmospheric variability. During WWB episodes, the resulting strong westerly wind stress over the western equatorial Pacific Ocean, may excite oceanic Kelvin waves that propagate zonally across the equatorial Pacific, deepening the thermocline, reducing upwelling, and initiating Bjerknes feedback. Despite this well-defined ENSO precursor mechanism, finding observational evidence may often be challenging, thus modeling studies are often preferred. Several numerical studies have shown that a WWB event can lead, depending on the ocean state, to both EPW and CPW flavors. In particular, in some modeling experiments, when the subsurface heat content is higher than normal (i.e., the system is recharged), a WWB event would likely produce an EPW event [*Lengaigne et al., 2004*], and when the subsurface heat content is in a neutral condition, a WWB would likely produce a CPW event [*Fedorov et al., 2014*].

The stochastic variability of ETWF can also excite the ENSO system. In particular, several studies have connected the variability of the North Pacific Oscillation (NPO, defined as the second mode of SLP variability in the North Pacific) with the extra-tropical SST anomaly precursor patterns of ENSO. The NPO pattern represents a dipole structure with anomalies of opposite signs located around the two centers of action, the Gulf of Alaska, and the region to the Northeast of Hawaii (Figure 1.1). During the negative phase of the winter NPO index, the negative SLP anomaly at the southern pole induces anomalous westerly winds to the south of this pole, which oppose the predominant easterly wind, resulting in a reduction in the wind speed, and thus in evaporation. These conditions induce a warming effect on the

underlying ocean, resulting in positive SST anomalies during the spring and the summer, when it subsequently influences ocean-atmosphere coupling over the tropical Pacific [*Alexander et al., 2010; Vimont et al., 2001*]. This mechanism, which takes place on a seasonal basis, is called the seasonal footprinting mechanism (SFM; see Figure 1.1a).

Although most studies connecting NPO-generated ETWF and ENSO variability rely on air-sea interactions among SST, evaporation, and wind speed, observational and numerical results suggest that the NPO-generated ETWF also influences subsurface temperature anomalies across the equatorial and off-equatorial Pacific [*Anderson, 2004; Anderson and Maloney, 2006*]. In fact, the weakening of the trade wind south of the NPO southern pole results in not only a warming effect for the underlying ocean but also a negative wind-stress curl. The latter, as expected from the Sverdrup balance theory, induces a southward meridional mass transport that in turn depresses the thermocline and increases the heat content of the tropical Pacific, which is known to promote the onset of El Niño [*Anderson et al., 2013b*]. This wind-induced charging (TWC) mechanism (Figure 1.1b) when initiated during a positive (negative) NPO phase produces positive (negative) anomaly of the subsurface heat content across the equatorial and off-equatorial Pacific. This condition of positive anomaly of the subsurface heat content is often referred to as a "recharged condition".

A simple statistical analysis based on observed anomalies in the sea-level pressure (SLP) and SST confirms the key role of NPO variability as a precursor of both EPW and CPW events (refer to Section 2.1). Lag-correlation maps of EPW and CPW indices with SST and SLP anomalies reveal NPO-like patterns preceding the mature phase of both El Niño flavors by about one year. The selection of the type of ENSO response likely depends on the state of the tropical ocean (charged vs. discharged) [*Alexander et al., 2010; Anderson, 2007*], as in the case of the WWB.

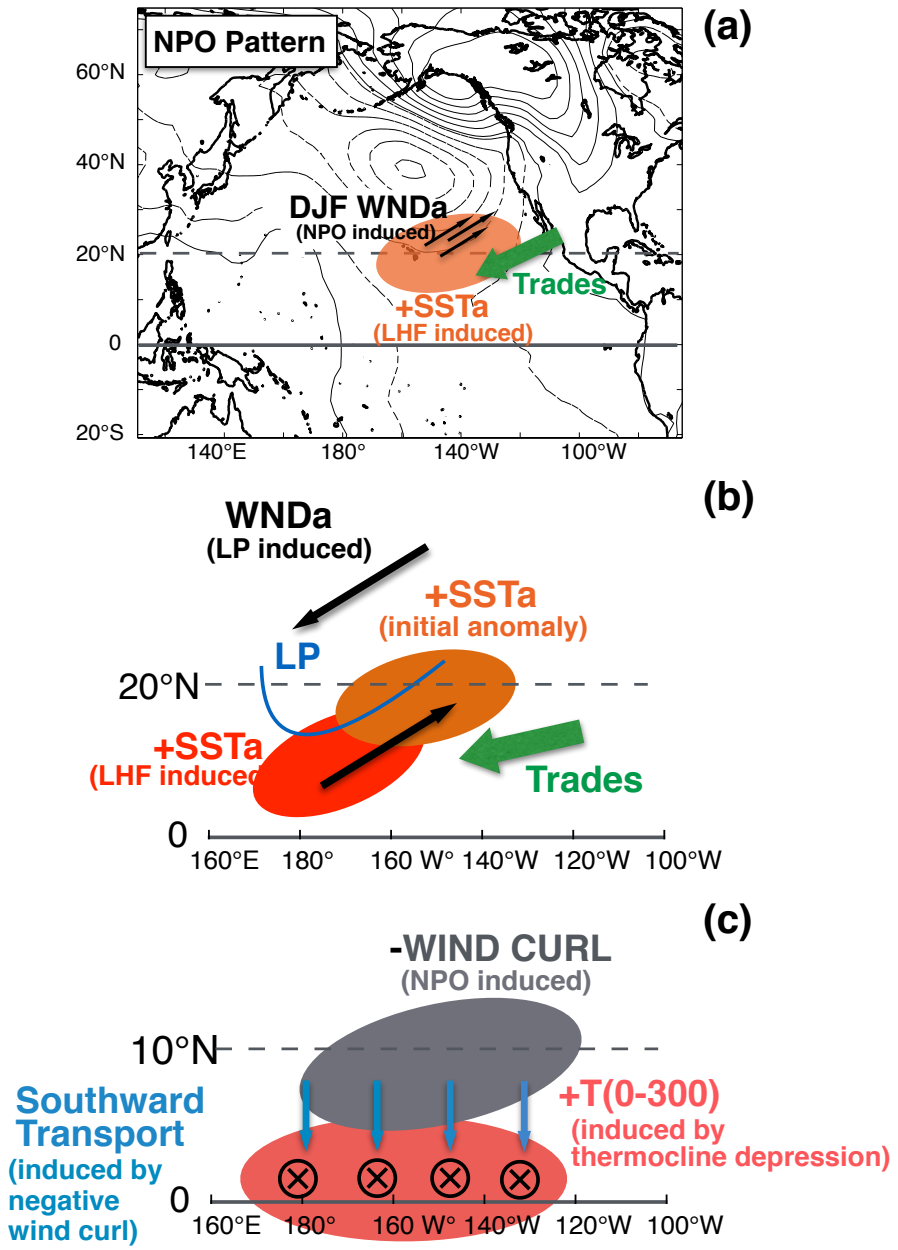

Figure 1.1. Schematic diagrams of the seasonal footprinting mechanism (SFM), the wind-evaporation-SST (WES) feedback, and the trade-wind charging (TWC) mechanism. (a) SFM: NPO stochastic variability during the winter (December/January/February, DJF) generates negative wind speed anomalies (WNDa) to the south of the Hawaiian Islands (blue arrows). The associated reduction in sea surface latent heat flux (LHF) loss leads to positive SST anomalies (light-red patch) later in the spring (March/April/May, MAM). (b) WES: An initial subtropical positive SST anomaly (e.g., the one propagated by SFM; light-red patch) induces a low-pressure anomaly trough (LP) and southwest wind anomalies, respectively, to the west and to the southwest of the warm SSTa. The wind anomalies oppose the persistent trade winds

and reduce LHF loss from the ocean, which results in a positive SSTa (red patch). (c) TWC: NPO variability can generate a negative wind stress curl which induces a southward meridional mass transport (Sverdrup balance theory) that in turn depresses the thermocline and increases the heat content from 0 to 300 meters (T(0-300)) of the tropical Pacific (i.e., a charged condition).

1.2 Meridional Modes and Extratropical Forcing of ENSO

The tropical Atlantic has a well-documented meridional mode of inter-annual-decadal atmosphere-ocean variability known as the Atlantic Meridional Mode [AMM; *Chang et al., 1997; Nobre and Shukla, 1996*]. This mode is characterized by variations in the meridional SST gradient, which drives surface winds that flow towards the warmer hemisphere, generally affecting the climate variability of this region and more specifically, the location of the ITCZ. Although less evident in the observations, a similar ocean-atmosphere coupled mode has been identified in the Pacific in both North and South Hemispheres and are known as the North Pacific Meridional Mode (NPMM) [*Chang et al., 2007; Chiang and Vimont, 2004*] and the South Pacific Meridional Mode (SPMM) [*Zhang et al., 2014*]. Both modes are connected to the ETWF mechanism, which also takes place along the meridional plane and plays a central role in connecting extratropical and tropical variability. In NPMM dynamics, the extratropical meridional gradient in SSTa, forced initially by a reduction in trade winds associated with NPO-type atmospheric variability, exerts positive feedback that further weakens the wind and strengthens the existing SSTa gradient. A similar mechanism is active in the southern hemisphere where the recently defined South Pacific Oscillation appears to be the optimal precursor of the SPMM [*You and Furtado, 2017*]. The feedback, which involves the impact of wind speed on anomalous evaporation, is also referred to as "wind evaporation–SST" (WES; Figure 1.1c) feedback [*S P Xie, 1999*]. In the North (South) Hemisphere this positive thermodynamic feedback supports a south-westward (north-westward) co-evolution of the

oceanic SSTa and winds that ultimately make it to the tropics, where they have the ability to favor ENSO anomalies through a weakening of the Walker cell associated with the positive SSTa.

The imprint of meridional mode dynamics is evident in the SSTa and SLPa patterns, which have been isolated as the precursors of EPW events with a lead of six to twelve months. However, recent studies also show that meridional mode dynamics energize CPW events) [*Kim et al., 2012; Yu and Kim, 2011*]. These findings suggest that extra-tropical stochastic forcing (e.g., NPO) can energize inter-annual variance in the tropical Pacific through meridional mode dynamics. Thus, the dynamics of the meridional mode are consistent with a red noise process (e.g., stochastic atmospheric forcing driving low-frequency variance in the ocean) without any preferential time scales, implying that meridional mode dynamics can also energize the decadal energy of the tropical Pacific. Moreover, components of NPMM ocean/atmosphere coupling individually and together exhibit important quasi-decadal variability. The characteristic SST pattern resembles both the NPGO [*Di Lorenzo et al., 2008*] and the CPW pattern [e.g., *Ashok et al., 2007*]. Furthermore, Furtado et al. [*2012*] demonstrated that the southern pole of the NPO (i.e., the center of action near Hawaii) exhibits strong low-frequency (i.e., 7-15 years) feedback with central tropical Pacific SSTs. In addition, the corresponding Atlantic meridional mode, which shares a number of similarities with the NPMM [*Chiang and Vimont, 2004*], is particularly active on decadal time scales [*Chang et al., 1997*]

1.3 Scientific Questions

From all evidence and suggestions supporting the potential key role of meridional mode dynamics in tropical Pacific decadal variability, several fundamental questions have arisen:

(1) What is the role of the NPMM in PDV?

(2) Does NPMM interact with the low-frequency modes of PDV, such as IPO, NPGO, and PDO?

(3) How is the NPMM sensitive to different mean states, such as a warmer planet resulting from anthropogenic forcing?

(4) What are the impacts of NPMM and SPMM in the statistics of the tropical Pacific variability from interannual to decadal timescale?

Questions (1) and (2) are addressed in Chapter II [*Di Lorenzo, Liguori et al., 2015*], question (3) is address in Chapter III [*Liguori and Di Lorenzo, 2018*], and question (4) in Chapter IV [*Liguori and Di Lorenzo*, *under review in GRL*].

1.4 References

Alexander, M. A. (1992), Midlatitude Atmosphere Ocean Interaction during El Nino .1. The North Pacific-Ocean, *Journal of Climate*, 5(9), 944-958.

Alexander, M. A., D. J. Vimont, P. Chang, and J. D. Scott (2010), The Impact of Extratropical Atmospheric Variability on ENSO: Testing the Seasonal Footprinting Mechanism Using Coupled Model Experiments, *Journal of Climate*, 23(11), 2885-2901.

Alexander, M. A., I. Blade, M. Newman, J. R. Lanzante, N. C. Lau, and J. D. Scott (2002), The atmospheric bridge: The influence of ENSO teleconnections on air-sea interaction over the global oceans, *Journal of Climate*, 15(16), 2205-2231.

Anderson, B. T. (2003), Tropical Pacific sea-surface temperatures and preceding sea level pressure anomalies in the subtropical North Pacific, *J Geophys Res-Atmos*, 108(D23).

Anderson, B. T. (2004), Investigation of a large-scale mode of ocean-atmosphere variability and its relation to tropical Pacific sea surface temperature anomalies, *Journal of Climate*, 17(20), 4089-4098.

Anderson, B. T. (2007), On the joint role of subtropical atmospheric variability and equatorial subsurface heat content anomalies in initiating the onset of ENSO events, *Journal of Climate*, 20(8), 1593-1599.

Anderson, B. T., and E. Maloney (2006), Interannual tropical Pacific Sea surface temperatures and their relation to preceding sea level pressures in the NCAR CCSM2*, Journal of Climate*, 19(6), 998-1012.

Anderson, B. T., R. C. Perez, and A. Karspeck (2013a), Triggering of El Nino onset through trade wind-induced charging of the equatorial Pacific, *Geophys Res Lett*, 40(6), 1212-1216.

Anderson, B. T., J. C. Furtado, K. M. Cobb, and E. Di Lorenzo (2013b), Extratropical forcing of El Nino-Southern Oscillation asymmetry, *Geophys Res Lett*, 40(18), 4916-4921.

Ashok, K., S. K. Behera, S. A. Rao, H. Weng, and T. Yamagata (2007), El Nino Modoki and its possible teleconnection, *Journal of Geophysical Research-Oceans*, 112(C11).

Barnett, T. P., D. W. Pierce, M. Latif, D. Dommenget, and R. Saravanan (1999), Interdecadal interactions between the tropics and midlatitudes in the Pacific basin*, Geophys Res Lett*, 26(5), 615-618.

Chang, P., L. Ji, and H. Li (1997), A decadal climate variation in the tropical Atlantic Ocean from thermodynamic air-sea interactions, *Nature*, 385(6616), 516-518.

Chang, P., L. Zhang, R. Saravanan, D. J. Vimont, J. C. H. Chiang, L. Ji, H. Seidel, and M. K. Tippett (2007), Pacific meridional mode and El Nino-southern oscillation, *Geophysical Research Letters*, 34(16).

Chavez, F. P., J. Ryan, S. E. Lluch-Cota, and M. Niquen (2003), From anchovies to sardines and back: Multidecadal change in the Pacific Ocean, *Science*, 299(5604), 217-221.

Chiang, J. C. H., and D. J. Vimont (2004), Analogous Pacific and Atlantic meridional modes of tropical atmosphere-ocean variability, *Journal of Climate*, 17(21), 4143-4158.

Chowdary, J. S., S. P. Xie, H. Tokinaga, Y. M. Okumura, H. Kubota, N. Johnson, and X. T. Zheng (2012), Interdecadal Variations in ENSO Teleconnection to the Indo-Western Pacific for 1870-2007, *Journal of Climate*, 25(5), 1722-1744.

Deser, C., A. S. Phillips, and J. W. Hurrell (2004), Pacific interdecadal climate variability: Linkages between the tropics and the North Pacific during boreal winter since 1900, *Journal of Climate*, 17(16), 3109-3124.

Di Lorenzo, E., K. M. Cobb, J. C. Furtado, N. Schneider, B. T. Anderson, A. Bracco, M. A. Alexander, and D. J. Vimont (2010), Central Pacific El Nino and decadal climate change in the North Pacific Ocean, *Nat Geosci*, 3(11), 762-765.

Di Lorenzo, E., et al. (2008), North Pacific Gyre Oscillation links ocean climate and ecosystem change, *Geophys Res Lett*, 35(8).

Fedorov, A. V. (2002), The response of the coupled tropical ocean-atmosphere to westerly wind bursts, *Q J Roy Meteor Soc*, 128(579), 1-23.

Fedorov, A. V., S. Hu, M. Lengaigne, and E. Guilyardi (2014), The impact of westerly wind bursts and ocean initial state on the development, and diversity of El Niño events, *Clim Dynam,* 44(5-6),1381-1401.

Furtado, J. C., E. Di Lorenzo, N. Schneider, and N. A. Bond (2011), North Pacific Decadal Variability and Climate Change in the IPCC AR4 Models, *Journal of Climate*, 24(12), 3049-3067.

Furtado, J. C., E. Di Lorenzo, B. T. Anderson, and N. Schneider (2012), Linkages between the North Pacific Oscillation and central tropical Pacific SSTs at low frequencies, *Clim Dynam*, 39(12), 2833-2846.

Gershunov, A., and T. P. Barnett (1998), Interdecadal modulation of ENSO teleconnections, *B Am Meteorol Soc*, 79(12), 2715-2725.

Kessler, W. S., and R. Kleeman (2000), Rectification of the Madden-Julian oscillation into the ENSO cycle, *Journal of Climate*, 13(20), 3560-3575.

Kim, S. T., J. Y. Yu, A. Kumar, and H. Wang (2012), Examination of the Two Types of ENSO in the NCEP CFS Model and Its Extratropical Associations, *Mon Weather Rev*, 140(6), 1908-1923.

Lengaigne, M., E. Guilyardi, J. P. Boulanger, C. Menkes, P. Delecluse, P. Inness, J. Cole, and J. Slingo (2004), Triggering of El Nino by westerly wind events in a coupled general circulation model, *Clim Dynam*, 23(6), 601-620.

Liguori G. and E. Di Lorenzo (2018), Meridional Modes and Increasing Pacific decadal variability under greenhouse forcing. *Geophys Res Lett,* 45(2), 983-991.

Liguori, G. and E. Di Lorenzo: Separating the North and South Pacific Meridional Modes contributions to ENSO and tropical decadal variability. *Geophys Res Lett*, *under review.*

Liu, Z. Y., and M. Alexander (2007), Atmospheric bridge, oceanic tunnel, and global climatic teleconnections, *Rev Geophys*, 45(2).

Luther, D. S., D. E. Harrison, and R. A. Knox (1983), Zonal Winds in the Central Equatorial Pacific and El-Nino, *Science*, 222(4621), 327-330.

Mantua, N. J., S. R. Hare, Y. Zhang, J. M. Wallace, and R. C. Francis (1997), A Pacific interdecadal climate oscillation with impacts on salmon production, *Bulletin of the American Meteorological Society*, 78(6), 1069-1079.

McPhaden, M. J. (1999), Genesis and evolution of the 1997-98 El Nino, *Science*, 283(5404), 950-954.

McPhaden, M. J., and X. Yu (1999), Equatorial waves and the 1997-98 El Nino, *Geophys Res Lett*, 26(19), 2961-2964.

Moore, A. M., and R. Kleeman (1996), The dynamics of error growth and predictability in a coupled model of ENSO, *Q J Roy Meteor Soc*, 122(534), 1405-1446.

Moore, A. M., and R. Kleeman (1997a), The singular vectors of a coupled ocean-atmosphere model of ENSO .1. Thermodynamics, energetics and error growth, *Q J Roy Meteor Soc*, 123(540), 953-981.

Moore, A. M., and R. Kleeman (1997b), The singular vectors of a coupled ocean-atmosphere model of ENSO .2. Sensitivity studies and dynamical interpretation, *Q J Roy Meteor Soc*, 123(540), 983-1006.

Newman, M., M. A. Alexander, and J. D. Scott (2011), An empirical model of tropical ocean dynamics, *Clim Dynam*, 37(9-10), 1823-1841.

Nobre, P., and J. Shukla (1996), Variations of sea surface temperature, wind stress, and rainfall over the tropical Atlantic and South America, *Journal of Climate*, 9(10), 2464-2479.

Power, S., T. Casey, C. Folland, A. Colman, and V. Mehta (1999), Inter-decadal modulation of the impact of ENSO on Australia, *Clim Dynam*, 15(5), 319-324.

Roemmich, D., and J. Mcgowan (1995), Climatic Warming and the Decline of Zooplankton in the California Current, *Science*, 267(5202), 1324-1326.

Salinger, M. J., J. A. Renwick, and A. B. Mullan (2001), Interdecadal Pacific Oscillation and South Pacific climate, *Int J Climatol*, 21(14), 1705-1721.

Schneider, N., and B. D. Cornuelle (2005), The forcing of the Pacific decadal oscillation, *Journal of Climate*, 18(21), 4355-4373.

Servain, J., I. Wainer, J. P. McCreary, and A. Dessier (1999), Relationship between the equatorial and meridional modes of climatic variability in the tropical Atlantic, *Geophys Res Lett*, 26(4), 485-488.

Vimont, D. J. (2005), The contribution of the interannual ENSO cycle to the spatial pattern of decadal ENSO-like variability, *Journal of Climate*, 18(12), 2080-2092.

Vimont, D. J., D. S. Battisti, and A. C. Hirst (2001), Footprinting: A seasonal connection between the tropics and mid-latitudes, *Geophys Res Lett*, 28(20), 3923-3926.

Vimont, D. J., J. M. Wallace, and D. S. Battisti (2003), The seasonal footprinting mechanism in the Pacific: Implications for ENSO, *Journal of Climate*, 16(16), 2668-2675.

Wang, H., and V. M. Mehta (2008), Decadal Variability of the Indo-Pacific Warm Pool and Its Association with Atmospheric and Oceanic Variability in the NCEP-NCAR and SODA Reanalyses, *Journal of Climate*, 21(21), 5545-5565.

You, Y. J., and J. C. Furtado (2017), The role of South Pacific atmospheric variability in the development of different types of ENSO, Geophys Res Lett, 44(14), 7438-7446.

Xie, S. P. (1999), A dynamic ocean-atmosphere model of the tropical Atlantic decadal variability, *Journal of Climate*, 12(1), 64-70.

Yu, J. Y., and S. T. Kim (2011), Relationships between Extratropical Sea Level Pressure Variations and the Central Pacific and Eastern Pacific Types of ENSO, *Journal of Climate*, 24(3), 708-720.

Zhang, H. H., A. Clement, and P. Di Nezio (2014), The South Pacific Meridional Mode: A Mechanism for ENSO-like Variability, *Journal of Climate*, 27(2), 769-783, doi:Doi 10.1175/Jcli-D-13-00082.1.

Zhang, Y., J. M. Wallace, and D. S. Battisti (1997), ENSO-like interdecadal variability: 1900-93, *Journal of Climate*, 10(5), 1004-1020.

CHAPTER II

ENSO AND MERIDIONAL MODES: A NULL HYPOTHESIS FOR PACIFIC CLIMATE VARIABILITY

Published as

Di Lorenzo, E., G. Liguori, N. Schneider, J. C. Furtado, B. T. Anderson and M. A. Alexander, 2015: ENSO and meridional modes: A null hypothesis for Pacific climate variability. *Geophysical Research Letters*, 42(21) 9440-9448, doi:10.1002/2015gl066281.

Abstract

Pacific low-frequency variability (timescale > 8 years) exhibits a well-known El Niño-like pattern of basin-scale sea surface temperature, which is found in all the major modes of Pacific decadal climate. Using a set of climate model experiments and observations, we decompose the mechanisms contributing to the growth, peak, and decay of the Pacific low-frequency spatial variance. We find that the El Niño-like interdecadal pattern is established through the combined actions of Pacific meridional modes (MM) and the El Niño–Southern Oscillation (ENSO). Specifically, in the growth phase of the pattern, subtropical stochastic excitation of the MM energizes the tropical low-frequency variance acting as a red noise process. Once in the tropics, this low-frequency variance is amplified by ocean-atmospheric feedbacks as the pattern reaches its peak phase. At the same time, atmospheric teleconnections distribute the variance from the tropics to the extratropics, where the pattern ultimately decays. In this stochastic red noise model of Pacific climate, the timescale of the extra-tropical/tropical

interactions (1–2 years) permits the stochastic excitation of the ENSO-like pattern of decadal and interdecadal variance.

2.1 Introduction

The observed decadal climate of the Pacific has been characterized in terms of statistical patterns of low-frequency oceanic variability, like the Interdecadal Pacific Oscillation [*Trenberth and Hurrell, 1994; Power et al., 1999; Deser et al., 2004*], the Pacific Decadal Oscillation [*Mantua et al., 1997*], and more recently the North Pacific Gyre Oscillation [*Di Lorenzo et al., 2008*]. Although these patterns track large-scale dynamics of the coupled ocean-atmosphere system and are useful for assessing the state of Pacific climate, the dynamics underlying the origin of the decadal and interdecadal Pacific variance are still debated. In the low-frequency limit (timescales > 8 years), these modes are all characterized by a spatially broad ENSO-like pattern [*Zhang et al., 1997*] (Figures 2.1a–2.1d), which is derived by computing the first empirical orthogonal function (EOF) of the 8-year low-pass sea surface temperature anomalies (SSTa) over the Pacific Ocean basin (45°S–65°N) (Figure 2.1a). The emergence of this ENSO-like pattern, and its spatial symmetry from the equator, suggests that an important fraction of this low-frequency variance originates from tropical Pacific dynamics linked to the ENSO system.

The influence of ENSO on the modes of Pacific decadal variability is well documented by previous studies showing how atmospheric and ocean teleconnections forced by ENSO, and its different eastern and central Pacific expressions, imprint a signal in the extratropics on the Pacific Decadal Oscillation (PDO) and North Pacific Gyre Oscillation (NPGO) [*Alexander et al., 2002; Vimont, 2005; Di Lorenzo et al., 2010; Furtado et al., 2012*]. However, despite the many theories proposed to explain the tropical interannual variability of ENSO [*Jin, 1997;*

Neelin et al., 1998, and others], few observationally constrained theories exist to explain the sources of tropical decadal variance itself [*Dommenget and Latif, 2008; Clement et al., 2011*]. We hypothesize that the observed ENSO-like pattern of decadal variability arises from the combined action of ENSO and the Pacific meridional mode [*Chiang and Vimont, 2004*].

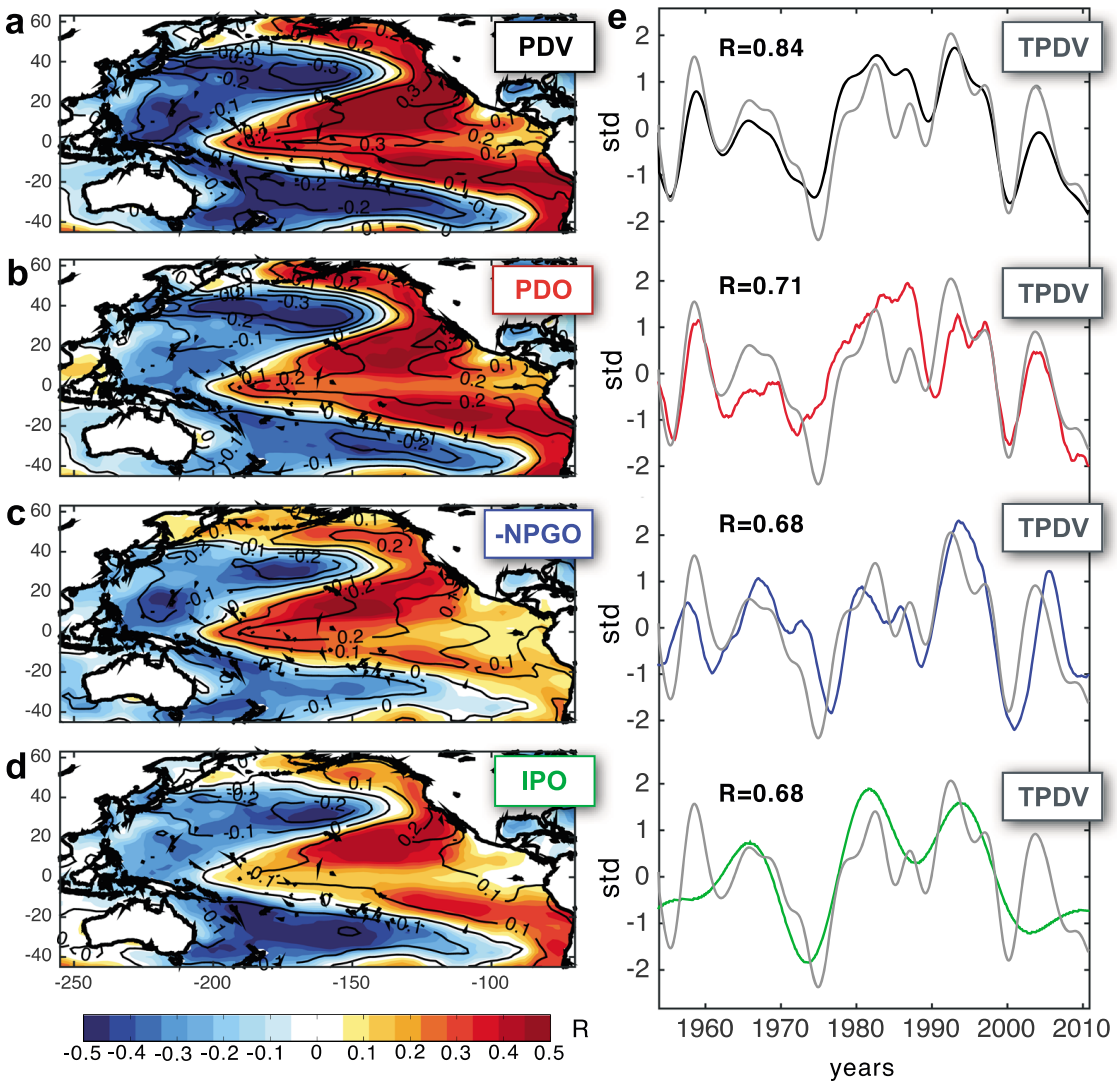

Figure 2.1. ENSO-like pattern of Pacific low-frequency variability. Correlation maps between monthly NOAA ERSST.v3 SSTa and (a) Pacific decadal variability (PDV) index defined as the PC1 of 8 year low-pass SSTa over Pacific basin (45°S–65°N), (b) 8 year low-pass Pacific Decadal Oscillation (PDO) index, (c) 8 year low-pass negative North Pacific Gyre Oscillation (NPGO) index, and (d) Interdecadal Pacific Oscillation (IPO) index. Regression

coefficients are shown as black contours in units of °C. The time series of the indices are shown in Figure 2.1e and compared against a Tropical Pacific Decadal Variability (TPDV) index defined as PC1 of 8 year low-pass SST over the equatorial Pacific (12°S-12°N).

2.2 Hypothesis for Pacific Climate Variability

On interannual timescales the ENSO system dominates the tropical variance. Perturbations in the tropical Pacific sea surface temperature and thermocline associated with stochastic atmospheric forcing (e.g., westerly wind bursts) can be amplified by positive feedbacks (e.g., zonal current and thermocline feedback) that involve coupling between the atmosphere and ocean dynamics [*Bjerknes, 1969; Suarez and Schopf, 1988; Jin, 1997*]. These positive feedbacks allow for the growth of dynamical modes along the equatorial zonal plane (e.g., zonal modes) that are collectively referred to as ENSO.

Although the dynamics of zonal modes are important in supporting and driving the ENSO system at the equator, several studies show that extratropical stochastic atmospheric forcing can also energize ENSO variance through thermodynamic and dynamic feedbacks [*Vimont et al., 2003; Chiang and Vimont, 2004; Anderson and Perez, 2015*]. Most importantly, for this study, it has been shown that the high-frequency variability of the North Pacific Oscillation (NPO) [*Rogers, 1981; Linkin and Nigam, 2008*] can generate winds and SSTa in the subtropics that amplify and propagate into the tropical Pacific through the wind-evaporation-SST (WES) feedback [*Xie, 1999*]. These sets of dynamical modes operate primarily along the north-south meridional plane and are referred to as meridional modes (MM). The imprint of meridional mode dynamics is evident in the SSTa and sea level pressure anomalies (SLPa) patterns of the ENSO extratropical precursors with a lead of 6–12 months, both for eastern and central Pacific El Niño events (Figure 2.2) [see also *Penland and Sardeshmukh, 1995; Vimont et al., 2003; Anderson, 2003; Zhang et al., 2014*]. These and other findings [*Chiang and Vimont,*

2004; Chang et al., 2007; Alexander et al., 2010] show that extratropical stochastic forcing (e.g., NPO) energize the interannual variance in the tropical Pacific through meridional mode dynamics (although not exclusively [*Anderson et al., 2013*]). Given that the dynamics of the meridional mode are consistent with a red noise process without any preferential timescales [*Larson and Kirtman, 2013*], it is plausible that meridional modes also play an important role in energizing the decadal and multidecadal energy of the tropical Pacific. As initial support for this hypothesis, we note that in the Atlantic basin where ENSO feedbacks are very weak, the dominant mode of tropical variability is controlled by meridional mode dynamics and is characterized by energy on the decadal and longer timescales [*Chiang and Vimont, 2004; Xie and Carton, 2013*].

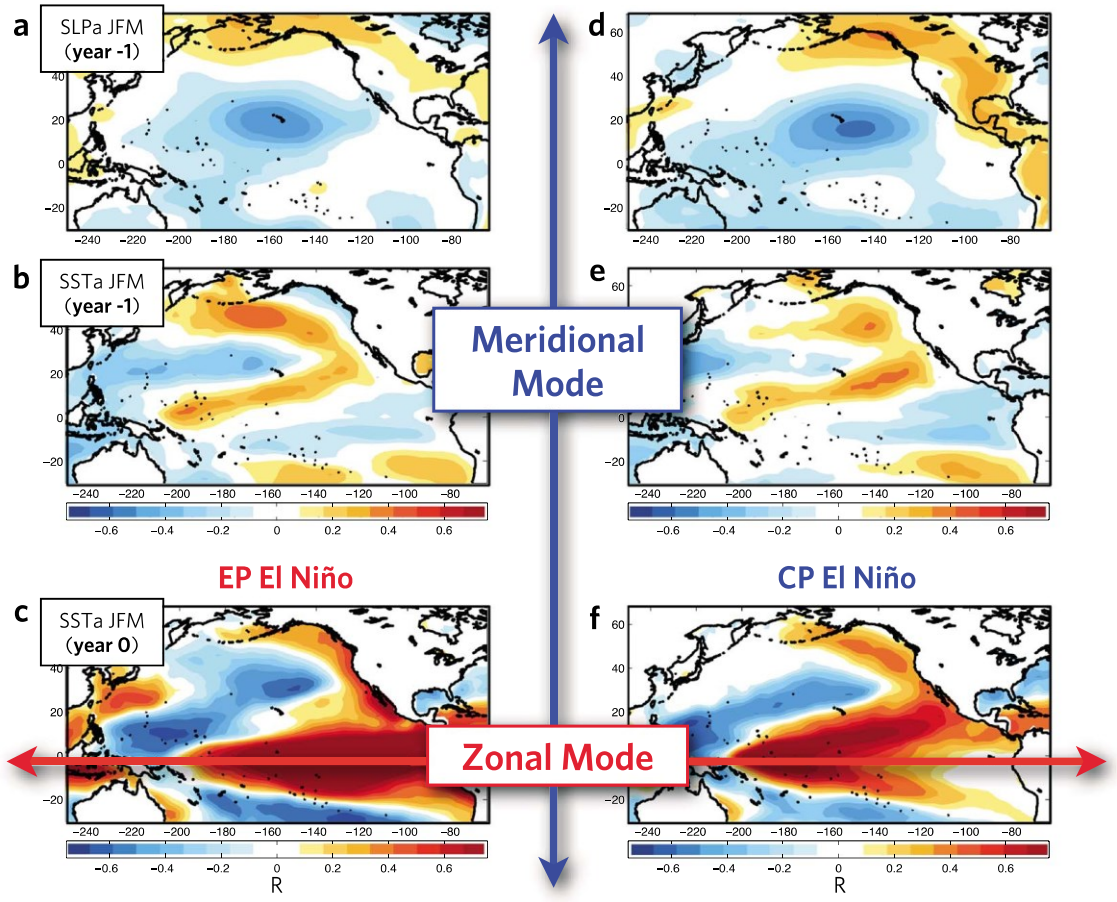

Figure 2.2. Precursor patterns to ENSO. Correlation map between winter (January–March (JFM)) Niño34 index and (a) SLPa in the prior winter, (b) SSTa in the prior winter, and (c) with concurrent SSTa. (e–g) The same analysis done with the CPW index is shown.

Building on these previous findings, we develop a red noise null hypothesis for Pacific decadal and multidecadal variability (Figure 2.3) whereby the NPO stochastic forcing in the extratropics excites meridional modes in the subtropics, which inject decadal-scale variance into the tropical system through the propagation of SSTa along the north-south plane (Figure 2.3, step 1). In the tropics, these SSTa are amplified by zonal mode dynamics (e.g., ENSO) and excite teleconnections that project the decadal-scale variance back into the extratropics (Figure 2.3, step 2). The extratropical projection of the decadal variance impacts both PDO and NPGO depending on the interannual state of ENSO. For example, while eastern Pacific

ENSO teleconnections preferentially energize the PDO pattern [e.g., *Alexander et al., 2002; Newman et al., 2003; Deser et al., 2004*], central Pacific ENSO events project onto the NPGO [e.g., *Di Lorenzo et al., 2010; Furtado et al., 2012*]. This hypothesis, which we will refer to as the Pacific climate null hypothesis, is essentially a red noise process [*Frankignoul and Hasselmann, 1977*], where the forcing is given by the atmospheric stochastic variability that energizes the MM (e.g., NPO) and the damping timescale arises from spatial/temporal evolution of the coupled system response to the MM perturbation. For example, following the diagram in Figure 2.3, the winter time NPO-type variability in a given year energizes ENSO-like variability along the equator that peaks in the following winter (~12 months) [*Anderson, 2003; Vimont et al., 2003*]. In turn, the ENSO teleconnections drive changes in the extratropical atmosphere, which drive ocean anomalies in the extratropics (e.g., SSTa) that decay over a period of 6–12 months [*Schneider and Cornuelle, 2005*]. The timescale resulting from this progression is ~18–24 months, which we interpret as the characteristic damping timescale in the red noise model. If we also account for the existence of feedbacks between ENSO and the MM (e.g., Central Pacific ENSO projecting onto NPO) [*Di Lorenzo et al., 2010; Furtado et al., 2012*], the low-frequency variance is further enhanced because the NPO spectrum is redden (e.g., driving an autoregressive model of order 1 with red noise provides a strong low-frequency filter).

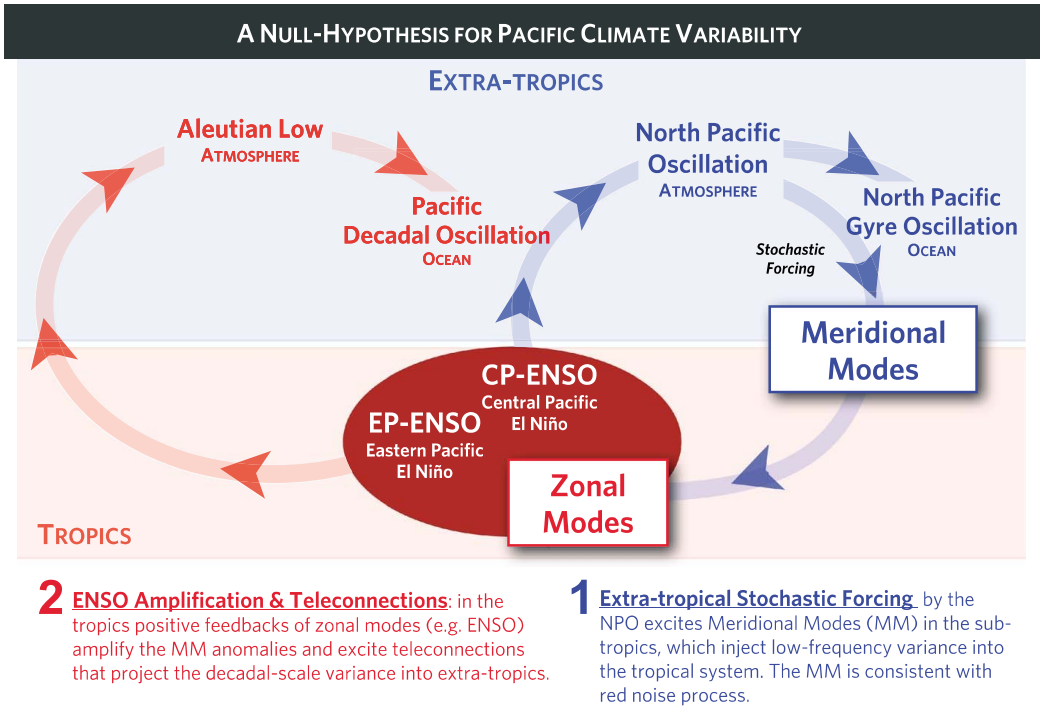

Figure 2.3. Diagram of the null hypothesis for Pacific climate variability. In this red noise model the stochastic variability of the North Pacific Oscillation (NPO) acts as the forcing, while the evolution of the ocean-atmosphere coupled system from extratropics to tropics and back to extratropics (1–2 years) provides the damping timescale. This progression and timescale provide the key memory for integrating the stochastic forcing of the atmosphere (e.g., NPO) into decadal-scale variance over the entire Pacific basin, beyond the generation region of the MM (see text for a detailed discussion).

The Pacific climate null hypothesis is consistent with previous theories and modeling work on stochastic Pacific climate variability [*Newman et al., 2011*] and global-scale Hyper Modes [*Dommenget and Latif, 2008*], which highlight the important interaction between the stochastic development of SSTa in the tropics (e.g., red noise process) and tropical atmospheric teleconnections in generating global multidecadal SSTa.

2.3 Observations and Models

Observations used for testing the Pacific climate null hypothesis (Figure 2.3) originate from two keys sources. SST data and anomalies are derived from the National Oceanic and

Atmospheric Administration (NOAA) Extended Reconstruction SST, version 3 (ERSST.v3) product [*Smith and Reynolds, 2004*]. Monthly mean fields are available on a 2° × 2° horizontal grid globally, with data available from 1854 to the present. For our work, we restrict the period of record to 1950–2012 to match the other data sets. Monthly mean SLP data and anomalies are taken from the National Centers for Environmental Prediction-National Center for Atmospheric Research reanalysis product [*Kalnay et al., 1996*] and exist on a 2.5° × 2.5° horizontal grid globally. For both observational products, we restrict our analysis primarily to the Pacific basin (i.e., 100°E–60°W, 45°S–65°N).

To diagnose the role of meridional modes, two sets of coupled ocean-atmosphere modeling experiments are conducted using the International Center for Theoretical Physics (ICTP) atmosphere general circulation model (AGCM) coupled to a 100m slab ocean. This AGCM, also known as SPEEDY, uses eight vertical layers and T30 horizontal resolution (3.758 3 3.758 on a longitude-latitude grid). Climatological heat fluxes corrected through observations are prescribed to account for ocean heat transport. The physical parameterizations of the model are described in Molteni [*2003*], and prior applications of this configuration can be found in Bracco et al. [*2004*]. The experimental designs are as follows.

2.3.1 The Zonal Mode Experiment

This experiment isolates the fraction of Pacific decadal variance that is deterministically forced within the equatorial Pacific and filters out any stochastic contributions from the MM. SSTa from 1950 to 2012 are prescribed in a narrow region in the equatorial Pacific (12°S–12°N) as a surface boundary condition to drive a 45-member ensemble of the ICTP AGCM with the slab ocean. Away from this tropical region, interactive fluxes between the AGCM and the slab ocean are implemented to determine the SSTa field.

By examining the ensemble mean SSTa from the 45 members, we effectively remove all contributions of stochastic forcing from the extratropics and therefore identify the SSTa variance that is driven by the equatorial Pacific.

2.3.2 The Meridional Mode Experiment

This experiment removes zonal mode dynamics and only retains thermodynamic coupling representative of MM dynamics. For this experiment, we perform a 2000-year integration of the AGCM with the interactive slab ocean over the entire global ocean. The absence of a dynamical ocean in the AGCM slab ocean model effectively removes the positive feedbacks of zonal modes (e.g., ENSO) along the equatorial plane while preserving the MM dynamics that rely on thermodynamic coupling (e.g., the WES feedback). To verify that tropical decadal variability in this experiment is driven by MMs we analyze the relationship between the dominant modes of SSTa variability in the subtropical North Pacific (12°N–30°N) and the tropical Pacific (12°S–12°N). In the subtropics, the leading empirical orthogonal function (EOF) of monthly SSTa exhibits the characteristic pattern of MMs (Figure 2.4a), while the leading EOF of monthly SSTa in the tropics exhibits maximum loading in the central tropical Pacific (i.e., around 180°W) consistent with the observed pattern of SSTa decadal variance (Figure 2.4b). The principal component (PC) time series of the modes exhibit strong low-frequency variability (Figure 2.4c), which is consistent with a red noise spectrum. The cross correlation between the leading subtropical and tropical PCs reaches a maximum correlationof R = 0.7 when the subtropical PC leads the tropical PC by 6 months (Figure 4c). This 6 month lead timescale agrees with the characteristic timescale of growth and propagation of the North Pacific MM into the equatorial Pacific [e.g., *Penland and Sardeshmukh, 1995*; *Vimont et al., 2003*; *Vimont, 2010*; *Alexander et al., 2008*].

This analysis confirms that the largest fraction of tropical low-frequency variability in this experiment is the results of meridional mode dynamics and that the MM can generate significant decadal variance. For this reason, we refer to this run as the MM experiment, although the MM is not the only active dynamics.

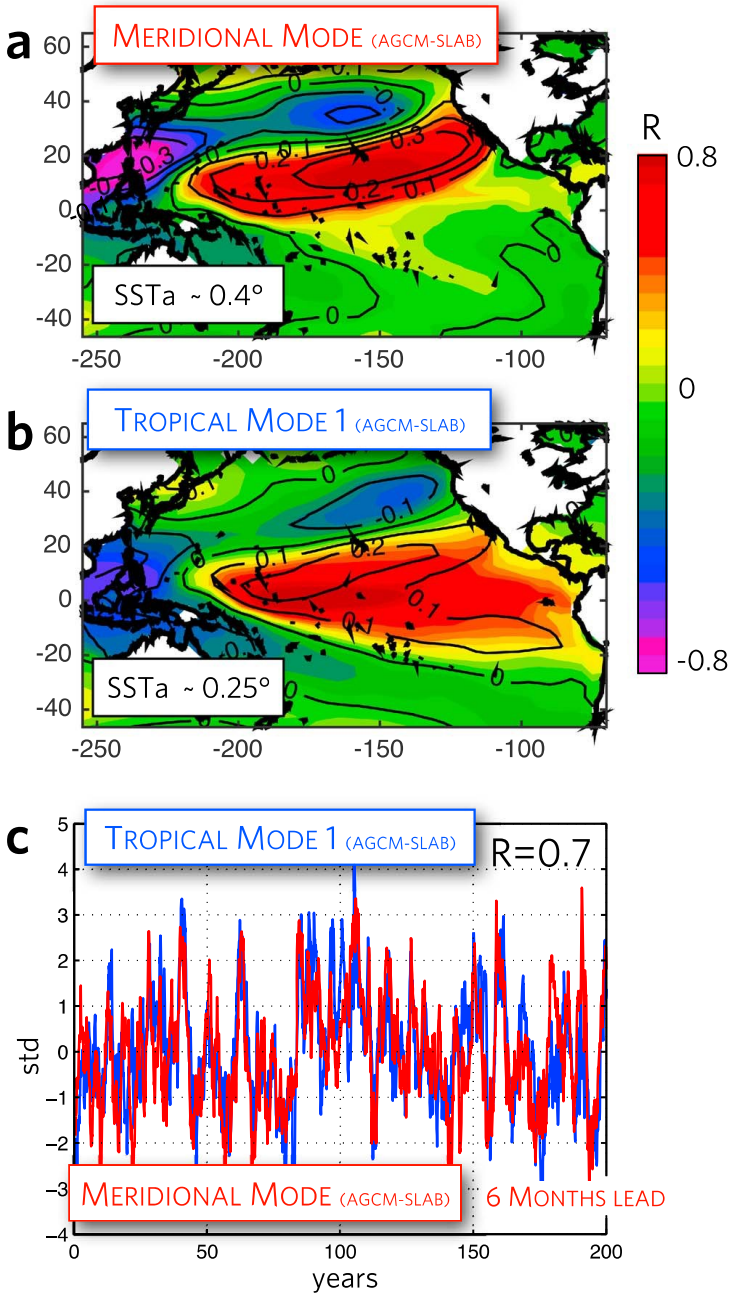

Figure 2.4. Tropical decadal variability of the meridional model experiment. (a) Correlation maps between monthly 2000 year long model SSTa and North Pacific meridional mode monthly index defined as PC1 of subtropical SSTa between (12°N–30°N). (b) Correlation maps between monthly model SSTa and monthly PC1 of tropical SSTa between 12°S and 12°N. Regression coefficients are shown as black contours in units of °C. The size of the maximum SSTa is reported in the bottom left of the panels. (c) Six month lead correlation between model meridional mode index (red line) and tropical PC1 (blue line) (shown only for the first 200 years).

2.4 Testing the Pacific Decadal Null Hypothesis

To test the tropical Pacific climate null hypothesis, we first characterize the observed spatial and temporal evolution of the tropical decadal variance associated with ENSO-like decadal pattern (Figure 2.1). After applying an 8 year low-pass filter to the observed SSTa, we perform a principal component analysis in the tropical Pacific (12°S–12°N) to extract the decadal-scale variability in the tropics. The first EOF explains about 50% of the total low-frequency variance, and its eigenvalue is well separated from subsequent eigenvalues. A correlation of the leading PC time series (PC1) with the monthly SSTa over the entire Pacific basin reveals the characteristic pattern of ENSO-like decadal variability in the Pacific (Figure 2.5b, compare with Figure 2.1). Furthermore, PC1 is correlated with the low-frequency component (8 year low pass) of other indices of Pacific decadal variability including the Interdecadal Pacific Oscillation (IPO) (R = 0.68), the PDO (R = 0.71), and the NPGO (R = 0.68) and shares a similar spatial structure especially in the tropics where all these modes significantly overlap (Figure 2.1). To characterize the growth and decay of this ENSO-like pattern, we compute 1.5 year lead and lag correlation maps of PC1 with Pacific monthly SSTa (Figures 2.5a and 2.5c). The 1.5 year timescale is chosen as it is the approximate e-folding timescale of the PC1 autocorrelation function (~1.67 years). Inspecting the lead and lag correlation maps (Figures 2.5a and 2.5c) reveals that the spatial patterns of the growing and decaying phases are not identical, indicating that the spatial expression of the autocorrelation function is not symmetric in space. The growing phase pattern (i.e., Figure 2.5a) exhibits a stronger loading pattern in the North Pacific resembling the pattern associated with the Pacific MM (compare Figure 2.5a with Figures 2c and 2e). By contrast, the decaying phase (Figure 2.5c) exhibits a more equatorially symmetric SSTa correlation pattern representative of the well-known ENSO teleconnection patterns.

Using the model experiments, our goal is to show that the meridional mode dynamics controls the growing phase of the ENSO-like decadal pattern, while zonal mode dynamics (e.g., ENSO) controls the decaying phase pattern. To do so, we examine the zonal mode and meridional mode AGCM experiments, which selectively exclude/include the contributions of the meridional mode dynamics.

We first examine the evolution of the ensemble mean SSTa from the zonal mode experiments which are forced with prescribed tropical SSTa forcing between 1950 and 2012. By construction, the ensemble mean SSTa removes all the variance contributions associated with extratropical stochastic forcing and meridional modes, and in the tropical forcing region (12°S–12°N) the evolution of the SSTa is identical to the observed. We compute the lead/lag correlation maps between the observed low-frequency PC1 of SSTa and the model monthly SSTa. We find that at lag 0 years (Figure 2.5e) and at lag 1.5 year (the decaying phase, Figure 2.5f) the model reproduces the observed structure of the ENSO-like decadal variability in the extratropics with anomaly correlation patterns (ACPs) ranging between ACP = 0.6 and 0.8, in the decaying and peak phase, respectively. However, at lead 1.5 year (Figure 2.5d) the model is unable to capture the North Pacific growing structure of the decadal pattern ($ACP_{NP} = 0$). This absence suggests that tropical forcing (e.g., ENSO) alone cannot explain the growing phase of the ENSO-like decadal variability. Although the North Pacific signal is missing in the growing phase, in the South Pacific we find a signature of the ENSO-like decadal variability ($ACP_{SP} = 0.62$), implying that a fraction of the precursor pattern in the South Pacific is forced by tropical dynamics (Figure 2.5d).

We now examine the meridional mode experiment using the 2000 year long integration of the AGCM slab coupled model. We have already verified that the dominant fraction of tropical variability in this model is contributed by the North Pacific meridional mode (e.g.,

Figure 2.4). An examination of the growing and decaying phases of the decadal pattern associated with the model tropical low-pass SSTa PC1 reveals that the inclusion of meridional mode dynamics allows us to recover the growing phase of the ENSO-like decadal pattern (Figure 2.5g; $ACP_{NP} = 0.68$). However, the decaying phase (Figure 2.5e) does not resemble the observations (ACPNP = 0) and most of the decay occurs along the equatorial Pacific with little signs of robust symmetric teleconnections from the tropics into the extratropics, which are visible in the observations.

To understand the nature of this local decay in the tropics, we compute the average size of the SSTa in the high loading regions of the growing and decaying phases. In the growing phase we find that both observations and the meridional mode experiment have an amplitude of ~0.3 C (compare Figure 2.5a with Figure 2.5g). However, at lag 0, while the SSTa of observations in the tropics continues to grow reaching ~0.5 C, in the meridional mode experiment the lack of zonal mode feedbacks (e.g., ENSO) prevents this anomaly from growing and instead negative feedbacks (e.g., damping) reduce the SSTa to ~0.1 C (compare Figure 2.5b with Figure 2.5h). In the meridional mode experiment, the lack of ENSO positive feedbacks and the decay of the SSTa prevent the system from exciting ENSO teleconnections, which are important in spreading the signal back to the extratropics as seen in the observations. Therefore, in the meridional mode experiment the tropical SSTa continues to decay locally in the tropics and at lag 1.5 year (Figure 2.5e, the decaying phase) its amplitude is further reduced to ~0.01 C. It is interesting to note that this local decay in the tropics is not evident in the observations, which show zero anomalies. Indeed, previous studies have reported how ocean waves dynamics related to the ENSO cycle are effective in terminating the SSTa along the equator [e.g., *Neelin et al., 1998*].

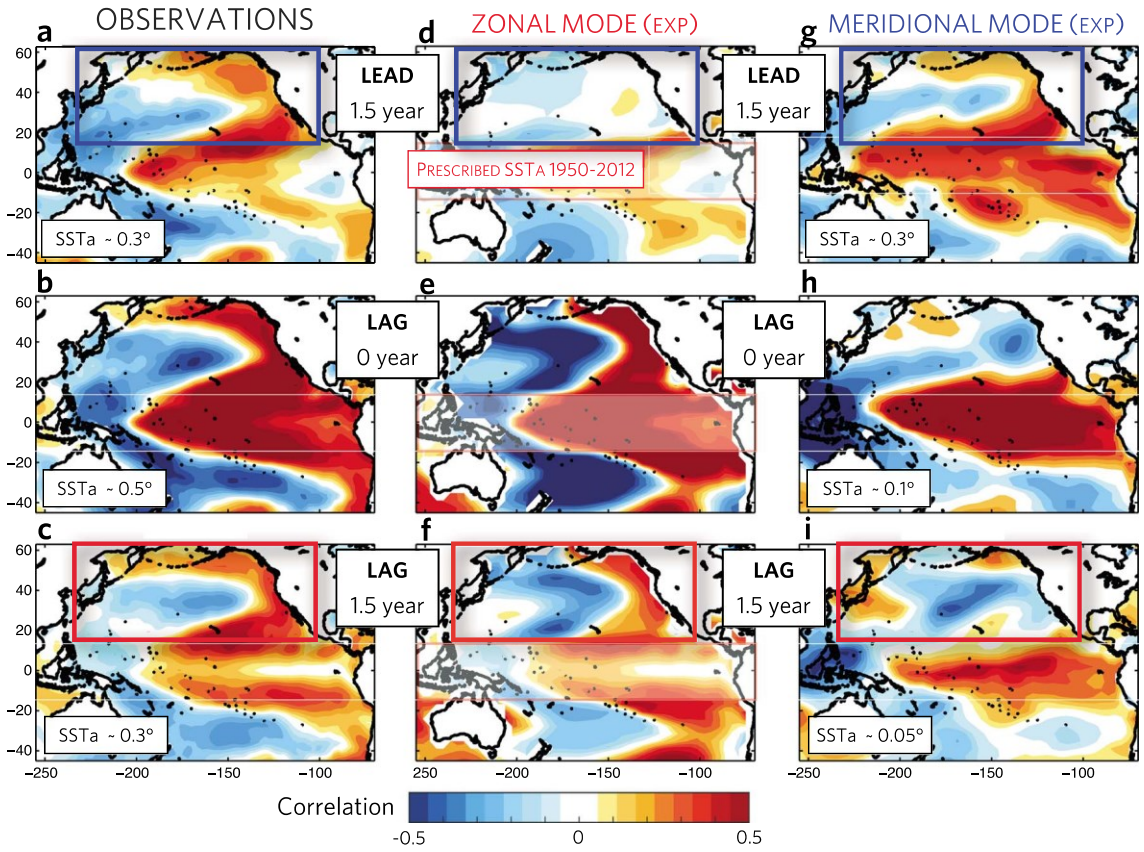

Figure 2.5. Spatial structure and temporal evolution of ENSO-like pattern of decadal variance in observations and models. Correlation between the observed tropical PC1 of 8 year low-pass SSTa defined between 12°S and 12°N and monthly mean SSTa at (a) lead 1.5 year the growing phase, (b) lag 0 the peak, and (c) lag 1.5 year the decaying phase. Same analysis done for the zonal mode experiments (d) growing, (e) peak, and (f) decaying phases. The white shadowing in Figures 2.5d–2.5f denotes the region where prescribed SSTa forcing was used in the zonal mode experiments. Same analysis done for the meridional mode experiment (g) growing, (h) peak, and (i) decaying phases. The average size of the SSTa in the regions of maximum correlation loading is indicated for the observations and meridional mode experiments in bottom left corner of each panel.

Before concluding, we also note that the growing phase of the MM experiment exhibits correlations along the entire equatorial strip, while observations show correlation only in the central tropical Pacific region. This difference is related to the dominant low-frequency character of the MM and tropical variability in the MM experiment (see time series Figure 2.4c). This implies that correlations computed with the low-pass PC1 of SSTa capture this

low-frequency signal. This is not true using the monthly data where we find no correlation in the tropics at lead 6 months (Figure 2.4). In the observations, ENSO interannual dynamics and the cold tongue upwelling region variability act as source for noise in the eastern tropical Pacific reducing the signal-to-noise ratio between the low-frequency expression of the MM in the extratropics at lead 1.5 years and the tropics at lag 0 year. Also, in the peak phase of the MM experiment, the amplitude of the SSTa in the tropics is smaller (~0.1 C) than at lead 1.5 year (~0.3 C), confirming that the dominant tropical mode is the manifestation of the decay of the Pacific meridional mode, which has originated in the subtropics earlier (see Figure 2.4, regression contours).

2.5 Summary and Discussion

Through analyses of the decadal variance of Pacific-wide SSTa in both observations and coupled ocean-atmosphere simulations, we offer significant evidence that the ENSO-like pattern of Pacific decadal variability arises from the interaction of meridional modes (e.g., MM) and the zonal modes (e.g., ENSO). While more sophisticated coupled model experiments are needed to separate the fraction of decadal variability that is driven by ENSO versus MMs, the main conclusion of our work is that the structure and evolution of the ENSO-like Pacific decadal variability (e.g., the growing and decaying phases) cannot be explained by the zonal mode (e.g., ENSO) or the MM in isolation. Although both modes can generate low-frequency variance in isolation, the interaction between both modes is required to explain the observations. In the growing phase, the MM supplies an important source of low-frequency variance through integration of extratropical stochastic atmospheric forcing (e.g., red spectrum), while the zonal mode dynamics (i.e., ENSO) amplify and distribute that low-frequency energy in the peak and decaying phases through global teleconnections. We refer to

this mechanism as the Pacific climate null hypothesis (as summarized in Figure 2.3) because the temporal dynamics energizing this evolution are consistent with a red noise process. However, the spatial progression of this ENSO-like decadal variance relies on specific patterns associated with the tropical coupled ocean/atmosphere response to the atmospheric stochastic forcing (e.g., MM and ENSO), and its teleconnected imprints in the extratropics (e.g., PDO, NPGO, and IPO). This red noise hypothesis is consistent with previous studies exploring Pacific decadal variance in a hierarchy of models, from linear inverse models [*Newman et al., 2011*] to AGCMs coupled to ocean mixed layers [*Dommenget and Latif, 2008; Clement et al., 2011*] and fully coupled climate models [*Yeh and Kirtman, 2004*].

Interestingly, the growth rates associated with the thermodynamic feedback of the MMs depend on the mean SST in subtropical and tropical regions [*Vimont, 2010*]. Hence, anticipated warming of global surface SSTs may amplify the SSTa associated with the growth of the MM. Using our new framework as a guide, this amplification would energize both the interannual and decadal variance of the entire Pacific basin (Figure 2.3). Consistent with this hypothesis, recent studies have suggested that the link between the North Pacific ENSO precursor pattern (e.g., NPO) and ENSO increases under enhanced greenhouse warming [e.g., *Wang et al., 2013, 2014*]. Actual quantification of this amplification and of the effects on ENSO and MM are aims for future studies.

These results provide an alternative set of dynamics that initiate and energize the Pacific decadal variability independently of ENSO and of other subsurface or wave dynamics [e.g., *Pierce et al., 2000; Solomon et al., 2008*]. The mechanism and forcing controlling these dynamics and their interaction with the ENSO system may prove useful as a framework for examining climate change projections for Pacific decadal variability in climate models, which may not reproduce the correct spatial patterns of the observed decadal dynamics, yet may

capture the underlying dynamics of interaction between zonal and meridional modes, along with the atmospheric forcing patterns that energize their variance.

2.6 References

Alexander, M. A., I. Blade, M. Newman, J. R. Lanzante, N. C. Lau, and J. D. Scott (2002), The atmospheric bridge: The influence of ENSO teleconnections on air-sea interaction over the global oceans*, J. Clim.*, 15(16), 2205–2231, doi:10.1175/1520-0442(2002).

Alexander, M. A., L. Matrosova, C. Penland, J. D. Scott, and P. Chang (2008), Forecasting Pacific SSTs: Linear inverse model predictions of the PDO, *J. Clim.*, 21(2), 385–402, doi:10.1175/2007jcli1849.1.

Alexander, M. A., D. J. Vimont, P. Chang, and J. D. Scott (2010), The impact of extratropical atmospheric variability on ENSO: Testing the seasonal footprinting mechanism using coupled model experiments, *J. Clim.*, 23(11), 2885–2901, doi:10.1175/2010jcli3205.1.

Anderson, B., and R. Perez (2015), ENSO and non-ENSO induced charging and discharging of the equatorial Pacific, *Clim. Dyn.*, 1–19, doi:10.1007/s00382-015-2472-x.

Anderson, B. T. (2003), Tropical Pacific sea-surface temperatures and preceding sea level pressure anomalies in the subtropical North Pacific, *J. Geophys. Res.*, 108(D23), 4732, doi:10.1029/2003JD003805.

Anderson, B. T., R. C. Perez, and A. Karspeck (2013), Triggering of El Niño onset through trade wind-induced charging of the equatorial Pacific, *Geophy. Res. Lett.*, 40, 1212–1216, doi:10.1002/grl.50200.

Bjerknes, J. (1969), Atmospheric teleconnections from equatorial Pacific, *Mon. Weather Rev.*, 97(3), 163–172, doi:10.1175/1520-0493(1969) 097<0163:Atftep>2.3.Co;2.

Bracco, A., F. Kucharski, R. Kallummal, and F. Molteni (2004), Internal variability, external forcing and climate trends in multi-decadal AGCM ensembles, *Clim. Dyn.*, 23(6), 659–678, doi:10.1007/S00382-004-0465-2.

Chang, P., L. Zhang, R. Saravanan, D. J. Vimont, J. C. H. Chiang, L. Ji, H. Seidel, and M. K. Tippett (2007), Pacific meridional mode and El Nino–Southern Oscillation, *Geophys. Res. Lett.*, 34, L16608, doi:10.1029/2007GL030302.

Chiang, J. C. H., and D. J. Vimont (2004), Analogous Pacific and Atlantic meridional modes of tropical atmosphere–ocean variability, *J. Clim.*, 17(21), 4143–4158, doi:10.1175/Jcli4953.1.

Clement, A., P. DiNezio, and C. Deser (2011), Rethinking the ocean's role in the Southern Oscillation, *J. Clim.*, 24(15), 4056–4072, doi:10.1175/2011jcli3973.1.

Deser, C., A. S. Phillips, and J. W. Hurrell (2004), Pacific interdecadal climate variability: Linkages between the tropics and the North Pacific during boreal winter since 1900*, J. Clim.*, 17(16), 3109–3124, doi:10.1175/1520-0442(2004)017.

Di Lorenzo, E., et al. (2008), North Pacific Gyre Oscillation links ocean climate and ecosystem change, *Geophys. Res. Lett.*, 35, L08607, doi:10.1029/2007GL032838.

Di Lorenzo, E., K. M. Cobb, J. C. Furtado, N. Schneider, B. T. Anderson, A. Bracco, M. A. Alexander, and D. J. Vimont (2010), Central Pacific El Niño and decadal climate change in the North Pacific Ocean*, Nat. Geosci.,* 3(11), 762–765, doi:10.1038/Ngeo984.

Dommenget, D., and M. Latif (2008), Generation of hyper climate modes, *Geophys. Res. Lett.*, 35, L02706, doi:10.1029/2007GL031087.

Frankignoul, C., and K. Hasselmann (1977), Stochastic climate models. Part II: Application to sea surface temperature anomalies and thermocline variability, *Tellus*, 29, 289–305.

Furtado, J. C., E. Di Lorenzo, B. T. Anderson, and N. Schneider (2012), Linkages between the North Pacific Oscillation and central tropical Pacific SSTs at low frequencies, *Clim. Dyn.*, 39(12), 2833–2846, doi:10.1007/s00382-011-1245-4.

Jin, F. F. (1997), An equatorial ocean recharge paradigm for ENSO. 1. Conceptual model, *J. Atmos. Sci.*, 54(7), 811–829, doi:10.1175/1520-0469 (1997)054.

Kalnay, E., et al. (1996), The NCEP/NCAR 40-Year Reanalysis Project, *Bull. Am. Meteorol. Soc.*, 77(3), 437–471, doi:10.1175/1520-0477(1996) 077.

Larson, S., and B. Kirtman (2013), The Pacific meridional mode as a trigger for ENSO in a high-resolution coupled model, *Geophys. Res. Lett.*, 40, 3189–3194, doi:10.1002/grl.50571.

Linkin, M. E., and S. Nigam (2008), The North Pacific Oscillation–West Pacific teleconnection pattern: Mature-phase structure and winter impacts, *J. Clim.*, 21(9), 1979–1997, doi:10.1175/2007jcli2048.1.

Mantua, N. J., S. R. Hare, Y. Zhang, J. M. Wallace, and R. C. Francis (1997), A Pacific interdecadal climate oscillation with impacts on salmon production, *Bull. Am. Meteorol. Soc.,* 78(6), 1069–1079, doi:10.1175/1520-0477(1997)078.

Molteni, F. (2003), Atmospheric simulations using a GCM with simplified physical parameterization. I: Model climatology and variability in multi-decadal experiments, *Clim. Dyn.,* 20, 175–191.

Neelin, J. D., D. S. Battisti, A. C. Hirst, F. F. Jin, Y. Wakata, T. Yamagata, and S. E. Zebiak (1998), ENSO theory, *J. Geophys. Res.*, 103(C7), 14,261–14,290, doi:10.1029/97JC03424.

Newman, M., G. P. Compo, and M. A. Alexander (2003), ENSO-forced variability of the Pacific Decadal Oscillation, *J. Clim.*, 16(23), 3853–3857, doi:10.1175/1520-0442(2003)016.

Newman, M., M. Alexander, and J. D. Scott (2011), An empirical model of tropical ocean dynamics, *Clim. Dyn.*, 37, 1823–1841, doi:10.1007/s00382-011-1034-0.

Penland, C., and P. D. Sardeshmukh (1995), The optimal-growth of tropical sea-surface temperature anomalies, *J. Clim.*, 8(8), 1999–2024, doi:10.1175/1520-0442(1995)008.

Pierce, D. W., T. P. Barnett, and M. Latif (2000), Connections between the Pacific Ocean tropics and midlatitudes on decadal timescales, *J. Clim.*, 13(6), 1173–1194, doi:10.1175/1520-0442(2000)013.

Power, S., T. Casey, C. Folland, A. Colman, and V. Mehta (1999), Inter-decadal modulation of the impact of ENSO on Australia, *Clim. Dyn.*, 15(5), 319–324, doi:10.1007/S003820050284.

Rogers, J. C. (1981), The North Pacific Oscillation, *Int. J. Climatol.*, 1(1), 39–57, doi:10.1002/joc.3370010106.

Schneider, N., and B. D. Cornuelle (2005), The forcing of the Pacific Decadal Oscillation, *J. Clim.*, 18(21), 4355–4373, doi:10.1175/jcli3527.1.

Smith, T. M., and R. W. Reynolds (2004), Improved extended reconstruction of SST (1854–1997), *J. Clim.,* 17(12), 2466–2477, doi:10.1175/ 1520-0442(2004)017.

Solomon, A., S.-I. Shin, M. Alexander, and J. McCreary (2008), The relative importance of tropical variability forced from the North Pacific through ocean pathways, *Clim. Dyn.*, 31(2–3), 315–331, doi:10.1007/s00382-007-0353-7.

Suarez, M. J., and P. S. Schopf (1988), A delayed action oscillator for ENSO, *J. Atmos. Sci.*, 45(21), 3283–3287, doi:10.1175/1520-0469(1988) 045.

Trenberth, K. E., and J. W. Hurrell (1994), Decadal atmosphere–ocean variations in the Pacific, *Clim. Dyn.*, 9(6), 303–319, doi:10.1007/bf00204745.

Vimont, D. J. (2005), The contribution of the interannual ENSO cycle to the spatial pattern of decadal ENSO-like variability, *J. Clim.*, 18(12), 2080–2092, doi:10.1175/Jcli3365.1.

Vimont, D. J. (2010), Transient growth of thermodynamically coupled variations in the tropics under an equatorially symmetric mean, *J. Clim.*, 23(21), 5771–5789, doi:10.1175/2010jcli3532.1.

Vimont, D. J., J. M. Wallace, and D. S. Battisti (2003), The seasonal footprinting mechanism in the Pacific: Implications for ENSO, *J. Clim.*, 16(16), 2668–2675, doi:10.1175/1520-0442(2003)016.

Wang, S. Y., M. L'Heureux, and J. H. Yoon (2013), Are greenhouse gases changing ENSO precursors in the Western North Pacific?, *J. Clim.*, 26(17), 6309–6322, doi:10.1175/jcli-d-12-00360.1.

Wang, S. Y., L. Hipps, R. R. Gillies, and J. H. Yoon (2014), Probable causes of the abnormal ridge accompanying the 2013–2014 California drought: ENSO precursor and anthropogenic warming footprint, *Geophys. Res. Lett.*, 41, 3220–3226, doi:10.1002/2014GL059748.

Xie, S. P. (1999), A dynamic ocean–atmosphere model of the tropical Atlantic decadal variability, *J. Clim.*, 12(1), 64–70, doi:10.1175/1520-0442-12.1.64.

Xie, S.-P., and J. A. Carton (2013), Tropical Atlantic variability: Patterns, mechanisms, and impacts, in Earth's Climate, edited by C. Wang, S. P. Xie and J. A. Carton, pp. 121–142, *AGU*, Washington, D. C., doi:10.1029/147gm07.

Yeh, S.-W., and B. P. Kirtman (2004), Tropical Pacific decadal variability and ENSO amplitude modulation in a CGCM, *J. Geophys. Res.*, 109, C11009, doi:10.1029/2004JC002442.

Zhang, Y., J. M. Wallace, and D. S. Battisti (1997), ENSO-like interdecadal variability: 1900–93, *J. Clim.*, 10(5), 1004–1020, doi:10.1175/ 1520-0442(1997)010.

Zhang, H., et al. (2014), The South Pacific meridional mode: A mechanism for ENSO-like variability*, J. Clim.*, 27(2), 769–783.

CHAPTER III

MERIDIONAL MODES AND INCREASING PACIFIC DECADAL VARIABILITY UNDER ANTHROPOGENIC FORCING

Published as

Liguori, G. and E. Di Lorenzo, 2018: Meridional Modes and Increasing Pacific Decadal Variability Under Anthropogenic Forcing. *Geophysical Research Letters*, 45, doi: 10.1002/2017GL076548.

Abstract

Pacific decadal variability has strong impacts on the statistics of weather, atmosphere extremes, droughts, hurricanes, marine heatwaves and marine ecosystems. Sea surface temperature (SST) observations show that the variance of the El Niño-like decadal variability has increased by ~30% (1920-2015) with a stronger coupling between the major Pacific climate modes. Although we cannot attribute these trends to global climate change, the examination of 30 members of the Community Earth System Model Large Ensemble (LENS) forced with the RCP8.5 radiative forcing scenario (1920-2100) suggests that significant anthropogenic trends in Pacific decadal variance will emerge by 2020 in response to a more energetic North Pacific Meridional Mode (PMM) -- a well-known El Niño precursor. The PMM is a key mechanism for energizing and coupling tropical and extra-tropical decadal variability. In the LENS, the increase in PMM variance is consistent with an intensification of

the winds-evaporation-SST thermodynamic feedback that results from a warmer mean climate.

3.1 Introduction

Understanding how decadal variability of the Pacific may change in the future is of great interest because of its direct and indirect impacts on ecosystems and weather, including ocean and atmosphere extremes [*Chavez et al., 2003; Di Lorenzo et al., 2016 Gershunov and Barnett, 1998; Mantua et al., 1997; Roemmich and Mcgowan, 1995*]. Previous studies examine changes in the Pacific decadal variability (PDV) of sea surface temperatures (SSTs) in the context of Empirical Orthogonal Function (EOF), such as the Pacific Decadal Oscillation (PDO; *Mantua et al. 1997*). While approaches such as these are useful for characterizing the decadal state of the Pacific basin, they do not provide a mechanistic basis for exploring the sensitivity of PDV to anthropogenic forcing.

Here we use a diagnostic framework of PDV that explains the dominant mode of low-frequency (timescale > 8 years) SST variability over the Pacific basin (i.e., the ENSO-like pattern [*Zhang et al., 1997*]) to explore the past and future changes in PDV across observational products and the Community Earth System Model (CESM) Large Ensemble (LENS). This framework, proposed by Di Lorenzo et al. [*2015*], decomposes the ENSO-like pattern into a growing, peak and decaying phase. The growth phase pattern is associated with ENSO precursor dynamics, such as North Pacific Meridional Modes (PMM) [*Chiang and Vimont, 2004; Alexander et al., 2010; Anderson et al., 2003; Zhang et al., 2013*] (Figure 3.1c) and the Trade Wind-induced Charging (TWC) of the equatorial thermocline [*Anderson et al., 2013*]. The peak phase is associated with the development of ENSO and its teleconnections to the mid-latitude (Figure 3.1d) with a hemispherically symmetric SST footprint, which then decays in both

tropics and extra-tropics (Figure 3.1e). This progression of events has an inherent timescale between 18-24 months and has been proposed as an important mechanism to explain the ENSO-like pattern of low-frequency variance (timescale > 8 years) [*Di Lorenzo et al., 2015*]. The advantage of this PDV diagnostic framework lies in the possibility of assessing the extent to which the PDV variance in LENS is consistent with the mechanisms inferred from observations, namely the interaction between PMM and ENSO.

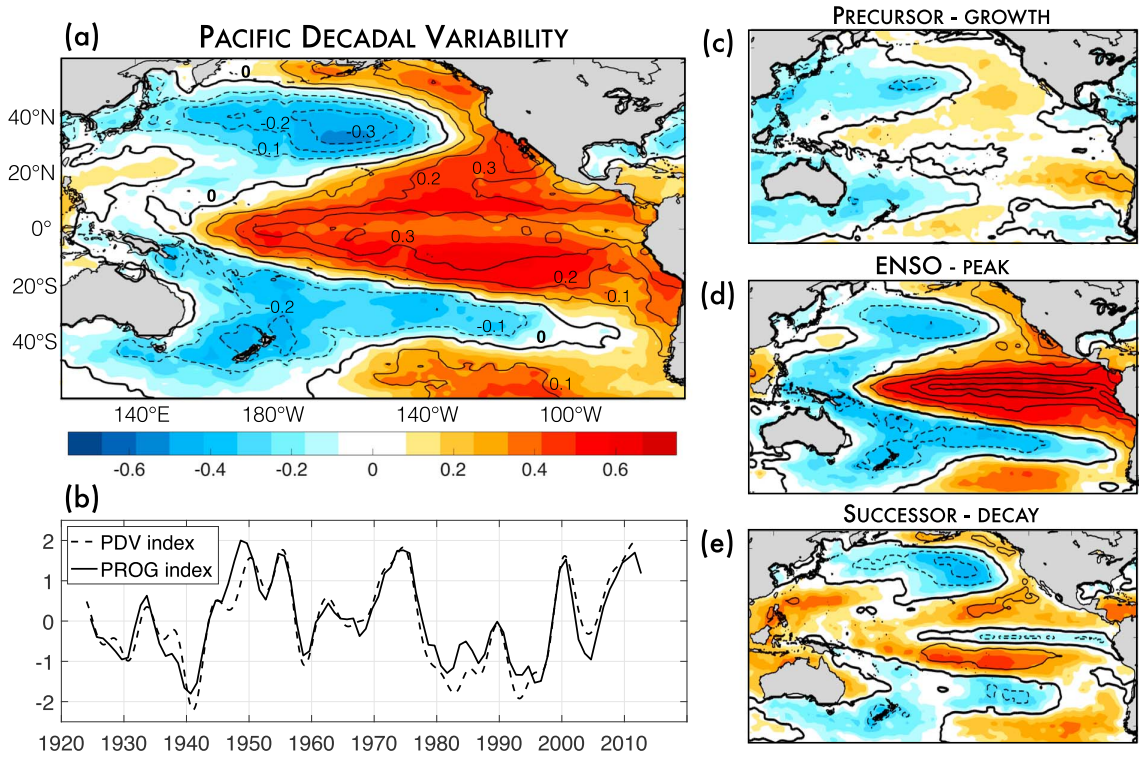

Figure 3.1. Pacific Decadal Variability. (a) Correlation and regression maps of the PDV index (i.e., leading PC of 8-yr low-passed SST over the Pacific domain) onto 8-yr low-passed Pacific SST. Color shading represents the correlation coefficient while the contours represent the regression coefficient. Contour interval 0.1 °C per standard deviation of the PDV index. Negative contours are dashed; the zero contour is thickened. (b) The PDV index shown together with the 8-yr low-passed PROG index (see text for the definition of the PROG index). (c-e) As in (a) but at different lags and using unfiltered SSTs and ENSO index (defined as the PC1 of SST anomalies between 20S-20N). When SSTs precede ENSO of 1 year, the

Precursor (c), when there is no lag between ENSO and SSTs, the Peak (d), and when ENSO leads the SSTs of 1 year, the Successor (e).

The main objective of this paper is to use the dynamical framework proposed by Di Lorenzo et al. [*2015*] to examine the sensitivity of the PDV to anthropogenic forcing. Using observations, we develop a new index that is designed to capture the ENSO-like decadal variability and the progression patterns associated with the growing (PMM), peak (ENSO), and decaying phases of Pacific SST variability. We then use this index to explore projected changes in the PDV variance under the RCP8.5 radiative forcing scenario and assess the role of the PMM.

3.2 Observations and Modeling

We use two sources of SST datasets, the National Oceanic and Atmospheric Administration (NOAA) Extended Reconstruction SST, version 3 (ERSST v3) product [*Smith and Reynolds, 2004*] and the Met Office Hadley Centre SST, version 1.1 (HadISST v1.1) dataset [*Rayner et al., 2003*]. ERSST v3 (HadISST v1.1) consists of monthly-mean values from 1854 (1870) to the present on a 2° × 2° (1° × 1°) horizontal grid globally. Except for SST-only analyses, which use data from 1920-2015 (i.e., Figure 3.1 and 3.2b), we restrict the period of record to 1950-2015 to match the other data sets. Monthly-mean values of sea level pressure (SLP), 10-m wind components (U and V), and latent heat flux (LHF) are taken from the National Centers for Environmental Prediction-National Center for Atmospheric Research reanalysis product [*Kalnay et al., 1996*] and exist on a 2.5° × 2.5° horizontal grid globally.

To investigate the PDV response under increasing greenhouse forcing, we analyze the output of the first 30 members of the CESM Large Ensemble simulations (hereafter LENS) from 1920–2100 under the RCP8.5 emission scenario available at

http://www.cesm.ucar.edu/projects/community-projects/LENS/ [*Kay et al., 2015*]. The 30-member ensemble uses historical radiative forcing for the period 1920–2005 and RCP8.5 radiative forcing thereafter. The simulation uses version 1 of CESM, with the Community Atmosphere Model, version 5 [CESM1(CAM5); *Hurrell et al. 2013*] at approximately 1° × 1° horizontal resolution in all model components. Unless otherwise stated, monthly-mean anomalies are computed by removing the climatological seasonal cycle (computed as long-term monthly mean of the record analyzed) from detrended fields. For the observational datasets, detrended fields are obtained by removing the linear fit at each grid point. For the LENS, they are obtained by removing at each grid point the signal associated with anthropogenic forcing, which is assumed to be the ensemble mean. Although each LENS realization starts with almost identical initial conditions in the ocean subsurface, it is reasonable to assume that each realization develops an independent natural (unforced) multi-decadal variability in the Pacific Ocean. In the Pacific, the surface decadal variability is not strongly coupled to the subsurface ocean state [*Liu and Di Lorenzo, 2018*]. This contrasts with the Atlantic where the surface decadal variability is linked to the Atlantic Meridional Overturning Circulation [e.g., *Delworth and Mann, 2000*, and references therein]. Thus, averaging all the ensemble members should be effective in extracting the anthropogenic forced signal in the Pacific Ocean.

Following Chang et al., [*2007*], the PMM pattern is obtained as leading Maximum Covariance Analysis (MCA) of boreal spring (defined as March-April-May or MAM) SST and surface wind stress anomaly with the ENSO signal removed by linear regression prior to the analysis. Timeseries of the PMM are then obtained by projecting the monthly-mean anomalies onto the leading MCA spatial pattern. As result of the projection we obtain two monthly-mean indices, an SST-based index, PMM_{sst}, and a 10-m-winds-based index, $PMM_{\boldsymbol{\tau}}$. The ENSO

index is computed as the leading Principal Component (PC1) of monthly-mean Tropical Pacific ([120E-80W 20S-20N]) SSTs. All the seasons in this manuscript are boreal seasons.

3.3 Increasing Pacific Decadal Variance: Observations versus LENS

To quantify the changes in decadal variance of the Pacific, we develop an index that captures the ENSO-like decadal variability that emerges from the PMM/ENSO interaction hypothesis. This index, which we will refer to as the progression (PROG) index, is designed to capture the progression associated with the growing, peak and decaying phases of the PDV [*Di Lorenzo et al., 2015*], namely the interaction between PMM in extra-tropics (growth), ENSO amplification in the tropics and teleconnections to extra-tropics (peak phase), and the extra-tropical decay. The progression is typically phase-locked with the seasonal cycles. For the North Pacific, a strong winter expression of the North Pacific Oscillation (NPO) [*Rogers, 1981*] will imprint an SST anomaly, which in the mid-latitude [30N-60N] is characterized by the North Pacific Gyre Oscillation (NPGO) pattern [*Di Lorenzo et al., 2008; Chhak et al., 2009*]. In the sub-tropics [10N-30N], the reduction of trade-winds associated with the NPO activates the PMMs [*Chang et al., 2007*], which typically grow during the spring and lead to an SST anomaly in the tropics [10S 10N] towards the end of spring and beginning of summer. In the tropics, these anomalies favor the development of ENSO, which grows during the summer and fall, and peaks in the winter. The ENSO teleconnections that follow imprint the ENSO signature into the mid-latitude during the fall and the following winter [30N-60N].

To capture this time/space progression of the anomalies, we obtain the PROG index by computing the first Empirical Orthogonal Function (EOF) of combined raw (unfiltered) data that consist of winter (defined as December-January-February or DJF) SST anomalies (SSTa) in the mid-latitude [30N-60N] a year prior ENSO (lag=-1yr), spring (defined as March-

April-May or MAM) SSTa in the sub-tropics [10N-30N] at lag=-1yr, fall (defined as September-October-November or SON) SSTa in the tropics [10S 10N] at lag=-1yr, and finally winter SSTa in the mid-latitude at lag zero. To recover the PMM footprint in winter and spring SSTa at lag=-1yr we linearly remove a commonly used ENSO index [Cold Tongue index, SSTa averaged over 6S-6N and 180W-90W] prior to the EOF analysis. This allows for the extraction of the PMM pattern in the winter/spring preceding ENSO as discussed in Chang et al. [*2007*]. In the observation, this modal decomposition results in a first principal component of annual values (i.e., PROG index) that explains ~67% of the variance and tracks closely both PDV temporal variations (Figure 3.1b) and seasonally-based spatial evolution (Figure 3.2a).

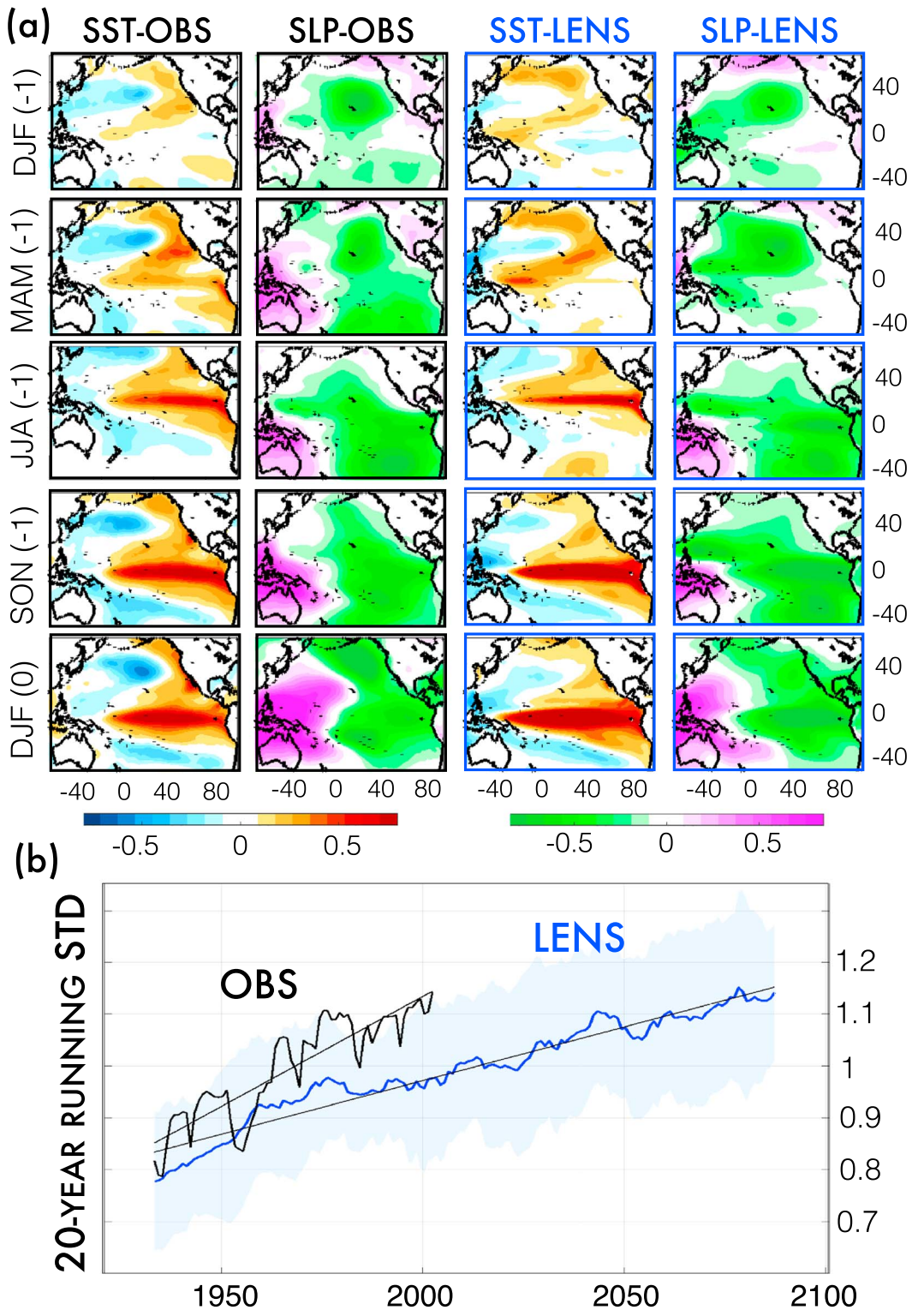

Figure 3.2. PMM progression. (a) Seasonal means of SSTa and standardized SLPa regressed onto PROG index in LENS (ensemble mean) and observations. Units for SST maps

are in [°C] per units of STD change of PROG index. SLP maps are in units of correlation. (b) Progression strength computed applying a 20-yr running STD to the PROG index. Observation (black) and LENS ensemble mean (blue) with its 1-STD spread envelope (shading).

Given that the PROG index is defined using an EOF analysis that maximizes variance but does not enforce the causality in the transition patterns from ENSO precursors to ENSO successors, we conducted additional tests. Specifically, we verified that the EOF patterns of the progression are consistent with the patterns obtained by lead/lag regression maps of the Niño3.4 index with SST and wind anomaly between -12 and +12 months (see the section supporting information at the end of Chapter III). We also developed a Monte Carlo approach to show that the observed order of the SSTa sequences (e.g., causality) is required in order to capture the largest fraction of the variance throughout the DJF to DJF+1 period.

We test the skill of the PROG index annual values in capturing PDV temporal variations by comparing the 8-year low-passed PROG index with the PDV index computed as Zhang et al., [*1997*], which is defined as the PC1 of 8-year low-passed monthly SST (Figure 3.1b). The high and significant correlation between the PROG and PDV indices (R=0.84) allow us to use the PROG index as a diagnostic tool to (i) test the PMM/ENSO interaction decadal framework in climate models, and (ii) quantify if the PDV variance is changing under anthropogenic climate change. The significance of the correlation coefficients throughout the study is estimated by computing empirical probability density functions (EPDFs) for the correlation coefficient of two red-noise time series which have the same lag-1 autoregressive coefficient of those estimated in the original signals. We assess the 99% significance levels using an EPDF obtained from 10,000 realizations of random red-noise time series. A similar approach is used to assess the significance of the trend.

An examination of the observed evolution of PDV variance inferred from the 20-yr running STD of the PROG index shows a marked trend in both observational products (Figure 3.2b; shows only the ERSST data, results for HadISST dataset are not shown), raising the question of whether this trend is part of a centennial-scale (or longer) natural fluctuation or if it is linked to the anthropogenic forcing. To explore the significance of these trends and their driving mechanisms, we look at the LENS projections, which span from 1920-2100 and are forced by the RCP8.5 radiative forcing scenario after 2005.

Following the same approach used for the observational dataset (Figure 3.1b), for each LENS member we compare the 8-yr low-passed PROG index with the PDV index computed as in Zhang et al., [*1997*]. The resultant mean correlation of R=0.82 shows that the PROG index captures the ENSO-like decadal variability. We then inspect the ensemble mean pattern (i.e., average of each individual pattern) associated with the phases of the progression in the models and compare it with observations. The different phases are revealed by regressing SST and sea level pressure (SLP) anomalies onto the PROG index (Figure 3.2a). In the winter prior to ENSO, DJF (lag=-1yr), we find patterns characterized by large regression coefficients in the North Pacific region resembling the NPGO-like and the NPO-like pattern, respectively for SST and SLP regressions. These patterns evolve in spring, MAM (lag=-1yr), in a stronger NPO-like pattern associated with a clear PMM signature in the SST. These ENSO precursors, NPO and PMM, promote the onset of El Niño and thus by fall, SON (lag=-1yr), both SST and SLP regressions are dominated by a mature phase of ENSO, which is characterized by a warm SST anomaly and a strong East-West pressure gradient anomaly in the tropical Pacific. In the following winter, DJF (0), these mature ENSO conditions begin to decay after exciting extratropical teleconnections, which energize PDO-like and Aleutian Low-like patterns in the North Pacific.

This mode progression from the NPGO/NPO-like patterns during the winter prior to ENSO to a PDO/Aleutian Low-like pattern during peak ENSO, shows that the PROG index captures the seasonal and spatial evolution of the Pacific variability in both observations and model simulations. The main discrepancies of LENS with respect to the observations are: (i) the stronger SST signature in the warm pool region (western equatorial pacific) during DJF (lag=-1yr) and MAM (lag=-1yr), and (ii) the very weak Aleutian Low signature in the SLP of the North Pacific region during ENSO peak phase in DJF (0). Both these discrepancies are likely due to LENS deficiencies in accurately representing ENSO and its extratropical teleconnection. For instance, the LENS tendency in overestimating the SST variability in the western equatorial Pacific is a known bias present in most global coupled models that has been linked to misrepresentation of the Bijerkness feedback [*Li and Xie, 2013*]. Nevertheless, LENS have been extensively validated in a number of recent studies [e.g., *Kay et al., 2015; Fasullo et al., 2016; Li et al., 2017*] and represents a valuable dataset to address the question of whether or not the PDV is likely to increase under greenhouse forcing. In both observational datasets, the variance of the LENS PDV inferred from the 20-yr running STD of the PROG index shows a marked trend that is consistent with the LENS response to anthropogenic forcing (Figure 3.2b). We can now diagnose the individual mechanisms of the PDV framework that are responsible for the PDV increase in LENS.

3.4 Diagnosing the Role of Meridional Mode Dynamics

To diagnose the origin of the trend in the PDV variance within the LENS, we examine the individual dynamics that are important in the progression, that is the PMM and ENSO. For each member we compute the PMM using the definition of Chang et al., [*2007*] (see section *Observations and Modeling*), which results in two monthly-mean indices: an SST-based

index, PMM_{sst}, and a 10-m-winds-based index, $PMM_{\boldsymbol{\tau}}$. The ENSO index is instead computed as the leading PC1 of monthly-mean Tropical Pacific ([120E-80W 20S-20N]) SSTs.

The cross-correlation between the monthly-mean PMM indices and the ENSO index confirms a known relationship in which the spring PMM index leads the winter ENSO index (R=.38 when the PMM index leads ENSO by 9 months; Figure 3.S3 in the supporting information). To explore if this coupling between the PMM and ENSO is changing under anthropogenic forcing, we compute the correlation between the PMM_{sst} index during spring and the ENSO index during the following winter (winter defined here as DJF mean; Figure 3.4b). We compare the coupling between two periods, one with weak and one with strong anthropogenic forcing (i.e., 1920-1960 vs 2060-2100). We find a moderate but robust increase, 21 out of 30 members, in the ensemble mean of ~19% (R=0.48 vs R=0.57) during the later period. Thus, if LENS projections are correct and we assume that each member of the ensemble is as likely to occur as the real climate, the increase in the PMM-ENSO coupling has a 70% chance of occurrence. Moreover, the 20-yr running variance of spring PMM_{sst} and $PMM_{\boldsymbol{\tau}}$ reveals a significant trend in both observations and LENS (Figure 3c), with the SST response (spring PMM_{sst}) being larger than the wind-stress response (spring $PMM_{\boldsymbol{\tau}}$). This amplification in the spring PMM_{sst} variance relative to spring $PMM_{\boldsymbol{\tau}}$ variance is consistent with the red-noise paradigm for the ocean-atmosphere interaction in which the ocean memory leads to an amplification of the atmospheric variance [*Frankignoul and Hasselmann, 1977*]. Since the spring PMM_{sst} index captures the oceanic expression of the ocean-atmosphere coupled PMM, it is expected for this index to have more low-frequency power than the spring $PMM_{\boldsymbol{\tau}}$, which captures the atmospheric expression of the coupled mode. In both LENS and observation, the trend in the variance of the spring PMM indices is accompanied by a marked trend in the 20-yr running variance of winter ENSO (Figure 3.3c). These trends in the variance of spring

PMM and winter ENSO are statistically significant in the ensemble mean of LENS but not in the observation, for which the record is too short to pass the significance test. In the model, the trends in the variance are accompanied by an increase in the spatial variance associated with each mode. This can be visualized by subtracting the pattern computed during 1960-2000 (i.e., weak anthropogenic forcing) from the one computed during 2060-2100 (i.e., strong anthropogenic forcing) (Figure 3.3a and 3.3b). The patterns are obtained by regressing the spring PMM_{sst} and winter ENSO indices onto SST and wind components.

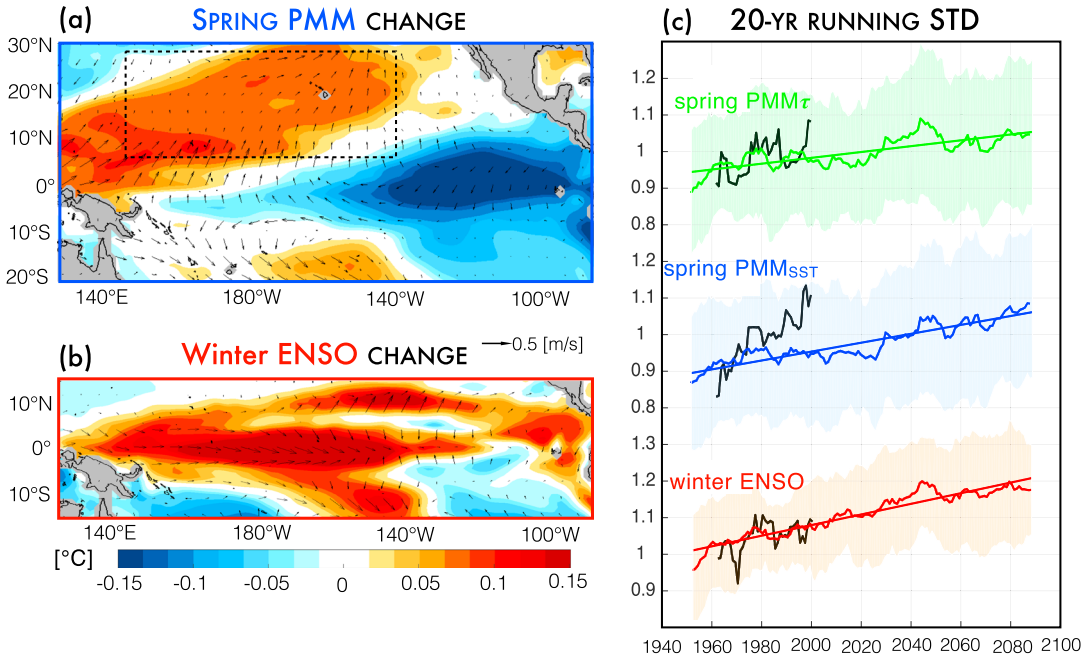

Figure 3.3. Projected change in the variance of PMM and ENSO. (a,b) Changes in PMM and ENSO obtained by subtracting the pattern computed during 1960-2000 (i.e., weak greenhouse forcing) to the one computed during 2060-2100 (i.e., strong greenhouse forcing). Patterns and wind vector are obtained by regressing spring PMM_{sst} and winter ENSO indices (see text for indices definitions) onto SST and wind components. Units are in [°C] per units of STD changes of the corresponding mode index. (c) Normalized 20-yr running standard deviation of spring PMM_{sst}, spring PMM_{τ}, and winter ENSO indices in LENS (green, blue, and red) and observations (NCEP reanalysis and ERSST v3; black).

Although ENSO variance has several contributions (e.g., westerly wind bursts, Harrison and Vecchi, 1997; Madden-Julian oscillation, Zhang and Gottschalck, 2002), the consistent slope between PMM and ENSO variance (Figure 3.3c) supports the hypothesis that the increase in the PMM variance resulting from anthropogenic forcing is an important contributor to the increase in ENSO variance. There are several mechanisms that can amplify the PMM and increase its variance: (i) Increase in the feedback (i.e., WES) between ocean and atmosphere that leads to larger growth of the mode, and (ii), increase in the variance of the extra-tropical atmospheric stochastic noise (i.e., NPO activity) that activates and energizes the PMM. In LENS, the increase in the PMM variance is consistent with an intensification of the WES feedback associated with changes in the background state. The nature of the WES feedback prevents its direct and precise quantification, but nevertheless Vimont [*2010*] proposed to use the change in latent heat flux per unit change in zonal wind speed as estimation of the WES feedback activity. Specifically, upon linearization of the standard bulk formula for the latent heat flux, he derived the so-called WES parameter (WESp),

$$WESp = \frac{\partial LH}{\partial |w|} = LH \cdot \frac{u}{|w|^2},$$

where, *LH* is the latent heat flux, *u* the zonal wind speed, and |w| the total wind speed (w $=\sqrt{u^2 + v^2 + w^2}$). We use the WESp to characterize this air-sea interaction since a large latent heat flux sensitivity to meridional wind variation is a necessary condition for an intense WES feedback in the subtropical Pacific. In both observation and LENS, we computed the spatially-averaged WESp in the region where the PMM is more active (i.e., dashed box shown in Figure 3.3a.). The timeseries of the WESp from LENS (Figure 3.4a) exhibits quadratic growth over the period 1960-2100, with a clear and significant trend emerging after 2020, and no significant trend prior 2000. Consistent with the WESp, a closer look at the trend lines in the spring PMM variance (Figure 3.3c) also show that most of the increase

occurs after 2020. This association is confirmed by comparing a quadratic fit of the WESp and spring PMM_{sst} variance (Figure 3.4a).

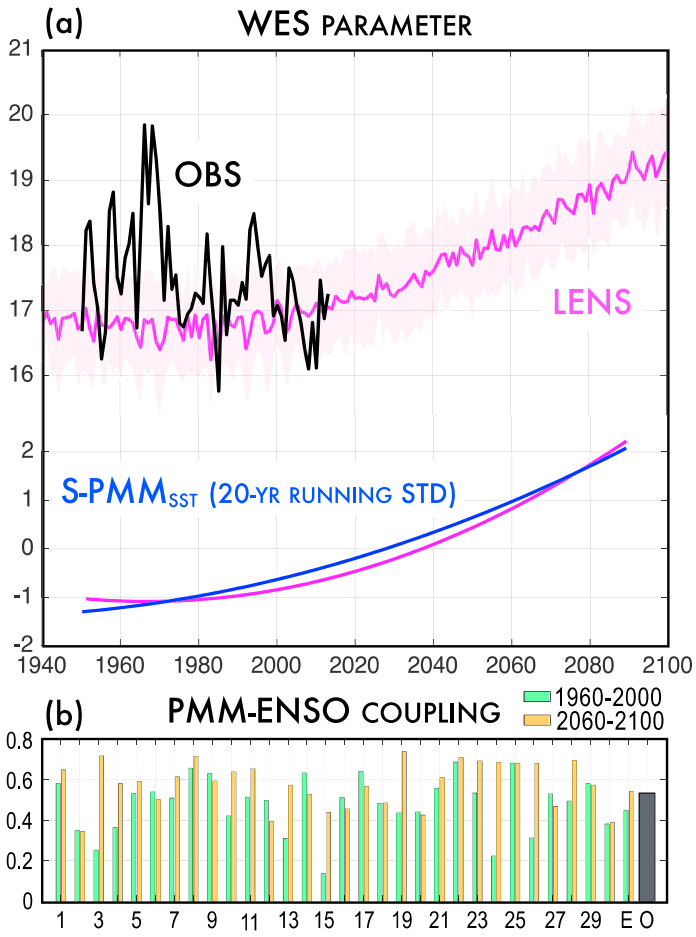

Figure 3.4. (a) Curves in the upper part indicate the WES parameter [*Vimont, 2010*] area-averaged over the dashed box shown in Figure 3.3a in the observation (black) and LENS ensemble mean (magenta). Units are in [W s m^{-3}] and the shading (light magenta) indicates the 1-STD spread envelope. Curves in the lower part compare quadratic fits of the normalized ensemble mean of the WES parameter (magenta) and the 20-yr running STD of the spring PMM_{sst} index (blue) (b) ENSO-PMM coupling estimated as correlation between spring PMM_{sst} and winter ENSO indices (see text for indices definitions). Correlation computed during 1920-1960 (green bars) and 2060-2100 (orange bars) for each LENS member (#), the ensemble mean (E), and the observations (O; 1960-2000).

3.5 Summary and Discussion

Using SST observations over the period 1920-2015 we find that the variance of the El Niño-like decadal variability in the Pacific basin has increased by ~30%, with a significant contribution from the North PMM. Combining available observations with a large ensemble of anthropogenic-forced model simulations (i.e., LENS), we offer evidence that the observed intensification in the PDV activity is consistent with anthropogenic-forced changes in the interaction between tropical and extratropical Pacific modes, namely ENSO and PMM. These mode interactions represent the core of a dynamical framework proposed by Di Lorenzo et al. [*2015*] to explain the nature of the PDV as a progression of Pacific modes (Figure 3.1). The statistical characterization of the mode progression in both observations and model outputs reveals a substantial intensification of the dynamics that energize the PDV (Figure 3.2). Specifically, ENSO and the PMM show a significant trend in variance (Figure 3.3c) that is accompanied in LENS by an increase in the coupling between the two modes (Figure 3.4b).

A diagnostic of the LENS suggests that these changes are significantly linked to anthropogenic forcing, which amplifies the variance of the PMM in subtropical and tropical regions. This amplification is consistent with an intensification of the winds-evaporation-SST thermodynamic feedback (i.e., WES) in the region of the North PMM. The WES, which controls the growth rate of the PMM SSTa [e.g., *Vimont, 2010*], exhibits an exponential increase in amplitude because of the nonlinear relationship between SSTa and evaporation in a warming mean climate [*Lindzen and Nigam, 1987; Gill, 1980*]. The increase in PMM amplitude also leads to a small but significant increase in coupling between PMM and ENSO in the CESM-LENS, a result that is consistent with previous studies suggesting that the link between the North Pacific ENSO precursor patterns (e.g., PMM) and ENSO increases under enhanced greenhouse warming [e.g., *Wang et al., 2013, 2014*]. Although these results suggest an important

role of the PMM dynamics, there are mechanisms other than PMM that can energize the decadal variance of Pacific SSTs. For instance, Wang et al. [*2013*] linked the increase in the PDV to greenhouse-forced changes in the relationship between ENSO and western North Pacific SST anomalies. Furthermore, by means of modelling experiments, Zhou et al. [*2014*] found that regardless of changes in the amplitude and spatial pattern of ENSO, the projected warming in the ENSO region will result in an overall increase in variance of ENSO teleconnections and hence of the oceanic response in the extra-tropics.

The analysis presented here provides support to the hypothesis that anthropogenic forcing may lead to an amplification of PDV through a strengthening of the PMM via the WES. However, the lack of a detectable trend in the WES parameter in the observational record does not allow for a clear attribution of the recent trends in PDV to anthropogenic forcing. According to the LENS, the trend in the WES begins to emerge in the period 2000-2020. Moreover, the computation of the WES parameter involves higher order statistics of quantities such as latent heat and wind speed that are not well constrained in observation. While this is especially true for estimates before the satellite era, even remote sensing-based estimates present a substantial uncertainty, which in the case of the latent heat flux, may be on the order of 20% or larger [*Jiang et al., 2004*, and reference therein]. The ensemble mean statistics from the LENS are very clear in projecting an increase in WES as a response to a warmer mean state. We anticipate that an amplification of this feedback in the next one or two decades will be accompanied by an intensification in both PMM and ENSO activity. In this respect, it is plausible that the record-breaking PMM index recorded in spring 2015 (https://www.esrl.noaa.gov/psd/data/timeseries/monthly/PMM/), followed by one of the strongest El Niño events ever recorded (winter 2016/2017) [e.g., *Hu and Fedorov, 2017*] represents a manifestation of this ongoing intensification.

3.6 Supporting Information

ENSO Precursor and Successor Patterns

The computation of the PROG index as the principal component of the seasonal anomalies of SST (e.g. DJF, MAM, SON, DJF+1) does not enforce causality in the transition from the ENSO precursors to the ENSO successor patterns (e.g. EOF maximizes variance). To test the degree to which the EOF analysis (e.g. PROG index) recovers the known ENSO precursors and successors we compare the EOF results against the patterns obtained from a lead/lag regression analysis of the Niño3.4 index against the monthly SSTa and wind anomalies from leads -12months to lags +12months (Figure S3.1). Given that ENSO peaks typically in winter, a lag=-12 month corresponds to the SSTa in the winter prior to the peak of ENSO (Figure S3.1). Likewise, the lag=+12 month reveals the anomalies in the winter after the peak of ENSO. During the winter prior to ENSO (lag=-12 months) the regression exhibits a weak NPGO-like and PMM signature in the subtropics (i.e., SSTa in association with southwesterly wind anomaly) that intensifies during spring and summer (~lag=-10 and -8). At lags -6 to 0 we see the development of the ENSO anomalies. Following the peak of ENSO (lag=-2,0 and 2), there is a clear shift in the North Pacific from a NPGO-like pattern to a PDO-like pattern (lag=+2) associated with the ENSO teleconnections. The ENSO and PDO-type pattern then decay over lags +4 to +12. The progression of patterns in the lead/lag ENSO regression analysis is captured by the combined EOF analysis used to compute the PROG index (Figure 3.2). This provides confidence that the PROG index is a good indicator of the seasonal evolution of the ENSO precursor/successor patterns.

To further test how important this pattern progression is in the observed SSTa seasonal variance, we developed a Monte Carlo test aimed at quantifying how much variance is captured by the PROG index in the absence of causality in the progression. Specifically, we

randomly re-order the sequences of each of the seasonal SSTa field (e.g. DJF, MAM, SON, DJF+1) that make up the vector used in the EOF calculation. This approach essentially removes any causality that may exist in the data. We then compute the EOF and quantify how much of the total variance is captures by the 1st principal component (e.g. the PROG index). We find (Figure S3.2) that none of the random permutation is able to capture more than 50% of the variance. The variance of the observed sequence captures 65%, which is outside any of the random permutations. We repeated this test by randomly permuting only the ENSO precursor field (DJF, MAM) and leaving SON and DJF+1 in the observed order. Although the explained variance increases the observed explained variance still lays outside any of the realizations. This gives us more confidence that the ENSO precursors patterns identified in DJF and MAM through the EOF of the observed sequence are dynamically linked to ENSO (SON) and its teleconnection to the PDO-like variability (DJF+1).

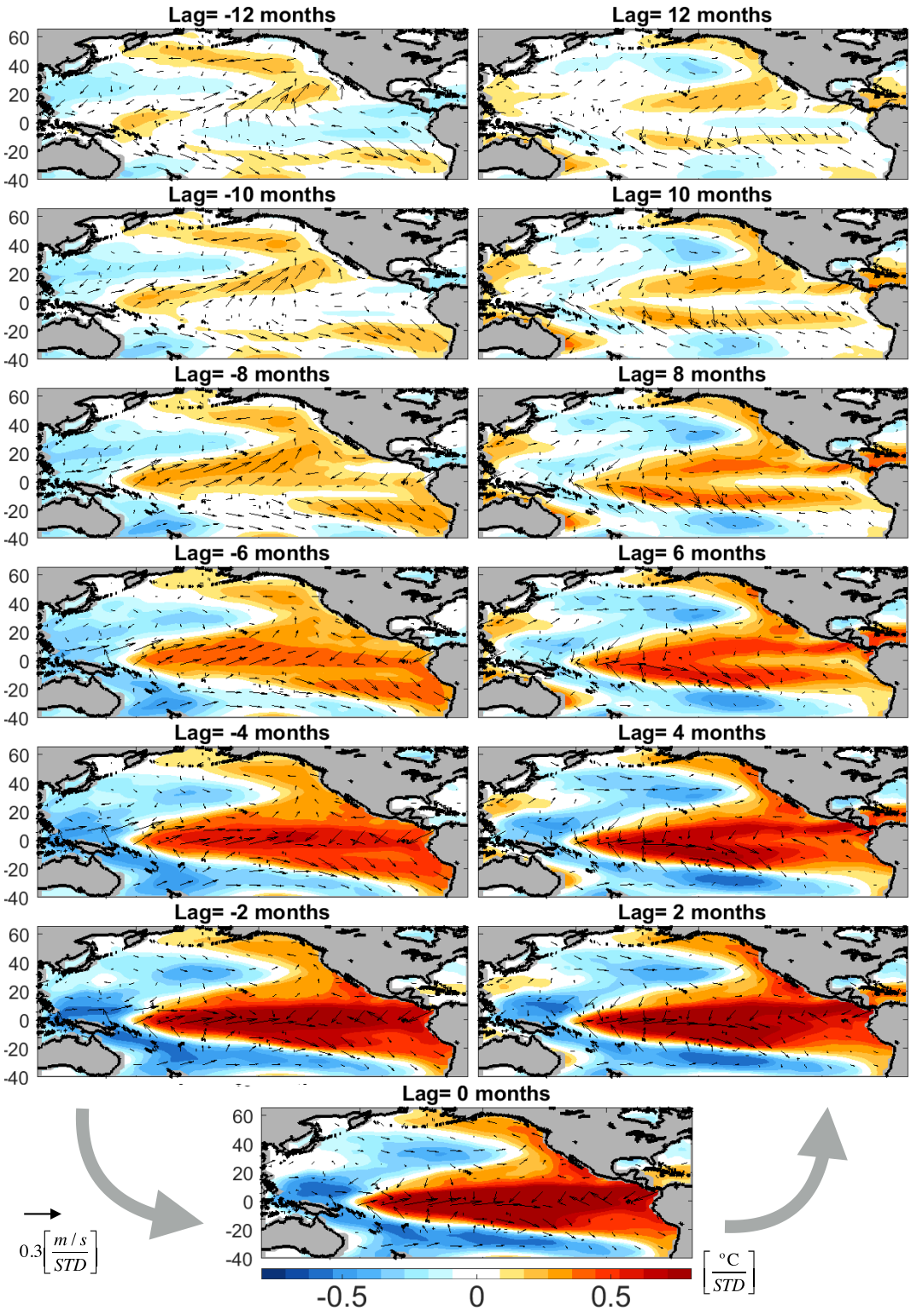

Figure S3.1. NOOA monthly mean SST anomaly (shading) and NCEP wind anomaly (vectors) regressed onto the Niño34 index at different lags for the period 1950-2015. Units are in [°C] and [m/s] per units of STD change of Niño34 index.

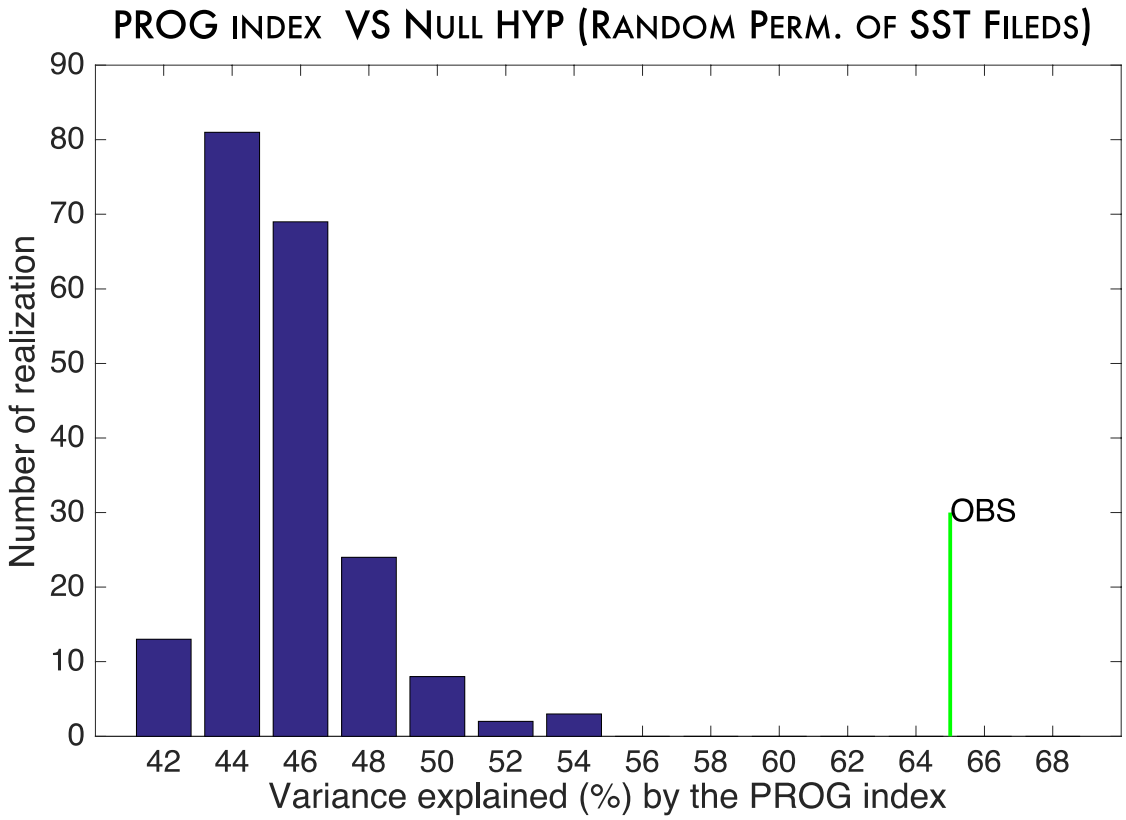

Figure S3.2. Histogram of 200 realizations of the variance explained by the PROG index when the sequences of each of the seasonal SSTa field (e.g., DJF, MAM, SON, DJF+1) are randomly re-ordered. The vertical line in green shows the variance explained by the actual PROG index (i.e., with unmodified SSTa sequences). ERSST.v3 SST from 1920-2015.

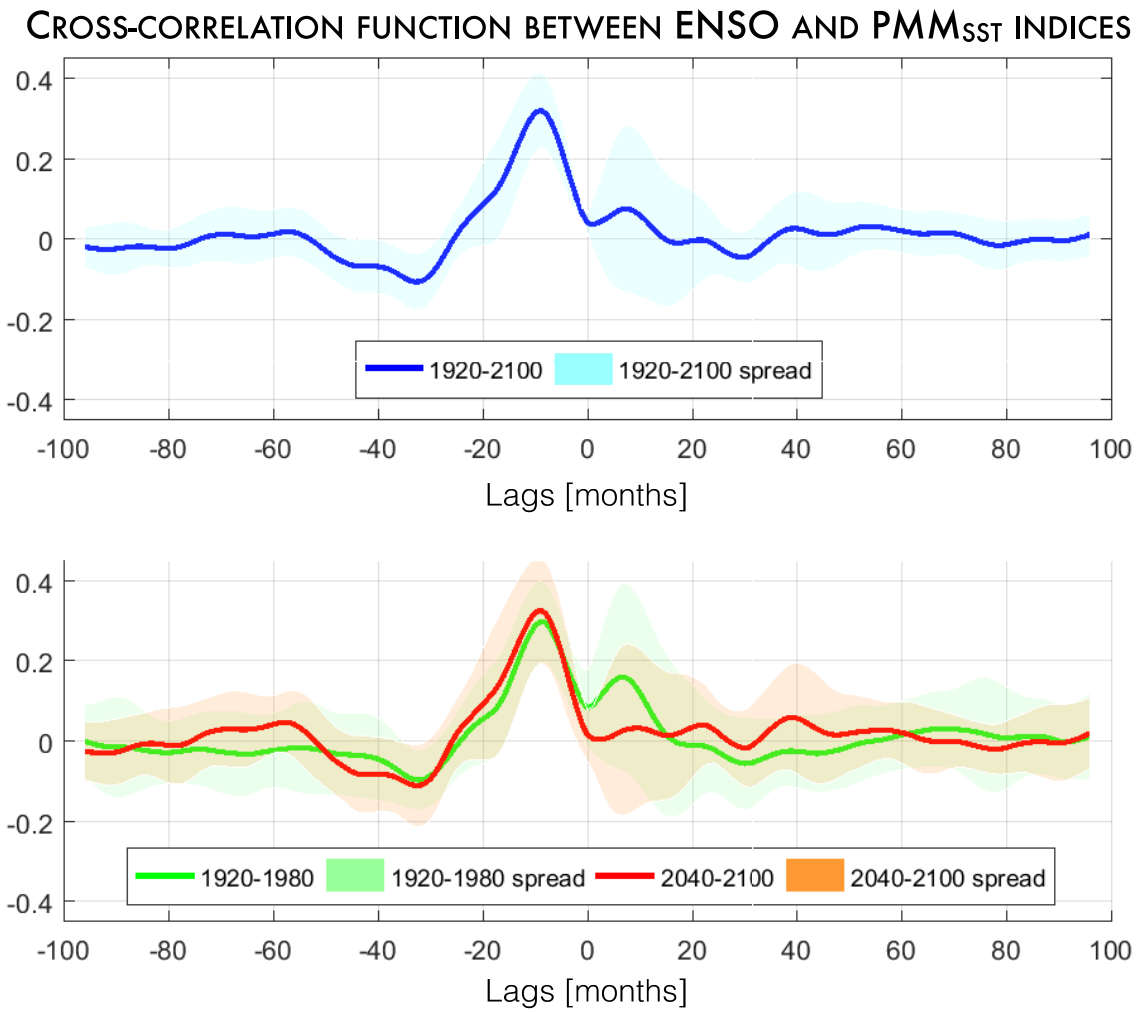

Figure S3.3. PMM-ENSO relationship. Cross-correlation function between monthly mean indices of ENSO and PMM_{sst} in LENS. In (a) the function is computed for the whole period, while in (b) the first 60 years (1920-1960) are compared to latest 60 years (2040-2100). Solid line indicates the ENSm while the shading represent the inter-member spread defined as 1 STD from the ENSm. The ENSO index is leading for positive lags, therefore the PMM index is leading for negative lags.

3.7 References

Alexander, M. A., D. J. Vimont, P. Chang, and J. D. Scott (2010), The Impact of Extratropical Atmospheric Variability on ENSO: Testing the Seasonal Footprinting Mechanism Using Coupled Model Experiments, *Journal of Climate*, *23*(11), 2885-2901.

Anderson, B. T. (2003), Tropical Pacific sea-surface temperatures and preceding sea level pressure anomalies in the subtropical North Pacific, *J Geophys Res-Atmos*, *108*(D23).

Chang, P., L. Zhang, R. Saravanan, D. J. Vimont, J. C. H. Chiang, L. Ji, H. Seidel, and M. K. Tippett (2007), Pacific meridional mode and El Nino-southern oscillation, *Geophys Res Lett*, *34*(16).

Chavez, F. P., J. Ryan, S. E. Lluch-Cota, and M. Niquen (2003), From anchovies to sardines and back: Multidecadal change in the Pacific Ocean, *Science*, *299*(5604), 217-221.

Chhak, K. C., E. Di Lorenzo, N. Schneider, and P. F. Cummins (2009), Forcing of Low-Frequency Ocean Variability in the Northeast Pacific, *Journal of Climate*, *22*(5), 1255-1276.

Chiang, J. C. H., and D. J. Vimont (2004), Analogous Pacific and Atlantic meridional modes of tropical atmosphere-ocean variability, *Journal of Climate*, *17*(21), 4143-4158.

Collins, M., et al. (2010), The impact of global warming on the tropical Pacific ocean and El Nino, *Nat Geosci*, *3*(6), 391-397.

Delworth, T. L., and M. E. Mann (2000), Observed and simulated multidecadal variability in the Northern Hemisphere, *Clim. Dyn.,* 16, 661–676.

Di Lorenzo, E., et al. (2008), North Pacific Gyre Oscillation links ocean climate and ecosystem change, *Geophys Res Lett*, *35*(8).

Di Lorenzo, E., G. Liguori, N. Schneider, J. C. Furtado, B. T. Anderson, and M. A. Alexander (2015), ENSO and meridional modes: A null hypothesis for Pacific climate variability, *Geophys Res Lett*, *42*(21), 9440-9448.

Di Lorenzo, E., and N. Mantua (2016), Multi-year persistence of the 2014/15 North Pacific marine heatwave, *Nat. Clim. Change*, doi:10.1038/nclimate3082

Fasullo, J. T., and R. S. Nerem (2016), Interannual Variability in Global Mean Sea Level Estimated from the CESM Large and Last Millennium Ensembles, *Water-Sui*, *8*(11).

Frankignoul, C., and K. Hasselmann (1977), Stochastic climate models. Part II: Application to sea surface temperature anomalies and thermocline variability, *Tellus*, 29, 289–305.

Jiang**,** L. Islam, S. and T. Carlson (2004), Uncertainties in latent heat flux measurement and estimation: implications for using a simplified approach with remote sensing data, *Cadadian Journal of Remote Sensing*, Vol. 30, Iss. 5

Gill, A. E. (1980), Some Simple Solutions for Heat-Induced Tropical Circulation, *Q J Roy Meteor Soc*, *106*(449), 447-462.

Harrison, D. E., and G. A. Vecchi (1997), Westerly wind events in the tropical Pacific, 1986-95, *Journal of Climate*, *10*(12), 3131-3156.

Hu, S. N., and A. V. Fedorov (2017), The extreme El Nino of 2015-2016 and the end of global warming hiatus, *Geophys Res Lett*, *44*(8), 3816-3824.

Hurrell, J., and Coauthors, (2013), The Community Earth System Model: A framework for collaborative research, *B Am Meteorol Soc*, 94, 1339–1360.

Kalnay, E., et al. (1996), The NCEP/NCAR 40-year reanalysis project, *B Am Meteorol Soc*, *77*(3), 437-471.

Kay, J. E., et al. (2015), The Community Earth System Model (Cesm) Large Ensemble Project a Community Resource for Studying Climate Change in the Presence of Internal Climate Variability, *B Am Meteorol Soc*, *96*(8), 1333-1349.

Li, G., and S. P. Xie (2014), Tropical Biases in CMIP5 Multimodel Ensemble: The Excessive Equatorial Pacific Cold Tongue and Double ITCZ Problems, *Journal of Climate*, *27*(4), 1765-1780.

Li, J., Z. W. Zhu, and W. J. Dong (2017), Assessing the uncertainty of CESM-LE in simulating the trends of mean and extreme temperature and precipitation over China, *Int J Climatol*, *37*(4), 2101-2110.

Lindzen, R. S., and S. Nigam (1987), On the Role of Sea-Surface Temperature-Gradients in Forcing Low-Level Winds and Convergence in the Tropics, *J Atmos Sci*, *44*(17), 2418-2436.

Linkin, M. E., and S. Nigam (2008), The North Pacific Oscillation–West Pacific Teleconnection Pattern: Mature-Phase Structure and Winter Impacts, *Journal of Climate*, *21*(9), 1979-1997.

Liu, Z. Y. and E. Di Lorenzo (2017), Mechanisms and Predictability of Pacific Decadal Variability. *Current Climate Change Reports*, accepted.

Mantua, N. J., S. R. Hare, Y. Zhang, J. M. Wallace, and R. C. Francis (1997), A Pacific interdecadal climate oscillation with impacts on salmon production, *B Am Meteorol Soc*, *78*(6), 1069-1079.

Rayner, N. A., D. E. Parker, E. B. Horton, C. K. Folland, L. V. Alexander, D. P. Rowell, E. C. Kent, and A. Kaplan (2003), Global analyses of sea surface temperature, sea ice, and night marine air temperature since the late nineteenth century, *J Geophys Res-Atmos*, *108*(D14).

Roemmich, D., and J. Mcgowan (1995), Climatic Warming and the Decline of Zooplankton in the California Current (Vol 267, Pg 1324, 1995), *Science*, *268*(5209), 352-353.

Rogers, J. C. (1981), The North Pacific Oscillation, *Journal of Climatology,* 1(1), 39-57.

Smith, T. M., and R. W. Reynolds (2005), A global merged land-air-sea surface temperature reconstruction based on historical observations (1880-1997), *Journal of Climate*, *18*(12), 2021-2036.

Vimont, D. J. (2010), Transient Growth of Thermodynamically Coupled Variations in the Tropics under an Equatorially Symmetric Mean, *Journal of Climate*, *23*(21), 5771-5789.

Wang, S. Y., M. L'Heureux, and J. H. Yoon (2013), Are Greenhouse Gases Changing ENSO Precursors in the Western North Pacific?, *Journal of Climate*, *26*(17), 6309-6322.

Wang, S. Y., L. Hipps, R. R. Gillies, and J. H. Yoon (2014), Probable causes of the abnormal ridge accompanying the 2013-2014 California drought: ENSO precursor and anthropogenic warming footprint, *Geophys Res Lett*, *41*(9), 3220-3226.

Zhang, C. D., and J. Gottschalck (2002), SST anomalies of ENSO and the Madden-Julian oscillation in the equatorial Pacific, *Journal of Climate*, *15*(17), 2429-2445.

Zhang, H., A. Clement, and P. Di Nezio (2014), The South Pacific Meridional Mode: A Mechanism for ENSO-like Variability, *Journal of Climate*, *27*(2), 769-783.

Zhang, Y., J. M. Wallace, and D. S. Battisti (1997), ENSO-like interdecadal variability: 1900-93, *Journal of Climate*, *10*(5), 1004-1020.

Zhou, Z.-Q., S.-P. Xie, X.-T. Zheng, Q. Liu, and H. Wang (2014), Global warming-induced changes in El Nino teleconnections over the North Pacific and North America, *J. Clim.*, **27**(24), 9050–9064.

CHAPTER IV

SEPARATING THE NORTH AND SOUTH PACIFIC MERIDIONAL MODES CONTRIBUTIONS TO ENSO AND TROPICAL DECADAL VARIABILITY

Manuscript under review as

Liguori, G. and E. Di Lorenzo, 2018: Separating the North and South Pacific Meridional Modes contributions to ENSO and tropical decadal variability, *Geophysical Research Letters, under review.*

Abstract

North and South Pacific Meridional Modes (NPMM and SPMM) are known precursors of El Niño–Southern Oscillation (ENSO) and Tropical Pacific decadal variability (TPDV). However, the relative importance of these precursors and the timescale on which they impact the tropics, remains unclear. Using a 30-member ensemble of the Community Earth System Model as the control climate, we generate two additional members where the NPMM and SPMM are selectively suppressed. We find that both meridional modes energize the tropical variance independently on different timescales. The absence of NPMM leads to a significant reduction of the tropical interannual variability (~35%), while the absence of the SPMM has no appreciable impact on ENSO but significantly reduces the TPDV (~30%). While the relative importance of the NPMM and SPMM may be model dependent, the

stochastic atmospheric variability in the extra-tropics that energizes the meridional modes emerges as a key source of TPDV.

4.1 Introduction

Sea surface temperatures (SSTs) in the equatorial Pacific associated with El Niño–Southern Oscillation (ENSO) exert significant control over the interannual variability of the basin climate [e.g., *Alexander et al.*, 2002; *Harrison and Larkin*, 1998; *McPhaden et al.*, 2006], which drives major societal and economic impacts [e.g., *Adams et al.*, 1999; *Berry and Okulicz-Kozaryn*, 2008; *Cashin et al.*, 2017; *Fisman et al.*, 2016]. To first order, ENSO can be thought of as a collection of modes that are amplified along the zonal equatorial plane by positive coupled feedbacks between the ocean and atmosphere [*Bjerknes*, 1969; *Jin*, 1997; *Suarez and Schopf*, 1988]. To understand and predict ENSO it is necessary to study all those oceanic and atmospheric processes that act prior to its extreme manifestation — the ENSO precursor dynamics. While important ENSO precursors (e.g., westerly wind burst and Madden-Julian oscillations) act along the equator and rely on equatorial wave dynamics [*Fedorov*, 2002; *Kessler and Kleeman*, 2000; *McPhaden*, 1999; *McPhaden and Yu*, 1999; *Zavala-Garay et al.*, 2005], extratropical precursors, such as North and South Pacific Meridional modes (NPMM,[*Chiang and Vimont*, 2004], and SPMM, [*Zhang et al.*, 2014]), have also been found to be very effective in energizing both ENSO [*Alexander et al.*, 2010; *Chang et al.*, 2007; *Larson and Kirtman*, 2013; 2014; *Thomas and Vimont*, 2016; *You and Furtado*, 2017; *L Zhang et al.*, 2009a; *L Zhang et al.*, 2009b] and tropical Pacific decadal variability [TPDV; *Di Lorenzo et al.*, 2015; *Liguori and Di Lorenzo*, 2018; *H Zhang et al.*, 2014; *Zhao and Di Lorenzo*, 2018].

Using reanalysis datasets, the spatial signature of the extratropical dynamics affecting ENSO is revealed by performing a simple analysis where the first principal component (PC1)

of October-November-December (OND) mean SST anomalies (SSTa) in the equatorial Pacific [12°S-12°N] (i.e., ENSO index, *Ei*) is regressed onto preceding SST and sea level pressure anomalies (SLPa) of January-December-February (JFM) of the same year. In the subtropics, the SST precursor shows a clear signature of the NPMM and SPMM (Figure 4.1c) that is consistent with the extratropical SLP precursor (Figure 4.1a), which shows low-pressure centers driving a weakening of the off-equatorial trade winds. This weakening of the trades is known to trigger several precursor dynamics, including the "seasonal foot-printing mechanism" (SFM) [*Vimont et al.*, 2001; *Vimont et al.*, 2003], the "trade wind charging" (TWC) mechanism [*Anderson*, 2003; *Anderson et al.*, 2013], and excitation of off-equatorial Rossby waves [*Knutson and Manabe*, 1998; *Wang et al.*, 2003].

In the northern hemisphere the atmospheric precursor pattern is characterized by the signature of the North Pacific Oscillation mode (NPO; [*Linkin and Nigam*, 2008; *Rogers*, 1981]), known to be the optimal forcing for the NPMM. Similarly, in the southern hemisphere the recently defined South Pacific Oscillation appears to be the optimal precursor of the SPMM [*You and Furtado*, 2017]. The importance of these extratropical patterns in driving the tropical Pacific variability can be quantified using time indices for the north and south precursor patterns (i.e., *Ni* and *Si*; Figure 4.1), which are obtained by projecting extratropical JFM anomalies onto the precursor patterns ([150°E-120°W, 12°N-50°N] for Ni and [160°E-75°W, 12°S-50°S] for Si), to predict the OND ENSO index (i.e., *Ei*). For both SST and SLP, an important fraction of the interannual ENSO variance (~38% and ~35%, respectively for SST and SLP) is predicted by linearly combining the contributions of *Ni* and *Si* time series (Figure 4.1g and 4.1h) which, in the observational record, are found to be largely independent (R=0.17 and R=0.13, for SST- and SLP-based indices, respectively; [*Ding et al.*, 2015; *Zhao and Di Lorenzo*, 2018]).

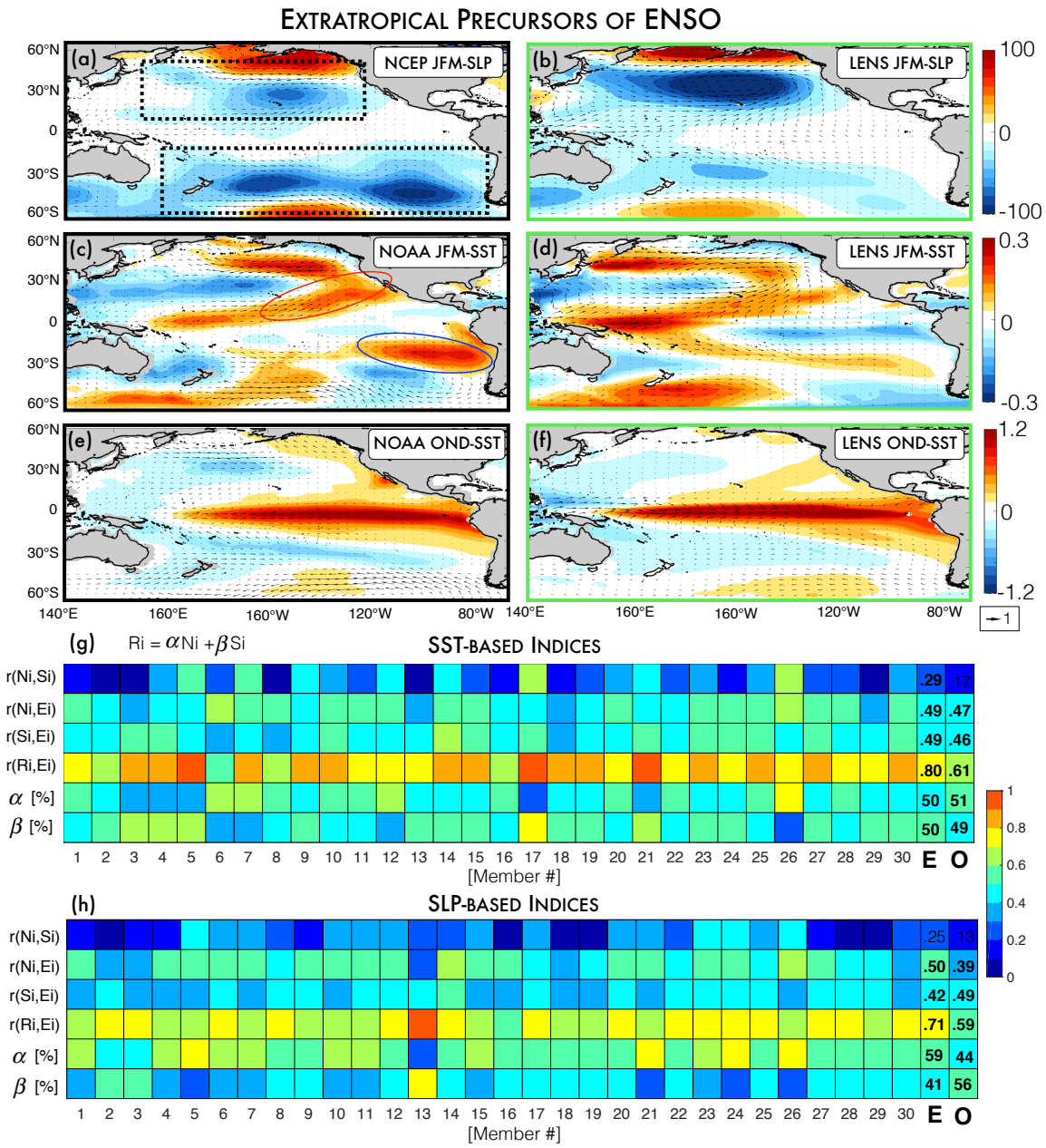

Figure 4.1. Precursor patterns of ENSO. Regression map between the SST-based October-November-December (OND) ENSO index (i.e., Ei, see text for the definition) and (a) preceding January-December-February (JFM) mean SLPa, (c) preceding JFM mean SSTa, and (e) concurrent OND mean SSTa. Vectors indicate regression with wind components, observational datasets are from NOAA ERSST v3 (SST) and NCEP (SLP and wind components), the period analyzed is 1950-2005, and units are in [°C] and [Pa]. (b, d, and e) The same analysis done with LENS (ensemble mean). (g) Correlation coefficients between Ei and SST-based north and South Pacific precursors, Ni and Si, respectively (see text for definitions): correlation between (first row) Ni and Si, (second row) Ni and Ei, (third row) Si

and Ei, and (forth row) Ei with the best linear model, Ri = α Ni + β Si. The relative weight (in %) of Ni (% α , fifth row) and Si (% β , sixth row) in the linear model is also shown. The correlation analysis is done for each LENS member (#1-30), the LENS ensemble mean (E), and the observational datasets (O). (h) as in (g) but for the SLP-based indices. The dash-lined boxes in (a) indicate the regions used to compute the projection indices Ni (upper box) and Si (lower box). The red-colored (blue-colored) ellipse in (c) indicates the area where the SST is restored for the noNPMM (noSPMM) experiment.

Recent studies suggest that although independent, synergies between South and North Pacific precursors (e.g., NPMM and SPMM) may be important for amplifying the tropical variance [*Ding et al.*, 2015; *You and Furtado*, 2017]. However, it remains unclear from these studies what the relative importance of these precursors is, on what frequency their influence on the tropics is more effective (i.e., interannual vs decadal timescales), and if destructive interference is also critical. While it is difficult to address these questions using exclusively observational analysis, experiments with coupled climate models can be designed to efficiently separate the contribution of ENSO precursor dynamics from the South and the North Pacific. Here we examine these dynamics in the Community Earth System Model (CESM) Large Ensemble (hereafter LENS) with a focus on the two dominant subtropical modes, the NPMM and SPMM, whose spatial signatures are highlighted by blue and red ellipses in the SST ENSO precursors shown in Figure 4.1c. In LENS, these precursor dynamics present a stronger than observed connection with ENSO that explain 64% and 50% of the ENSO variance, respectively for SST and SLP precursors (Figure 4.1g and 4.1h). However, given the large internal model variability, LENS can be considered consistent with the observations (Figure 4.1a, 4.1c, and 4.1e). In addition to the LENS simulations, we perform two extra LENS-like simulations in which either the NPMM or the SPMM variability is suppressed. These additional experiments, which differ from any other LENS member only for a regional

restoring of SST, allow us to investigate the role and the relative importance of NPMM and SPMM in the tropical Pacific variability, and establish the significance of the changes against the CESM ensemble. Using observational datasets and model simulations, our goals are to (1) identify the role of NPMM and SPMM precursors dynamics in the development of ENSO and (2) quantify the impact of both precursors in the statistics of the tropical Pacific variability from interannual to decadal timescale.

4.2 Datasets and Methodology

We use two SST data sets, the Met Office Hadley Centre SST, version 1.1 (HadISST v1.1) data set [*Rayner et al.*, 2003] and the National Oceanic and Atmospheric Administration Extended Reconstruction SST, version 3 (ERSST v3) product [*Smith and Reynolds*, 2005]. HadISST v1.1 (ERSST v3) consists of monthly mean values from 1870 (1854) to the present on a 1° x 1° (2° x 2°) horizontal grid globally. SLP and 10-m wind components, U and V, are taken from the National Centers for Environmental Prediction-National Center for Atmospheric Research reanalysis product [*Kistler et al.*, 2001] and consist of monthly mean values from 1950 to present on a 2.5° x 2.5° horizontal grid globally. Except for Figure 4.1, which uses observation from 1950 to 2005, we analyzed the period of record 1920–2005 to match the historical segment of LENS simulations.

We analyze the first 30 members of the LENS for the period forced by historical greenhouse gas and aerosol concentrations (i.e., radiative forcing) that span 1920-2005. The simulation uses CESM version 1, with the Community Atmosphere Model, version 5 (CESM1-CAM5; [*Hurrell et al.*, 2013]) at approximately 1° x 1° horizontal resolution in all model components. Throughout the manuscript, monthly mean anomalies are computed by removing the climatological seasonal cycle (i.e., long-term monthly mean of the record

analyzed) from detrended fields. While for the observational datasets, detrended fields are obtained by removing the linear trend at each grid point, in LENS, they are obtained by removing at each grid point the ensemble mean, which is assumed to be the signal associated with the historical radiative forcing.

The NPMM (SPMM) pattern is obtained as leading maximum covariance analysis (MCA) of monthly mean SST and surface wind stress anomaly in the region [175°E-95°W, 0°-32°N] ([165°W-95°W, 32°S-0°]) with ENSO removed by linear regression prior to the analysis. This calculation is similar to the one performed by *Chiang and Vimont* [2004] but computes the MCA on monthly mean value rather than on Spring anomalies, which introduces a preference on a specific season in the analysis. All the seasons in this manuscript are boreal seasons. The significance of the correlation coefficients throughout the study is estimated by computing empirical probability density functions (EPDFs) for the correlation coefficient of two red-noise time series which have the same lag-1 autoregressive coefficient of those estimated in the original signals. We assess the 99% significance levels using an EPDF obtained from 10,000 realizations of random red-noise time series.

4.3 Coupling Experiment Design

To investigate the role and relative importance of NPMM and SPMM in driving ENSO and TPDV, we extend the CESM ensemble (i.e., LENS) by adding two extra members in which either the NPMM or the SPMM variability is suppressed by restoring the SST (2 days restoring factor) to the monthly mean climatology only in the region where these modes are most active (see Figure S4.1 in the section *Supporting information* at the end of Chapter IV). Although this strong restoring removes any SST variability longer then few days, and not exclusively the ones linked with meridional mode dynamics, we assume that statistically

significant changes between the experiments and LENS are largely due to NPMM and SPMM dynamics. Hereafter we will refer to these experiments as noNPMM and noSPMM for suppressed NPMM and suppressed SPMM, respectively. The regions where these modes are most active, which do not include the tropical pacific band between [10°S-10°N], are identified by computing the LENS ensemble mean pattern of both NPMM and SPMM (Figure S4.1). These two extra members are highly comparable with LENS since they use same CESM code and configuration parameters, including numerical grids and radiative forcing. This is crucial given the very high internal variability that characterizes the model (e.g., Figure 4.1g and 4.1h) and presumably nature. Without a robust null hypothesis for the Pacific climate variability, as the one provided by LENS, it would not be possible to evaluate and assess the significance of the changes in the statistics of the Pacific climate driven by the suppression of the meridional modes variability.

4.4 Impacts of North and South Pacific Meridional mode on ENSO

The impacts of NPMM and SPMM on ENSO is assessed by comparing noNPMM and noSPMM experiments with LENS. Except in the region where the SST restoring is applied, ENSO precursor patterns of the noSPMM experiment are largely unchanged. Both SLP and SST during the preceding JFM season are substantially similar to the ones of LENS. In the North Pacific, the NPO-like pattern emerges in the SLP (Figure 4.2b) and an NPGO-like pattern in the SST (Figure 4.2d). Major changes are instead visible in the precursor patterns for the noNPMM experiment. Specifically, the SLP precursor lacks the characteristic NPO-like pattern and the North Pacific is instead characterized by an Aleutian Low-like pattern. Even more remarkable are the changes in the SST precursor: while in both LENS and noSPMM the equator band presents an east-west dipole structure, in noNPMM this is replaced

by a positive anomaly that extend across the whole basin. This remarkable change in ENSO precursors results in a significant reduction of ENSO activity during the succeeding OND season (Figure 4.2e).

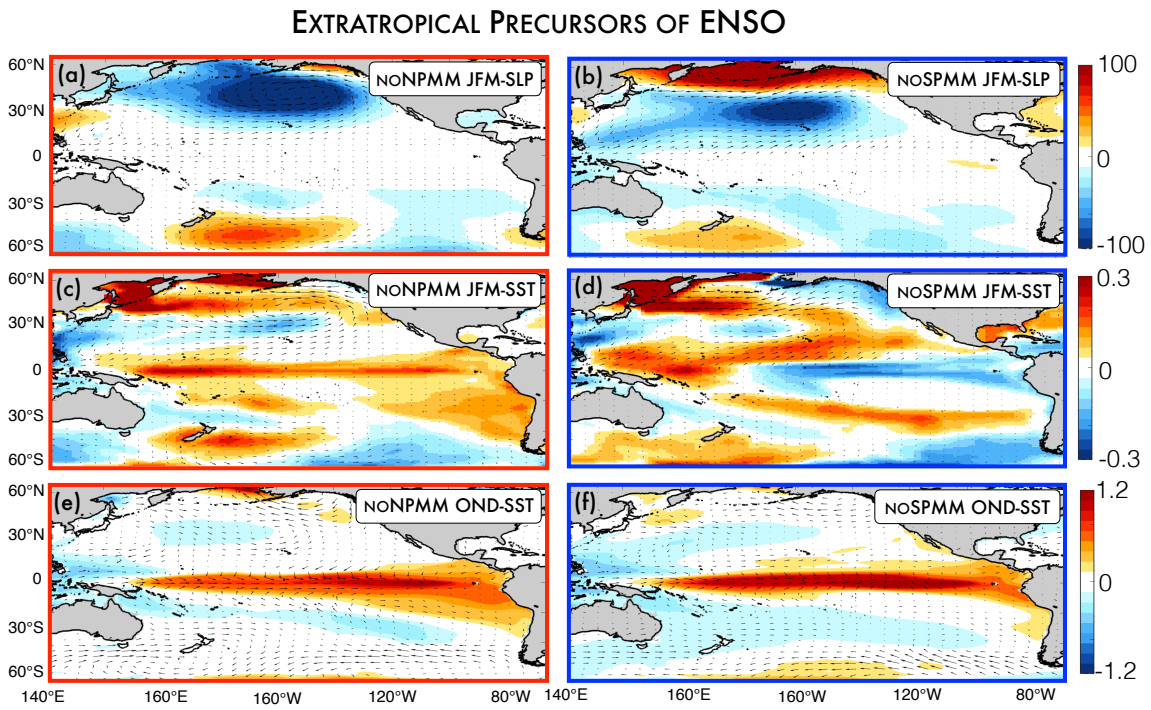

Figure 4.2. Precursor patterns of ENSO in the CESM experiments. Same as Figure 4.1 but for the experiments (a, c, and e) noNPMM and (b, d, and f) noSPMM.

To further explore the changes in tropical Pacific variance, we examine the first three empirical orthogonal functions (EOF) of the SST in the tropics [120°E-70°W, 25S°-25°N], which in LENS track ENSO, the NPMM and the SPMM, respectively for the first, the second, and the third mode (Figure 4.3a-c). While this simple classification may appear as an over simplification, it is confirmed by the modal decomposition of noNPMM and noSPMM experiments (Figure 4.3d-i). Specifically, the suppression of the NPMM variability results in a second mode (Figure 4.3e) which closely resembles the third mode of LENS (Figure 4.3c). Accordingly, the suppression of the SPMM variability only affects the third mode and leaves

the first two leading modes mostly unchanged, which is analogous to LENS-EOF1 and LENS-EOF2. Although this three-mode framework explains well the equatorial variability in the CESM simulations (i.e., LENS, noNPMM, and noSPMM), its third mode, which represents the SPMM, differs substantially from the one computed using an observational product such as the HadISST (Figure 4.3j, 4.3k, and 4.3l). Moreover, using the North's rule (North et al. 1982) we find that the third and the second mode in HadISST are not completely separated, which makes the mode-by-mode comparison difficult between model and observation. The first mode, ENSO, is similar in both observation and CESM simulations. Nevertheless, the simulations all present a bias in the extension of the equatorial anomaly, which extends too far east (Figure 4.3a, 4.3d, and 4.3g).

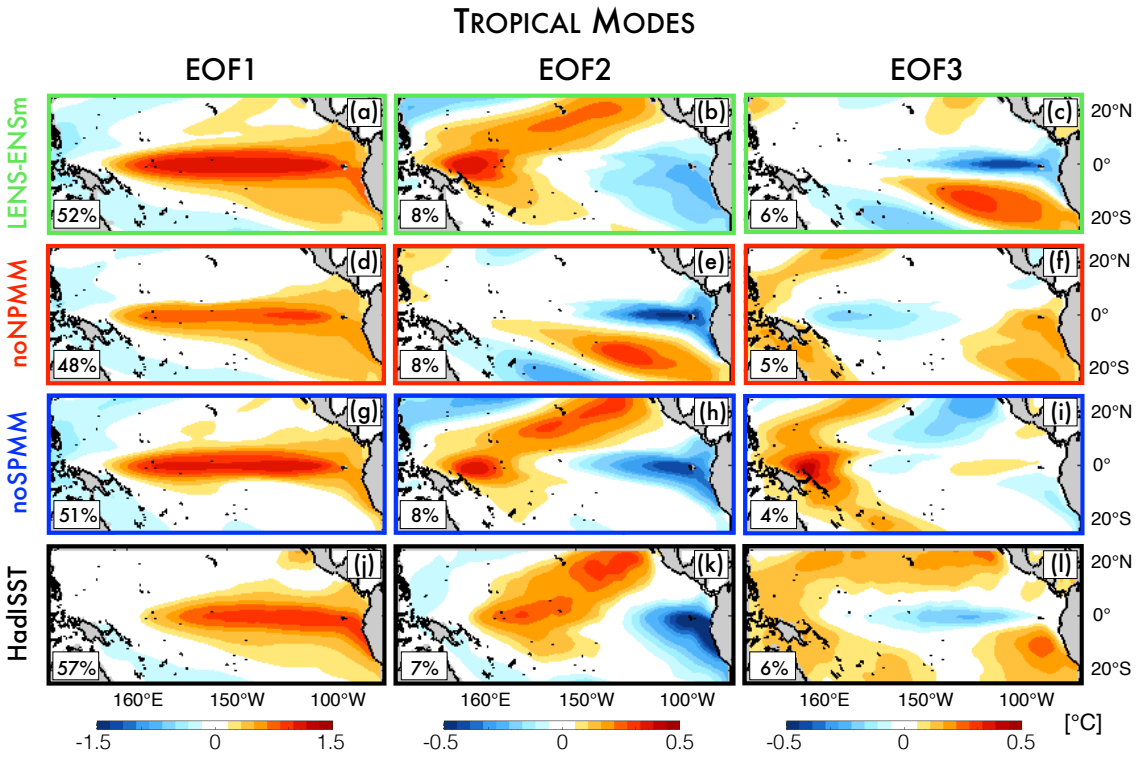

Figure 4.3. First three leading modes of tropical Pacific SSTa in (a-c) LENS, (d-f) noNPMM, (g-i) noSPMM, and (j-l) HadISST v1.1. The numbers in the lower-left corner of each figure indicates the amount of explained variance and units are in [°C].

The impacts of NPMM and SPMM on the equatorial SSTa spectrum is examined through the standard deviation (SD) of the monthly mean SSTa along the equatorial line (Figure 4.4a). When the NPMM is suppressed (i.e., noNPMM) there is a substantial reduction of tropical variance compared with LENS in the SD at all longitudes. This reduction, which for most latitudes (i.e., [170°W-110°W]) amounts to -35%, is highly statistically significant because all LENS members exhibit substantially higher values for the SD. However, it must be noted that LENS, and more generally this CESM version (i.e., version 1.1), presents a clear positive bias in the variance of the equatorial Pacific. When compared to LENS, the noSPMM experiment does not show any significant differences in SST SD along equator (Figure 4.4a). However, separating the SST variability in an interannual (<8 year) and a decadal (>8 year) component suggests a more complex situation (Figure 4.4b and 4.4c). While suppression of the SPMM (i.e., noSPMM) does not impact the interannual tropical variance, it leads to a significant reduction in the decadal-scale variability. In contrast, the suppression of the NPMM (i.e., noNPMM) reduces significantly the interannual variability (Figure 4b) but not the decadal variability (Figure 4.4c). For a view of the El Niño cycle in both experiments and LENS see the Figure S4.2 in the section *Supporting information* at the end of Chapter IV.

4.5 Impacts of North and South Pacific Meridional mode on Tropical Pacific Decadal Variability (TPDV)

The reduction of the decadal-scale equatorial variance in the noSPMM experiment (Figure 4.4c) is confirmed by the power spectrum of the Niño3.4 index (Figure 4.4d), which shows a sharp decrease in the power for periods longer than about 4 years. Such a sharp decrease in low-frequency energy is not as clear in the power spectrum of the noNPMM experiment, which presents instead a broad-spectrum weakening including a strong

suppression of the ENSO band (3-7 years) (Figure 4.4c; see also the normalized power spectrum of Figure S4.3 in the section *Supporting information* at the end of Chapter IV). To further characterize the role of meridional mode dynamics on the TPDV, we looked at the basin signature of the TPDV in both experiments and LENS. After applying an 8-year low-pass filter to the SSTa, we perform an EOF decomposition in the tropical Pacific sector that is not affected by the restoring ([10°S–10°N]) to extract the decadal-scale climate signal.

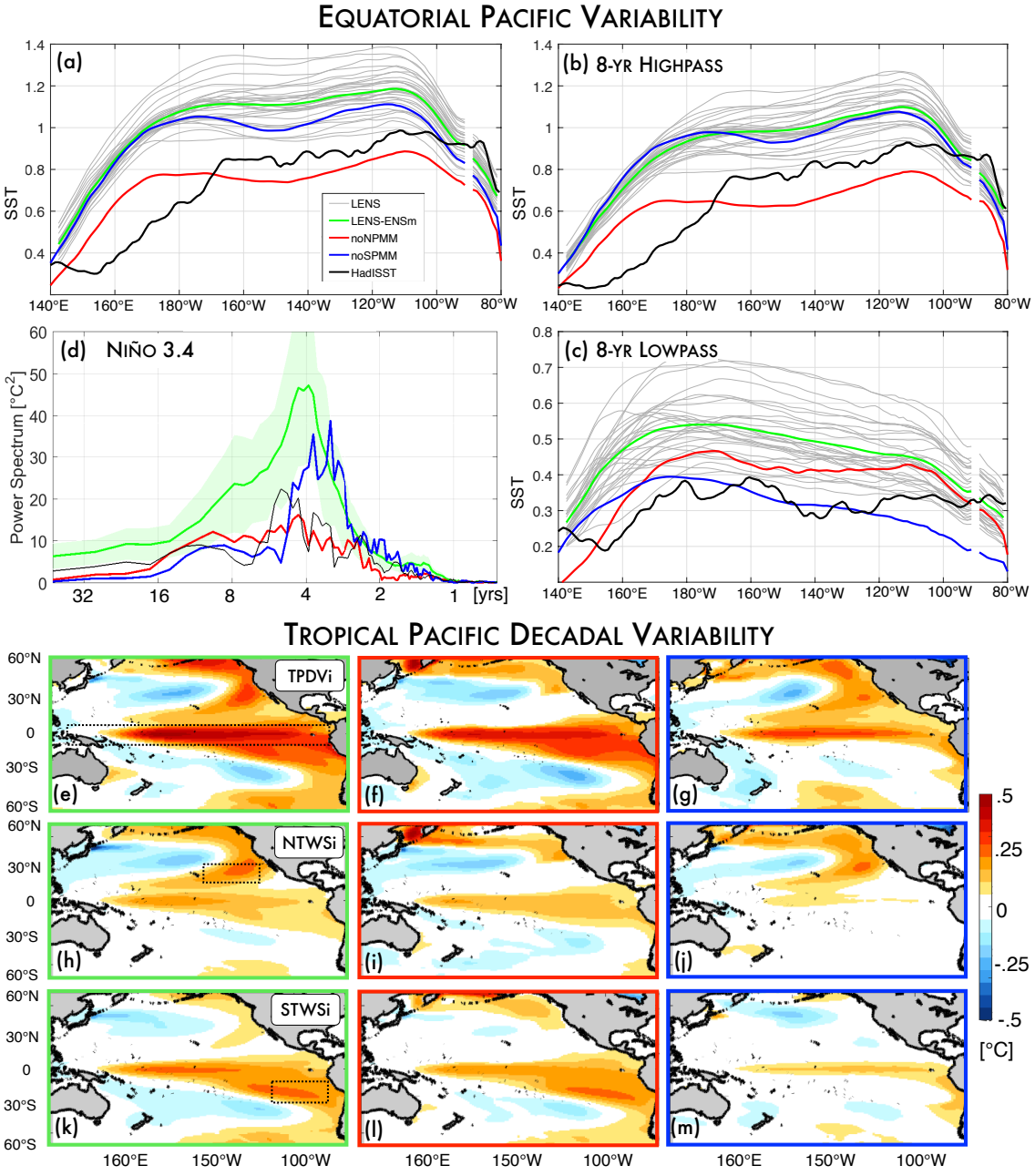

Figure 4.4. (a) Standard deviation in [°C], SD, of the monthly mean SSTa along the equatorial line (i.e., latitudinally averaged between 3°S-3°N) for each LENS members (grey), LENS ensemble mean (green), noNPMM (red), noSPMM (blue), and HadISST v1.1 (black). (b-c) As in (a) but for interannual (i.e., 8-year high-passed) and decadal (i.e., 8-year low-passed) SSTa. (d) Power spectrum in [°C2] of Niño 3.4 index for LENS ensemble mean (green; shading indicates 1 SD spread envelope), noNPMM (red), noSPMM (blue), HadISST v1.1 (black). (e, h and k) LENS 8-year low-passed SSTa regressed upon (e) the tropical Pacific decadal variability index (i.e., PC1 of 8-year low-passed SSTa over [10°S-10°N]), (h) the

northeasterly trade winds strength index (i.e., 8-year low-passed wind speed averaged over [150°W-120°W, 15°N-25°N]), and (k) the southeasterly trade winds strength index (i.e., 8-year low-passed wind speed averaged over [110°W-80°W, 25°S-15°S]). The same analysis is repeated for (f, i, and l) noNPMM and (g, j, and m) noSPMM experiments.

The first EOF mode, which represent the TPDV, explains most of the low-frequency variance (85%, 90% and 73%, in LENS, noNPMM and noSPMM, respectively) and is statistically distinct from higher-order modes [*North et al.*, 1982]. Excluding the region where the SST restoring is applied, the spatial signature of the TPDV that is obtained by regressing the PC1 onto the monthly SSTa over the entire Pacific basin reveals the characteristic equatorially symmetric pattern of ENSO-like decadal variability [*Zhang et al.*, 1997] in both LENS and noNPMM (Figure 4e and 4f), but not in the noSPMM (Figure 4g), which present substantially weaker anomalies in the tropics and important spatial differences in the southern hemisphere. Excluding the region where the SST restoring is applied, the spatial signature of the TPDV in LENS and noNPMM are similar in both hemispheres while the one of noSPMM differs substantially in the southern hemisphere. Specifically, the noSPMM lacks the negative anomaly pole centered at about [35°S,110°W], the positive anomaly near eastern side of the Australian continent, and the positive anomaly band in the extratropics that extends longitudinally from 140°W to the South America coastline.

4.6 Summary and Discussion of Mechanisms

Using observational data for SST and SLP over the period 1950-2005, we show that a significant fraction (~37% for SST and ~35% for SLP) of the late-fall (i.e., OND) interannual variability in the tropical Pacific, which is largely dominated by ENSO, can be explained by the state of the atmosphere (i.e., SLP) and ocean (i.e., SST) in the extratropics 9-month prior

(i.e., JFM mean; Figure 4.1g and 4.1h). Although these prior SST and SLP conditions (i.e., ENSO precursors) are characterized by the signature of both the NPMM in the north and the SPMM in south (Figure 4.1a and 4.1c), the contribution of each meridional mode to the tropical Pacific variability differs substantially. Experiments with the CESM model reveals that the SPMM does not have a significant impact on the interannual statistics of the tropical Pacific while the NPMM plays a key role in initiating ENSO. Moreover, in CESM most of the tropical Pacific variability (~65%) is explained by the first three leading EOF modes, which generally track ENSO, the NPMM, and the SPMM, respectively. While the SPMM has a weak influence on ENSO and explains only ~6% of the TPV, it plays a key role in the decadal statistics of the tropical Pacific. This finding provides an alternative hypothesis for the generation of TPDV, which previous studies have ascribed to residual variability of ENSO [e.g., *Vimont*, 2005] or to local coupled ocean-atmosphere dynamics in the tropical and North Pacific region [*Liu et al.*, 2002]. Further support for the idea that ENSO dynamics is not the primary source of TPDV is revealed by the experiment where the NPMM is suppressed, which leads to weaker ENSO but no significant decrease in the TPDV.

These results confirm a more recent view proposed by *Okumura* [2013] and consistent with observational analyses [*Deser et al.*, 2004; *Garreaud and Battisti*, 1999; *Zhao and Di Lorenzo*, 2018] and modeling studies [*Clement et al.*, 2011; *Matei et al.*, 2008] in which the TPDV is tightly linked to the South Pacific. Specifically, *Okumura* [2013] proposed that the latitudinal asymmetry of the central and eastern tropical Pacific climate, with the intertropical convergence zone displaced north of the equator during most of the year, allows the extratropical atmospheric variability to drive SST changes in the southeast equatorial Pacific by modulating the intensity of the southeasterly trade winds. This important role of the southeasterly trade winds in the TPDV is somewhat evident in LENS. Regression maps of 8-

year low-passed SSTa with indices of the northeasterly and southeasterly trade winds strength (NTWSi and STWSi) (Figure 4.4) reveal that the STWSi presents a larger signal in the Tropics that resemble more closely the TPDV pattern (Figure 4.4e). Repeating this analysis for noNPMM and noSPMM experiments confirms LENS results and suggests a negligible constructive interference between south and north precursors (Figure 4.4i, 4.4j, 4.4l, and 4.4m). Specifically, the suppression of the SST variability in the NPMM region results in southeasterly trade winds with a TPDV signature similar in shape and size of the anomaly to the ones in LENS (compare Figure 4.4k and 4.4l), suggesting a dominant and independent role of the south precursor in the TPDV. Although the noNPMM and noSPMM experiments helped revealing important characteristics of the two main extratropical ENSO precursors, the possibility that some results may be model-dependent requires further confirmation in other climate models.

Supporting Information

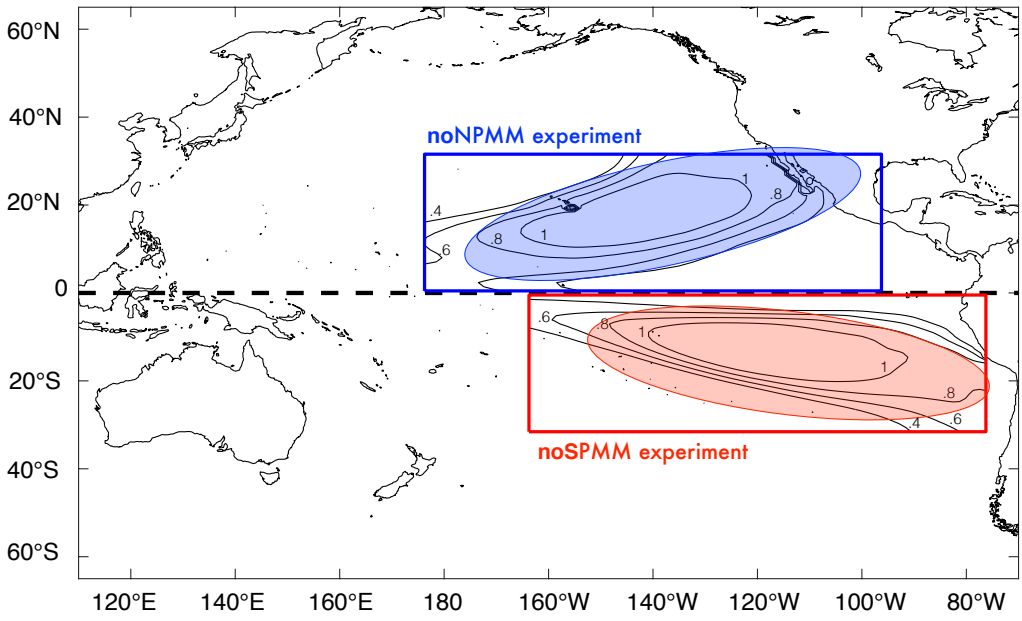

Figure S4.1. Experiment design. To suppress the NPMM and SPMM variability (i.e., noNPMM and noSPMM experiments, respectively), we restore the SST (2 days restoring factor) to the monthly mean climatology of LENS ensemble mean in the region where these modes are most active (blue and red shading ellipses, for noNPMM and noSPMM, respectively), which overlaps the normalized NPMM and SPMM patterns indicated by the contours in the blue and red rectangles, respectively (see Datasets and Methodology for detail on how the modes are computed). To blue ellipse is slightly larger than the red ellipse to ensure a similar extension of the SST-restored area in both experiments. The Blue and red rectangles indicate the region used for the calculation of the NPMM and SPMM, respectively. To avoid abrupt changes in the SST field, a buffer zone, in which the climatology combines with model values, is used within 3° of the restoring ellipse.

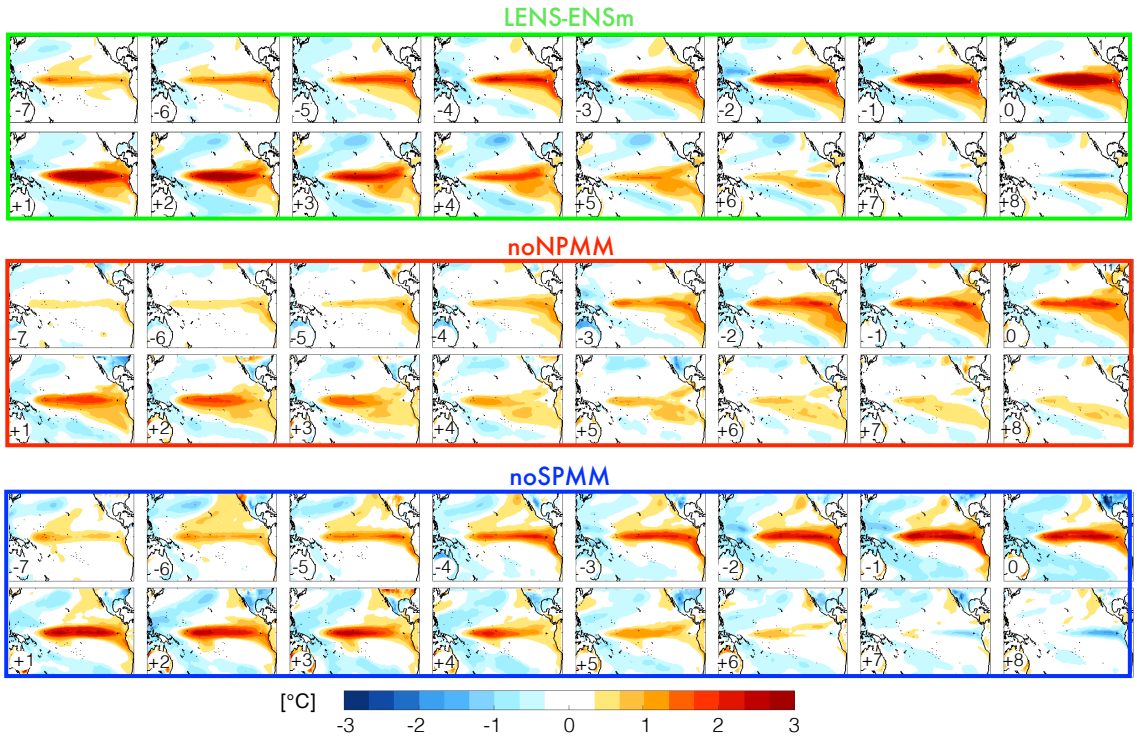

Figure S4.2. El Niño cycle. Composite anomalies of monthly mean SST for strong El Niño events during the period 1920-2005 (i.e., cold tongue index (CTI) > 2°C) in LENS (ensemble mean), noNPMM, and noSPMM. Progression of anomalies from 7 months before (-7) to 8 months after (+8) the CTI peak (0). The suppression of the SPMM variability does not impact substantially the progression of El Niño anomalies. In both LENS and noSPMM the progression appears to originate from warm anomalies in the western/central equatorial Pacific and evolve from west to east. It ends with cold anomalies in the eastern equatorial Pacific (i.e., La Niña conditions). Significant changes are instead visible when the NPMM variability is suppressed. In noNPMM the progression presents significantly weaker anomalies,

it appears to originate from warm anomalies in the eastern equatorial Pacific and evolve from east to west. it ends mostly with neutral condition in equatorial Pacific.

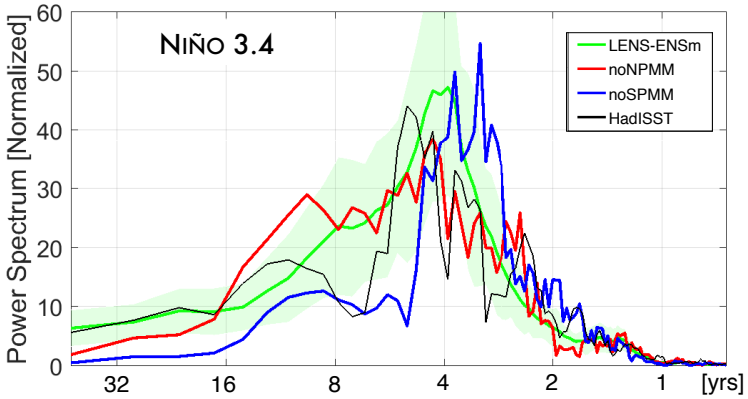

Figure S4.3. Normalized power spectrum of Niño 3.4 index for LENS ensemble mean (green; shading indicates 1 SD spread envelope), noNPMM (red), noSPMM (blue), HadISST v1.1 (black). The period analyzed is 1920-2005.

4.8 References

Adams, R. M., C. C. Chen, B. A. McCarl, and R. F. Weiher (1999), The economic consequences of ENSO events for agriculture, *Climate Research*, *13*(3), 165-172.

Alexander, M. A., D. J. Vimont, P. Chang, and J. D. Scott (2010), The Impact of Extratropical Atmospheric Variability on ENSO: Testing the Seasonal Footprinting Mechanism Using Coupled Model Experiments, *Journal of Climate*, *23*(11), 2885-2901.

Alexander, M. A., I. Blade, M. Newman, J. R. Lanzante, N. C. Lau, and J. D. Scott (2002), The atmospheric bridge: The influence of ENSO teleconnections on air-sea interaction over the global oceans, *Journal of Climate*, *15*(16), 2205-2231.

Anderson, B. T. (2003), Tropical Pacific sea-surface temperatures and preceding sea level pressure anomalies in the subtropical North Pacific, *J Geophys Res-Atmos*, *108*(D23).

Anderson, B. T., R. C. Perez, and A. Karspeck (2013), Triggering of El Nino onset through trade wind-induced charging of the equatorial Pacific, *Geophys Res Lett*, *40*(6), 1212-1216.

Berry, B. J. L., and A. Okulicz-Kozaryn (2008), Are there ENSO signals in the macroleconomy?, *Ecol Econ*, *64*(3), 625-633.

Bjerknes, J. (1969), Atmospheric Teleconnections from Equatorial Pacific, *Mon Weather Rev*, *97*(3), 163-&.

Cashin, P., K. Mohaddes, and M. Raissi (2017), Fair weather or foul? The macroeconomic effects of El Nino, *J Int Econ*, *106*, 37-54.

Chang, P., L. Zhang, R. Saravanan, D. J. Vimont, J. C. H. Chiang, L. Ji, H. Seidel, and M. K. Tippett (2007), Pacific meridional mode and El Nino-southern oscillation, *Geophys Res Lett*, *34*(16).

Chiang, J. C. H., and D. J. Vimont (2004), Analogous Pacific and Atlantic meridional modes of tropical atmosphere-ocean variability, *Journal of Climate*, *17*(21), 4143-4158.

Clement, A., P. DiNezio, and C. Deser (2011), Rethinking the Ocean's Role in the Southern Oscillation, *Journal of Climate*, *24*(15), 4056-4072.

Deser, C., A. S. Phillips, and J. W. Hurrell (2004), Pacific interdecadal climate variability: Linkages between the tropics and the North Pacific during boreal winter since 1900, *Journal of Climate*, *17*(16), 3109-3124.

Di Lorenzo, E., G. Liguori, N. Schneider, J. C. Furtado, B. T. Anderson, and M. A. Alexander (2015), ENSO and meridional modes: A null hypothesis for Pacific climate variability, *Geophys Res Lett*, *42*(21), 9440-9448.

Ding, R. Q., J. P. Li, and Y. H. Tseng (2015), The impact of South Pacific extratropical forcing on ENSO and comparisons with the North Pacific, *Clim Dynam*, *44*(7-8), 2017-2034.

Fedorov, A. V. (2002), The response of the coupled tropical ocean-atmosphere to westerly wind bursts, *Q J Roy Meteor Soc*, *128*(579), 1-23.

Fisman, D. N., A. R. Tuite, and K. A. Brown (2016), Impact of El Nino Southern Oscillation on infectious disease hospitalization risk in the United States, *Proceedings of the National Academy of Sciences of the United States of America*, *113*(51), 14589-14594.

Garreaud, R. D., and D. S. Battisti (1999), Interannual (ENSO) and interdecadal (ENSO-like) variability in the Southern Hemisphere tropospheric circulation, *Journal of Climate*, *12*(7), 2113-2123.

Harrison, D. E., and N. K. Larkin (1998), El Nino-Southern Oscillation sea surface temperature and wind anomalies, 1946-1993, *Rev Geophys*, *36*(3), 353-399.

Hurrell, J. W., et al. (2013), The Community Earth System Model A Framework for Collaborative Research, *B Am Meteorol Soc*, *94*(9), 1339-1360.

Jin, F. F. (1997), An equatorial ocean recharge paradigm for ENSO .1. Conceptual model, *J Atmos Sci*, *54*(7), 811-829.

Kessler, W. S., and R. Kleeman (2000), Rectification of the Madden-Julian oscillation into the ENSO cycle, *Journal of Climate*, *13*(20), 3560-3575.

Kistler, R., et al. (2001), The NCEP-NCAR 50-year reanalysis: Monthly means CD-ROM and documentation, *B Am Meteorol Soc*, *82*(2), 247-267.

Knutson, T. R., and S. Manabe (1998), Model assessment of decadal variability and trends in the tropical Pacific Ocean, *Journal of Climate*, *11*(9), 2273-2296.

Larson, S., and B. Kirtman (2013), The Pacific Meridional Mode as a trigger for ENSO in a high-resolution coupled model, *Geophys Res Lett*, *40*(12), 3189-3194.

Larson, S., and B. Kirtman (2014), The Pacific Meridional Mode as an ENSO Precursor and Predictor in the North American Multimodel Ensemble, *Journal of Climate*, *27*(18), 7018-7032.

Liguori, G., and E. Di Lorenzo (2018), Meridional Modes and Increasing Pacific Decadal Variability Under Anthropogenic Forcing, *Geophys Res Lett*, *45*(2), 983-991.

Linkin, M. E., and S. Nigam (2008), The North Pacific Oscillation–West Pacific Teleconnection Pattern: Mature-Phase Structure and Winter Impacts, *Journal of Climate*, *21*(9), 1979-1997.

Liu, Z., L. Wu, R. Gallimore, and R. Jacob (2002), Search for the origins of Pacific decadal climate variability, *Geophys Res Lett*, *29*(10).

Matei, D., N. Keenlyside, M. Latif, and J. Jungclaus (2008), Subtropical forcing of tropical Pacific climate and decadal ENSO modulation, *Journal of Climate*, *21*(18), 4691-4709.

McPhaden, M. J. (1999), Genesis and evolution of the 1997-98 El Nino, *Science*, *283*(5404), 950-954.

McPhaden, M. J., and X. Yu (1999), Equatorial waves and the 1997-98 El Nino, *Geophys Res Lett*, *26*(19), 2961-2964.

McPhaden, M. J., S. E. Zebiak, and M. H. Glantz (2006), ENSO as an integrating concept in Earth science, *Science*, *314*(5806), 1740-1745.

North, G. R., T. L. Bell, R. F. Cahalan, and F. J. Moeng (1982), Sampling Errors in the Estimation of Empirical Orthogonal Functions, *Mon Weather Rev*, *110*(7), 699-706.

Okumura, Y. M. (2013), Origins of Tropical Pacific Decadal Variability: Role of Stochastic Atmospheric Forcing from the South Pacific, *Journal of Climate*, *26*(24), 9791-9796.

Rayner, N. A., D. E. Parker, E. B. Horton, C. K. Folland, L. V. Alexander, D. P. Rowell, E. C. Kent, and A. Kaplan (2003), Global analyses of sea surface temperature, sea ice, and night marine air temperature since the late nineteenth century, *J Geophys Res-Atmos*, *108*(D14).

Rogers, J. C. (1981), The North Pacific Oscillation, *Journal of Climatology*, *1*(1), 39-57.

Smith, T. M., and R. W. Reynolds (2005), A global merged land-air-sea surface temperature reconstruction based on historical observations (1880-1997), *Journal of Climate*, *18*(12), 2021-2036.

Suarez, M. J., and P. S. Schopf (1988), A Delayed Action Oscillator for Enso, *J Atmos Sci*, *45*(21), 3283-3287.

Thomas, E. E., and D. J. Vimont (2016), Modeling the Mechanisms of Linear and Nonlinear ENSO Responses to the Pacific Meridional Mode, *Journal of Climate*, *29*(24), 8745-8761.

Vimont, D. J. (2005), The contribution of the interannual ENSO cycle to the spatial pattern of decadal ENSO-like variability, *Journal of Climate*, *18*(12), 2080-2092.

Vimont, D. J., D. S. Battisti, and A. C. Hirst (2001), Footprinting: A seasonal connection between the tropics and mid-latitudes, *Geophys Res Lett*, *28*(20), 3923-3926.

Vimont, D. J., J. M. Wallace, and D. S. Battisti (2003), The seasonal footprinting mechanism in the Pacific: Implications for ENSO, *Journal of Climate*, *16*(16), 2668-2675.

Wang, X. C., F. F. Jin, and Y. Q. Wang (2003), A tropical ocean recharge mechanism for climate variability. Part I: Equatorial heat content changes induced by the off-equatorial wind, *Journal of Climate*, *16*(22), 3585-3598.

You, Y. J., and J. C. Furtado (2017), The role of South Pacific atmospheric variability in the development of different types of ENSO, *Geophys Res Lett*, *44*(14), 7438-7446.

Zavala-Garay, J., C. Zhang, A. M. Moore, and R. Kleeman (2005), The linear response of ENSO to the Madden-Julian oscillation, *Journal of Climate*, *18*(13), 2441-2459.

Zhang, L., P. Chang, and M. K. Tippett (2009a), Linking the Pacific Meridional Mode to ENSO: Utilization of a Noise Filter, *Journal of Climate*, *22*(4), 905-922.

Zhang, L., P. Chang, and L. Ji (2009b), Linking the Pacific Meridional Mode to ENSO: Coupled Model Analysis, *Journal of Climate*, *22*(12), 3488-3505.

Zhang, Y., J. M. Wallace, and D. S. Battisti (1997), ENSO-like interdecadal variability: 1900-93, *Journal of Climate*, *10*(5), 1004-1020.

Zhao, Y., and E. Di Lorenzo (2018), South and North Pacific ENSO precursors control the phase of tropical decadal variability, *Nat Geosci.*, submitted

CHAPTER V

CONCLUDING REMARKS AND FUTURE RESEARCH

5.1 Concluding Remarks

A large part of this dissertation is based on the novel idea that interaction and exchange dynamics between the extra-tropics and the tropics are a key source of the multi-year climate memory that supports the basin-scale expressions of the ENSO-like tropical Pacific decadal variability (Chapter II). In the extra-tropics, stochastic atmospheric forcing that activate ENSO precursor dynamics such as NPMM energize ENSO (blue path of Figure 5.1), and its teleconnection back to the extra-tropics (red path of Figure 5.1). The seasonal sequence from ENSO precursors, to ENSO peak, to ENSO teleconnections (with decay in the extra-tropics) provides a mechanism to integrate the short-memory, seasonally-varying, stochastic forcing from both the extra-tropics and tropics into Pacific decadal-scale variance. We referred to this process in Chapter II as the "reddening" of Pacific climate.

In this PDV framework outlined in Figure 5.1, the extra-tropical modes of Pacific decadal variability (e.g., PDO, NPGO) are connected and capture different phases of this TPDV reddening. Specifically, the modes of North Pacific decadal variability are the result of a collection of processes that involve the integration of different atmospheric forcing both internal (i.e., stochastic forcing such as the NPO) and external to the extra-tropics (e.g. teleconnections from tropics and other oceanic basins). The integration of these forcing is enabled by the memory dynamics of the ocean-atmosphere system associated with tropical/extra-tropical winter (boreal) to winter coupling but also with reemergence processes [*Alexander and Deser, 1995*] and westward propagating Rossby waves [*Qiu, 2003; 2007; Ceballos, Di Lorenzo et al. 2009; Perkins and Holbrook, 2001*]. Although the schematic of Figure 5.1

represents the teleconnections and processes as deterministic, the links between tropics/extra-tropics and the climate modes are affected by internal noise of the climate system, which can override these teleconnections at any time during an event (e.g., ENSO precursor, ENSO, and ENSO teleconnections events). Furthermore, the strength and types of coupled ocean/atmosphere feedbacks that are activated by the stochastic forcing play a key role in the magnitude and spatial distribution of the decadal variance over the Pacific basin.

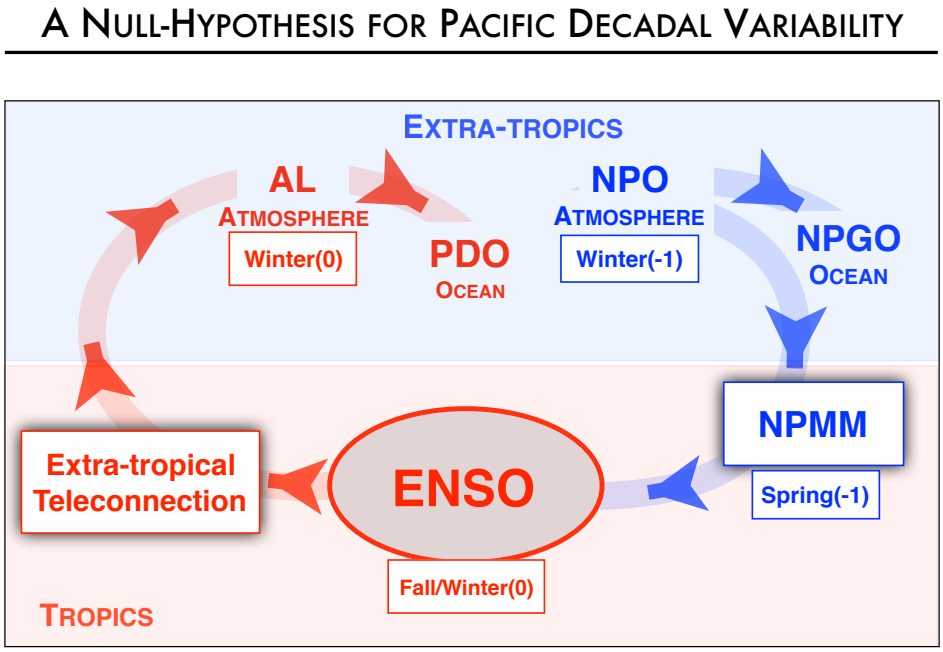

Figure 5.1. Schematic of observational-based hypothesis of PDV processes and teleconnections

This interpretative framework proved for be useful for exploring how the PDV has changed in the observational record, and how PDV is expected to change according to the Community Earth System Model (CESM) Large Ensemble (LENS) under the RCP8.5 radiative forcing scenario (Chapter III). Using a seasonally-spatially stratified EOF analysis to capture the PDV mechanisms, we found that the variance of the PDV increases in both observational dataset and LENS. In LENS, further analyses linked this increase to an

intensification of the ocean-atmosphere thermodynamical coupling associated with the WES feedback, which is dependent on the mean background state (i.e., warming of SST generates a stronger response in evaporation) and modulates the amplitude of the growth of NPMM (Figure 5.2).

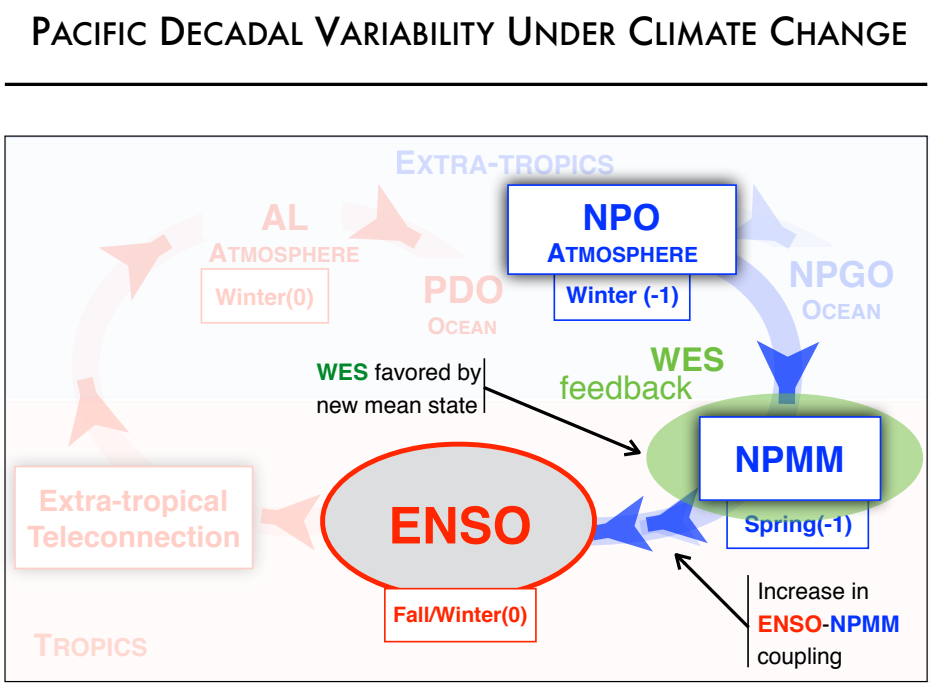

Figure 5.2. Schematic of changes in the PDV dynamics under anthropogenic forcing (RCP8.5 radiative forcing scenario) in the Community Earth System Model (CESM) Large Ensemble (LENS).

In Chapter IV, inspired by recent studies suggesting an important role of the SPMM in the Pacific climate variability [e.g., *Zhang et al., 2014; Okumura, 2013; You and Furtado, 2017*], we investigate the relative importance of the NPMM and South PMM (SPMM) in ENSO and TPDV by performing "surgical" experiments with the CESM model in which NPMM and SPMM are selectively suppressed. We find that the absence of NPMM leads to a significant reduction of ENSO (~35%), while the absence of the SPMM has no appreciable impact on

ENSO but significantly reduces the TPDV (~30%). The NPMM and SPMM modes impact the tropical variance independently on interannual and decadal timescale, respectively (Figure 5.3).

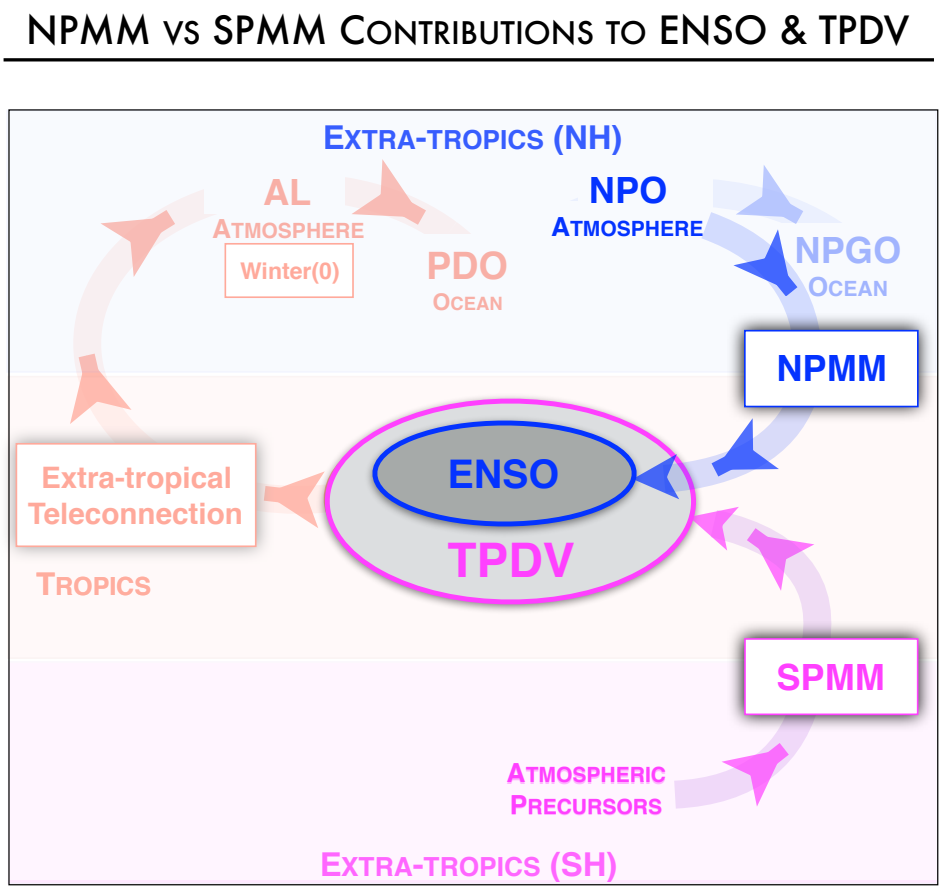

Figure 5.3. Schematic of North and South Pacific Meridional Modes (NPMM and SPMM) contributions to ENSO and TPVD as inferred from idealized simulations performed with the CESM version 1.1.

5.2 Future Research

The research presented in this dissertation significantly improved our understanding of the mechanisms responsible for the Pacific climate variability. However, our findings on the impact of climate change on PDV dynamics as well as on the relative contributions of

NPMM and SPMM to ENSO and TPDV, were based on the analysis of a single-model ensemble and might show model dependences. Therefore, it is important to validate these findings in other Earth System Models (ESMs) large ensemble simulations, such as the ones recently produced by the Geophysical Fluid Dynamics Laboratory and the Max-Planck Institute of Meteorology. Given the significance of internal variability shown in LENS (e.g., Figure 3.4b and Figure 4.1g-h), ESM large ensemble simulations are a requirement for robust projections of the impacts of anthropogenic climate change with a given model.

Given that the PDV framework has proved a powerful tool to diagnose PDV mechanisms in both observational datasets and models, we envisage a great benefit for the climate science community in analyzing simulations from the Coupled Model Intercomparison Project Phase 6 (CMIP6) models under both 20th century and projected future conditions. Specifically, a comprehensive analysis of the mechanisms energizing PDV and ENSO using the PDV framework would allow us to assess the ability of CMIP6 models in reproducing observed PDV dynamics, and understand how these mechanisms interact/depend on climate change trends.

5.3 References

Alexander, M. A., and C. Deser (1995), A mechanism for the recurrence of wintertime midlatitude SST anomalies, *J. Phys. Oceanogr.,* 25, 122–137.

Ceballos, L. I., E. Di Lorenzo, C. D. Hoyos, N. Schneider, and B. Taguchi (2009), North Pacific gyre oscillation synchronizes climate fluctuations in the eastern and western boundary systems, *J. Clim.,*22, 5163–5174.

Qiu, B. (2003). Kuroshio Extension variability and forcing of the Pacific decadal oscillations: Responses and potential feedback. Journal of Physical Oceanography 33(12): 2465-2482.

Perkins ML, Holbrook NJ. (2001), Can Pacific Ocean thermocline depth anomalies be simulated by a simple linear vorticity model? *J Phys Oceanogr.,* 31(7):1786–806.

You, Y. J., and J. C. Furtado (2017), The role of South Pacific atmospheric variability in the development of different types of ENSO, *Geophys Res Lett*, 44(14), 7438-7446.

Okumura, Y. M. (2013), Origins of Tropical Pacific Decadal Variability: Role of Stochastic Atmospheric Forcing from the South Pacific, *Journal of Climate*, 26(24), 9791-9796.

Zhang, H., A. Clement, and P. Di Nezio (2014), The South Pacific Meridional Mode: A Mechanism for ENSO-like Variability, *Journal of Climate*, 27(2), 769-783.

PUBLICATIONS

Ortiz Beviá M.J., Álvarez García F.J., Ruiz de Elvira A., **Liguori, G.**, Hernández-Carretero J., 2012: The Western Mediterranean Summer Variability and its Feedbacks. *Climate Dynamics*, doi: 10.1007/S00382-012-1409-X.

Iermano I., **Liguori G.**, Iudicone D., Buongiorno B., Colella S., Zingone A., Saggiomo V., Ribera d'Alcalà M., 2012: Filament formation and evolution in buoyant coastal waters: observation and modelling. *Progress in Oceanography*, doi: 10.1016/j.pocean.2012.08.003.

Dominguez M., Romera R., Sanchez E., Fita L., Fernandez J., Jimenez-Guerrero P., Montalvo J.P., Cabos W.D., **Liguori G.**, Gaertner M.A., 2013: Precipitation and temperature extremes under present climate over Spain from a set of high resolution RCMs. *Climate Research*, doi: 10.3354/cr01186.

Jimenez-Guerrero P., Montalvo J.P., Dominguez M., Romera R., Fita L., Fernandez J., Cabos W.D., **Liguori G.**, Gaertner M.A., 2013: Description of mean fields and interannual variability in an ensemble of RCM evaluation simulations over Spain: Results from the ESCENA project. *Climate Research*, doi: 10.3354/cr01165.

Gomez G., Cabos W., **Liguori G.**, Lozaon S., Fita L., Fernández J.,Magariño E., Jiménez-Guerrero P., Montalvez J., Domínguez M., Romera R., Gaertner M., 2014: Characterization of the wind speed variability and future change in the Iberian Peninsula and the Balearic Islands. *Wind Energy,* doi: 10.1002/we.1893.

Di Lorenzo E., **Liguori G.**, Schneider N., Furtado J. C., Anderson B. T., Alexander M. A., 2015: ENSO and Meridional Modes: a null hypothesis for Pacific climate variability. *Geophysical Research Letters*, doi:10.1002/2015GL066281.

Ruti P., Somot S., Dubois C., Calmanti S., Ahrens B., Aznar R., Bartholy J., Béranger K., Bastin S., Brauch J., Calvet J.C., Carillo A., Alias A., Decharme B., Dell'Aquila A., Djurdjevic V., Drobinski P., Elizalde Arellano A., Gaertner M., Galan P., Gallardo C., Giorgi F., Gualdi S., Bellucci A., Harzallah A., Herrmann M., Jacob D., Khodayar S., Krichak S., Lebeaupin C., Lheveder B., Li L., **Liguori G.**, Lionello P., Baris O., Rajkovic B., Sevault F., Sannino G., 2016: MED-CORDEX Initiative for Mediterranean Climate Studies. *Bulletin of the American Meteorological Society*, doi:10.1175/BAMS-D-14-00176.1.

Liguori G., Di Lorenzo E. , Cabos W., 2017: A multi-model ensemble view of winter heat flux dynamics and the dipole mode in the Mediterranean Sea. *Climate Dynamics*, doi: 10.1007/s00382-016-3129-0.

Liguori G and Di Lorenzo E, 2018: Meridional Modes and Increasing Pacific decadal variability under greenhouse forcing. *Geophysical Research Letters*, 45. doi: 10.1002/2017GL076548.

Fernandez J., Frias M. D., Cabos W.D., Cofino A. S., Dominguez M., Fita L., Gaertner M. A., Garcıa-Dıez M., Gutierrez J. M., Jimenez-Guerrero P., **Liguori G.**, Montavez J. P.,

Romera R., Sanchez E., 2018: Consistency of climate change projections from multiple global and regional model intercomparison projects. *Climate Dynamics*, *doi:* 10.1007/s00382-018-4181-8.

Cabos Narvaez, W, Sein, D. V., Durán-Quesada, A., **Liguori, G**., and et al.: Dynamical downscaling of historical climate over CORDEX Central America domain with a regionally coupled atmosphere-ocean model. *Climate Dynamics*, *doi*: 10.1007/s00382-018-4381-2.

Liguori, G. and E. Di Lorenzo: Separating the North and South Pacific Meridional Modes contributions to ENSO and tropical decadal variability. *Geophysical Research Letters,* submitted.

Grothe, P. R., Cobb K.M., **Liguori G.**, and et al.: Central Pacific El Niño Southern Oscillation stronger in last decades than pre-industrial period. *Nature Geoscience*, submitted.